

# Spontaneous Symmetry Breaking In Four Fermion Theories



---

seit 1558

FRIEDRICH-SCHILLER-UNIVERSITÄT JENA  
Physikalisch Astronomische Fakultät

MASTERARBEIT  
zur Erlangung des akademischen Grades  
MASTER OF SCIENCE (M. SC.)  
im Studiengang Physik

eingereicht am 17.07.2018 von

*Julian Johannes Lenz*

geb. am 30.07.1994 in Elmshorn

Betreut und begutachtet von  
Prof. Dr. Andreas WIPF  
Dr. Björn WELLEGEHAUSEN

**Abstract.** This thesis investigates spontaneous symmetry breaking in four fermion theories. To obtain concrete results from this broad field of theories, the setting is specialized to GROSS-NEVEU models in three spacetime dimensions. In a first step, the critical behavior and thermodynamics of the large flavor number approximation are discussed. After further specifying the model to one irreducible flavor, Monte Carlo lattice simulation results are shown. On the one hand, precise estimates for the critical behavior at zero temperature are given including the critical coupling and critical exponents of the parity/chiral phase transition as well as the lattice artifact phase transition. On the other hand, a first glance into an investigation of the finite temperature phase diagram is provided.

# Contents

<b>1</b>	<b>Introduction</b>	<b>4</b>
<b>2</b>	<b>General Preliminaries</b>	<b>7</b>
2.1	Physical Preliminaries . . . . .	7
2.1.1	Phase Transitions And Critical Behavior . . . . .	7
2.1.2	(Lattice) Quantum Field Theory . . . . .	8
2.2	Numerical Preliminaries . . . . .	9
2.2.1	Monte Carlo Methods And Importance Sampling . . . . .	10
2.2.2	Finite Size Scaling . . . . .	11
2.2.3	Fermions On The Lattice . . . . .	13
<b>3</b>	<b>Four Fermion Theories</b>	<b>16</b>
3.1	Spinors And Representations . . . . .	16
3.2	General Four Fermion Theories . . . . .	17
3.3	Symmetries Of Four Fermion Theories . . . . .	19
3.4	Symmetry Breaking In Four Fermion Theories . . . . .	22
3.5	Bosonization Of Four Fermion Theories . . . . .	23
<b>4</b>	<b>Large-<math>N_f</math> Limit</b>	<b>25</b>
4.1	Calculation Of The Partition Function . . . . .	26
4.2	Chiral Condensate And Critical Behavior . . . . .	28
4.3	Thermodynamics . . . . .	33
<b>5</b>	<b>Lattice Results for <math>N_f = 1</math></b>	<b>38</b>
5.1	Dualization Of GROSS-NEVEU . . . . .	38
5.2	Observables In Dual Formulation . . . . .	40
5.3	Evaluation Details . . . . .	42
5.4	Remarks On The Sign Problem . . . . .	45
5.5	Results For Vanishing Temperature . . . . .	48
5.5.1	Investigation Of The Physical Phase Transition . . . . .	48
5.5.2	Investigation Of The Lattice Artifact PhaseTransition . . . . .	54
5.6	The Phase Diagram Of GROSS-NEVEU . . . . .	59
5.6.1	Preliminary Discussion . . . . .	59
5.6.2	Results . . . . .	63
5.6.3	Comparisons . . . . .	68
<b>6</b>	<b>Conclusions And Outlook</b>	<b>70</b>

## 1 Introduction

Symmetry is one of the most fundamental concepts in physics. It led to the formulation of general relativity, the state-of-the-art description of macroscopic physics, and can be used to derive the complete particle content of the standard model of particle physics – the best description of microscopic physics nowadays. Symmetry is strongly connected to conservation laws and can hence, in retrospective, also be understood as important building block of earlier theories like NEWTON’s classical mechanics or MAXWELL’s electrodynamics.

Symmetry basically means that a transformation of the mathematical formulation of a theory does not change the physically relevant quantities. The most intuitive example might be translational invariance stating that the laws of physics should not depend on the location they are formulated at. But there are many more symmetries in nature that all can be divided into global and local symmetries. The former include symmetries, the transformations of which are the same at every point in spacetime. The paradigmatic example is the ISING model [1] with spins with value  $\pm 1$  at every point of a lattice. A global transformation (under which it is invariant) would be the flip  $\pm 1 \rightarrow \mp 1$  at *every* point on the lattice. A local transformation, in contrast, is allowed to vary between different points in spacetime; that would mean a flip of *only some* of the spins. Though the latter is, of course, no symmetry of the ISING model, local symmetries are a common phenomenon in physical theories. Nevertheless, the focus of this thesis lies on global symmetries.

At this point, it should be clear that formulating theories with a high degree of symmetry is desirable and potentially even necessary to describe nature. However, in a lot of cases we observe a smaller symmetry than the original theory allows. This is called *spontaneous symmetry breaking* (SSB) and occurs whenever the ground state of the underlying theory is not invariant under the full symmetry. Then, by symmetry there are other ground states with the same properties and no a priori principle to choose one exists. Thus, it seems that the choice of a ground state was spontaneous – justifying the naming. This concept allows to combine high symmetry assumptions with seemingly contradicting experimental data like in the case of the HIGGS mechanism [2–4] which, by SSB, gives rise to the experimentally observed masses of particles that should have no mass by symmetry restrictions.

Unfortunately, a lot of non-perturbative effects in state-of-the-art physics are hard to compute and thus there are a lot of open questions concerning the long established standard model. One way to tackle this issue is the use of toy models conjectured to have similar properties like parts of the original theory but evaluated more easily. Some *four fermion theories* (4FT) are candidates for such toy models. Fermions are the building blocks of matter which interact via gauge bosons in

the standard model. There, they obey a flavor symmetry (mixing different kinds of fermions) and a chiral symmetry. Both are also shared (to some extent) by 4FT where no bosons exist as fundamental degrees of freedom but the fermions interact directly via a point interaction. An exploration of the chiral symmetry in the conceptually simpler 4FT can then build up an understanding of what might happen in the hard to handle general theory.

But this was not the advent of 4FT. The first models of such kind were proposed by NAMBU and JONA-LASINIO [5, 6] as models for nuclei which were later found to be described by *quantum chromodynamics* (QCD) instead [7]. Later, it was additionally found that 4FT arise as effective models from tight binding Hamiltonians in solid state physics. In that setting, they can describe the electronic properties of graphene [8, 9] and similar materials – also in the second sense, that a particular 4FT, the THIRRING (TH) model, has strong parallels with *3-dimensional quantum electrodynamics* (QED<sub>3</sub>) [10]. Nowadays, another 4FT, GROSS-NEVEU (GN) [11], gains attention because it is asymptotically safe [12] – a scenario potentially similar to a theory of quantum gravity.

This thesis is intended to investigate SSB in 4FT. 4FT are a rather general class of theories where the details concerning symmetries and potential SSB depend on the concrete model and further parameters like the dimensionality and the number of *flavors*, i.e. copies of fermions in use. We will therefore specialize the setting to get concrete results: first to three dimensions – sticking close to the applications to graphene and QED<sub>3</sub> – and later even to one irreducible flavor. The latter is a setting poorly discussed in the literature because of technical difficulties. In particular, to the best of our knowledge we will show the first *Monte Carlo* (MC) lattice simulation results for this model including the critical coupling of the so-called chiral phase transition (which is actually a parity breaking phase transition) and the critical exponents of this transition. Furthermore, we will contribute insights to the discussion of the *lattice artifact phase* (LAP) – a phenomenon encountered in various 4FT when discussed on the lattice. Finally, we will present our first results and insights about the phase diagram in the temperature-coupling plane. However, this part is a glimpse into ongoing research and therefore not intended to be an exhaustive investigation.

This thesis is organized as follows: The next section, Sec. 2, is intended to give an overview over general concepts used in this thesis. This implies that the explanations in there are not specific to 4FT, to which a subsequent section (Sec. 3) is dedicated. Sec. 2 is divided into two subsections: one concerned with the more physical aspects (Sec. 2.1), i.e. *phase transitions* (Sec. 2.1.1) and *quantum field theories* (QFT) (Sec. 2.1.2), the other (Sec. 2.2) with the basic notions and means exploited in this work, namely MC methods (Sec. 2.2.1), *finite size scaling* (FSS) (Sec. 2.2.2) and the pitfalls commonly encountered in the work with fermions on

## 1 Introduction

the lattice (Sec. 2.2.3). Afterwards, Sec. 3 goes into detail about 4FT. Starting from the general description of fermions by spinors (Sec. 3.1), 4FT are introduced (Sec. 3.2), discussed (Sec. 3.3 and Sec. 3.4) and reformulated for further mathematical treatment (Sec. 3.5). To build up a physical intuition for the models under investigation, the first (Sec. 4) of the two results sections employs the well-known *large- $N_f$  approximation* scheme to explore the SSB and critical behavior (Sec. 4.2) as well as some thermodynamical aspects (Sec. 4.3). Finally, the announced lattice results of the three-dimensional GN model with one irreducible flavor are presented in Sec. 5. After working out a proper formulation of the theory in Sec. 5.1 as well as observables to inspect (Sec. 5.2), some rather technical aspects are discussed in Sec. 5.3 and Sec. 5.4. Finally, we show the results obtained for vanishing temperature (Sec. 5.5) and the phase diagram in the temperature-coupling plane (Sec. 5.6). This whole thesis works in natural units setting  $\hbar = k_B = c = 1$ .

## 2 General Preliminaries

This first section is dedicated to the general principles fundamental for this work. It is broadly divided in rather physical discussions in Sec. 2.1 and more numerical topics in Sec. 2.2. However, it should be mentioned here that this division is by no means strict, since we will see that the rather numerical properties have a lot of physical implications.

### 2.1 Physical Preliminaries

#### 2.1.1 Phase Transitions And Critical Behavior

Consider a physical system with one or more external parameters – collected in the symbol  $\lambda$  – in thermodynamical equilibrium. If we now vary  $\lambda$ , we would usually expect a mostly smooth behavior of macroscopic quantities describing the state of the system. The connected regions where this expectation is correct, we want to call a *phase* of the system.<sup>1</sup> Typical phases are the state of aggregation of water (the solid, liquid or gaseous phase) or the ferro- and paramagnetic phase of some solids.

Phases are separated by so-called *phase transitions* at which the smoothness of physical quantities does not apply. Phase transitions can be broadly divided into two categories: First order phase transitions are characterized by a latent heat. This usually involves discontinuous behavior of at least one extensive quantity and coexistence of phases right at the critical point. The typical processes with such a behavior are liquid-gas transitions. Since we will only shortly touch this topic in the following, we do not go into detail here but refer the reader to the pertinent literature, e.g. [13].

A second order phase transition is characterized by a divergent correlation length  $\xi$ . Contrary to the first-order case, the two phases are identical at the critical point allowing for a continuous behavior of extensive quantities and first derivatives while their second derivatives may jump. The paradigmatic example exhibiting such a transition is the Ising model [1]. Observables  $\mathcal{O}$  for such systems usually behave like [14]

$$\langle \mathcal{O} \rangle \sim \tau^{\kappa_{\mathcal{O}}} \quad (2.1)$$

with the *reduced parameter(s)*  $\tau = \frac{\lambda - \lambda_c}{\lambda_c}$  and critical exponent  $\kappa_{\mathcal{O}}$ .<sup>2</sup> The critical exponents are universal quantities in a sense that they are not affected by the concrete microscopic nature of the regarded system but only by general properties

---

<sup>1</sup>This is a working definition that includes all commonly implied application as given in [13].

<sup>2</sup>The symbol  $\langle \cdot \rangle$  denotes the expectation value rigorously defined in Eq. (2.2).

## 2 General Preliminaries

Tab. 2.1: Conventional notation of various critical exponents as found in [16]. In this table,  $m$  denotes a mass parameter of the theory and  $p$  the momentum argument of the two-point function. Historically  $\tau$  was used for the reduced temperature but in this work the symbol (and the corresponding exponents) will also be used for other reduced parameters such as coupling constants.

Observable $\mathcal{O}$	Exponent $\kappa_{\mathcal{O}}$	Relation
Specific Heat	$-\alpha$	$\sim \tau^{-\alpha}$
Order Parameter	$\beta$	$\sim \tau^{\beta}$
Susceptibility	$-\gamma$	$\sim \tau^{-\gamma}$
Correlation Length	$-\nu$	$\sim \tau^{-\nu}$
Order Parameter	$\frac{1}{\delta}$	$\sim m^{\frac{1}{\delta}}$
Two-Point Correlation Function	$\eta$	$\sim p^{-D+2-\eta}$

like symmetries and dimensionality of the theory.<sup>3</sup> Thus, theories can be clustered into large *universality classes* with the same universal behavior. Some conventional notations for the various critical exponents have been developed over the years. Tab. 2.1 gives an overview over the most common ones.

One important observation regarding this thesis is the following: As the correlation length diverges at the critical point, all other length scales become irrelevant. This particularly implies that a finite lattice spacing  $a$  – as it will be introduced during the discretization of the system (cf. Sec. 2.1.2) – does not change the physics. Hence, the continuum limit of a discretized theory is obtained by tuning external parameters to the critical point [7].

### 2.1.2 (Lattice) Quantum Field Theory

This work is concerned with QFT on the lattice. As in classical field theory, our quantum field theoretical studies start from an action  $S$  that – if we assume locality – can be written as spacetime integration of a corresponding Lagrangian density  $\mathcal{L}$ . In the so-called path integral formulation an observable  $\mathcal{O}$  can be seen as a functional on the space of configurations of this system and its expectation value

<sup>3</sup>For bosonic systems, it is known that adding the range of interactions to the above exhausts the list of properties dividing the universality classes. For fermionic systems, there is still an open discussion about this topic [15].



is then given by a weighted average over all possible configurations  $\phi$  via

$$\langle \mathcal{O} \rangle = \frac{1}{Z} \int \mathcal{D}\phi \mathcal{O}[\phi] e^{iS} \quad (2.2)$$

where the normalisation constant  $Z$  is fixed by demanding  $\langle 1 \rangle = 1$ . The measure  $\mathcal{D}\phi$  on the space of configurations can be hard to define in general. However, if we assume our spacetime to be a  $D = d + 1$  dimensional, finite lattice  $\Lambda$ , one can simply use a<sup>4</sup>  $|\Lambda|$  dimensional product of Lebesgue measures

$$\mathcal{D}\phi = \prod_{x \in \Lambda} d\phi_x. \quad (2.3)$$

From this starting point, one might try to find a well-defined continuum version of the theory by  $|\Lambda| \rightarrow \infty$  and lattice spacing  $a \rightarrow 0$  but this is usually not possible in MINKOWSKI spacetime [17].

The way to go for actually computing Eq. (2.2) is usually an analytic continuation to imaginary time arguments  $t \rightarrow i\tau$ , called *WICK rotation*. Then the action is converted to an EUCLIDEAN action and the imaginary unit in the exponent changes to a minus sign. Beside its mathematical advantages, this has a direct physical interpretation: If one imposes (anti-)periodic boundary conditions in  $\tau$ -direction for (fermions) bosons and sets the length in time direction to be  $L_t = \beta$ , the path integral becomes

$$Z = \int \mathcal{D}\phi e^{-S_E} = \text{tr} e^{-\beta H} \quad (2.4)$$

the canonical *partition function* of our system at inverse temperature  $\beta = \frac{1}{T}$  with its Hamiltonian  $H$ . The effective EUCLIDEAN action  $S_E$  is then given by the Hamiltonian. Later, we will work in the EUCLIDEAN (or WICK rotated) formulation but omit the subscript  $E$  for notional convenience.

## 2.2 Numerical Preliminaries

From the various approaches developed to solve QFT since its early days, the method of choice in this work is *Monte Carlo* (MC) simulations on the lattice. It has been very successfully applied to various theories involving prominent examples like the standard model (e.g. *quantum chromodynamics* (QCD) [7]), condensed matter systems (including *four fermion theories* (4FT) [8]) and various beyond-the-standard-model theories (e.g. [18]).

The basic idea of lattice QFT arises naturally from the approach of Sec. 2.1.2. There, for the sake of well-definedness we defined the measure on the space of

---

<sup>4</sup>We use  $|\cdot|$  on a finite set to denote the number of its elements.

## 2 General Preliminaries

configurations for a finite spacetime lattice (cf. Eq. (2.3)). Physical quantities like observables (Eq. (2.2)) or the partition function (Eq. (2.4)) now are finite dimensional integrals to be solved and lattice simulations are meant to provide efficient ways for finding numerical approximations of those integrals.

It should be pointed out that this method is – apart from technical issues – applicable to any theory and parameter regime without approximations (besides numerical uncertainties). This is the great advantage over other approaches like perturbation theory [19] or functional renormalization group [20]. However, there are two drawbacks, since one is usually interested in the continuum and infinite-volume limit of a theory. First, the results must be extrapolated carefully from the data obtained on the lattice. This can be done via FSS explained in Sec. 2.2.2. Second, the theory has to be formulated consistently on the lattice. This particularly includes that important properties like symmetries remain intact or at least get restored during the extrapolation. An example of such restrictions is met in Sec. 2.2.3.

### 2.2.1 Monte Carlo Methods And Importance Sampling

Our aim in this subsection is to find a method for efficiently computing expectation values of observables  $\mathcal{O}$  or, more abstractly speaking, high-dimensional integrals of the form

$$I = \int_G dx f(x) \quad (2.5)$$

for some integrable function  $f : G \rightarrow \mathbb{C}$ . Numerically  $I$  will be approximated via a finite number  $N \in \mathbb{N}$  of sampling points  $x_i \in G$ ,  $i \in \{1, \dots, N\}$  for example by the average  $\bar{I}$

$$I \approx \bar{I} = \frac{1}{N} \sum_{i=1}^N f(x_i) \quad (2.6)$$

or some more complicated scheme<sup>5</sup>. For slowly varying integrands  $f$ , a uniformly distributed random choice of sample points in  $G$  yields a convergence rate  $\sim \frac{1}{\sqrt{N}}$  [17]. By this convergence rate, it usually outperforms systematic sampling methods as soon as the dimensionality of the integral gets high. This is called the *Monte Carlo* (MC) method.

If  $f$  does not fit the assumption “slowly varying”, this can be taken care of by changing the distribution to sample from. More concretely, if one uses sampling points distributed according to  $p(x)dx$  for a probability density  $p : G \rightarrow [0, \infty)$

---

<sup>5</sup>Examples can e.g. be found in [17].

such that  $\int p(x)dx = 1$  and  $\frac{f(x)}{p(x)}$  is slowly varying,  $I$  is again well-approximated by

$$\bar{I} = \frac{1}{N} \sum_{i=1}^N \frac{f(x_i)}{p(x_i)}. \quad (2.7)$$

This idea of choosing the sample points according to their importance for the approximation Eq. (2.6) is called *importance sampling*.

The final problem is the generation of points according to  $p$ . In this work we will use a *Metropolis algorithm* that works as follows: Given some sampling point  $x$  we propose a random change to  $x'$  and draw a uniformly distributed random number  $r \in [0, 1]$ . If  $\frac{p(x')}{p(x)} > r$ , we append  $x'$  to the sample and use it as starting point for the next iteration; else, we start again from  $x$ . The generated configurations form a *Markov chain* meaning that the choice and acceptance of every configuration depends only on the last preceding configuration. It fulfills the so-called *detailed balance* condition such that it can be shown to converge to the desired distribution  $p$  (see [17] for details). However, the intermediate distributions, particularly at the beginning of the chain may differ significantly from  $p$  because we did not specify any condition on the (overall) starting point  $x$ . Thus, a *thermalization phase* at the beginning of which the configurations do not contribute to Eq. (2.7) is required in general [14].

Last, we translate this abstract description to our lattice QFT setting: The integral  $I = \langle \mathcal{O} \rangle$  with integrand<sup>6</sup>  $f(\phi) = \mathcal{O}[\phi] \frac{e^{-S[\phi]}}{Z}$  is defined on the space of configurations. If  $S[\phi]$  is real for all  $\phi$ ,<sup>7</sup> this can be split into a probability density  $p[\phi] = \frac{e^{-S[\phi]}}{Z}$  and a usually slowly varying observable such that we find the average  $\bar{\mathcal{O}}$  to be an estimate for

$$\langle \mathcal{O} \rangle \approx \bar{\mathcal{O}} = \frac{1}{N} \sum_{i=1}^N \mathcal{O}[\phi_i]. \quad (2.8)$$

### 2.2.2 Finite Size Scaling

As already mentioned, one key problem of lattice simulations usually is the extrapolation to the thermodynamic limit, i.e. to infinite volume. The theory concerned with this subject is called *finite size scaling* (FSS) [14, 21]. Its fundamental assumption is that the correlation length  $\xi$  is the only relevant length scale of the theory<sup>8</sup> and from this it derives asymptotic scaling laws relating the expectation

<sup>6</sup>The a priori unknown normalization  $Z$  is not important for the Metropolis algorithm described above and can be set to one for the algorithm. If desired, it can then be measured for  $\mathcal{O} = 1$ .

<sup>7</sup>If this condition is not met, the formulation has a *sign problem* (SP) which is discussed in Sec. 2.2.3.

<sup>8</sup>Interestingly, in the context of 4FT in large- $N_f$  limit (see Sec. 4) this is found not to be true. Instead, a non-vanishing chemical potential provides a second length scale and introduces

## 2 General Preliminaries

values  $\langle \cdot \rangle_L$  on a finite lattice with its linear size  $L$ . For simplicity, we assume the lattice  $\Lambda$  to be (hyper-)cubic and lattice spacing  $a$  to be one, i.e.  $V = |\Lambda| = L^D$ .

Near a second order critical point  $\lambda_c$ , any observable  $\mathcal{O}$  exhibits a critical behavior governed by a critical exponent  $\kappa_{\mathcal{O}}$  according to Eq. (2.1). In particular, for the correlation length where we denote  $\nu = -\kappa_{\xi}$  we find

$$\xi \sim \tau^{-\nu} \Rightarrow \tau \sim \xi^{-\frac{1}{\nu}} \quad (2.9)$$

for  $\tau = \frac{\lambda - \lambda_c}{\lambda_c}$ . On the lattice of linear size  $L$ , the lattice correlation length  $\xi_L$  is restricted to  $\xi_L \leq L$  and thus a reasonable assumption is  $\xi_L = \min\{\xi, L\}$ . If  $L \gg \xi$ , we expect to describe the infinite-volume physics well such that

$$\lim_{L/\xi \rightarrow \infty} \langle \mathcal{O} \rangle_L = \langle \mathcal{O} \rangle. \quad (2.10)$$

If  $\xi \gg L$ ,  $L$  replaces  $\xi$  as the physically relevant scale. This introduces lattice artifacts. Combining Eq. (2.1) with Eq. (2.9), we conclude that

$$\langle \mathcal{O} \rangle_L \sim \tau_L^{\kappa_{\mathcal{O}}} [1 + \dots] \sim \xi_L^{-\frac{\kappa_{\mathcal{O}}}{\nu}} [1 + \dots] \sim L^{-\frac{\kappa_{\mathcal{O}}}{\nu}} [1 + \dots] \quad (2.11)$$

where the dots include higher order behavior in  $\tau$ . Thus, there exists a function  $f_{\mathcal{O}}$  obeying

$$f_{\mathcal{O}}(s) \rightarrow \begin{cases} 1, & s \rightarrow 0 \\ L^{\frac{\kappa_{\mathcal{O}}}{\nu}} \langle \mathcal{O} \rangle, & s \rightarrow \infty \end{cases} \quad (2.12)$$

and interpolating between these limiting behaviors such that

$$\langle \mathcal{O} \rangle_L = L^{-\frac{\kappa_{\mathcal{O}}}{\nu}} f_{\mathcal{O}}(s) [1 + \dots] \quad (2.13)$$

for the scaling variable  $s = \frac{L^{\frac{1}{\nu}}}{\xi(\tau)^{\frac{1}{\nu}}}$ .

From these considerations, one is now able to extrapolate observables of interest to the infinite-volume limit, e.g. an order parameter or the susceptibility of the system. An equally interesting observation is that (to leading order) functions  $U$  of observables the exponents of which cancel exhibit an  $L$ -independent value at criticality, i.e.  $s = 0$ . By this property,  $U$  allows the determination of the critical point independent of the critical exponents. Furthermore, its derivative at the critical point

$$\ln \left. \frac{dU}{d\lambda} \right|_{\lambda=\lambda_c} = \frac{1}{\nu} \ln L + \dots \quad (2.14)$$

---

additional finite size effects strongly dependent on the ratio between the linear system size  $L$  and the length scale from the chemical potential [22].

yields direct access to the correlation length critical exponent  $\nu$  [16].<sup>9</sup> This was first observed by BINDER [23] who recommended to use the cumulants of the distribution as such functions. This will be made concrete in Sec. 5.2.

After all, the above discussion is a good approximation only sufficiently close to criticality where the higher orders – hidden in the dots – are negligible. Otherwise, one can continue the expansion to

$$\langle \mathcal{O} \rangle_L = L^{-\frac{\kappa_{\mathcal{O}}}{\nu}} f_{\mathcal{O}}(s) [1 + L^{-w_{\mathcal{O}}} f_{\mathcal{O}}^{(C)}(s) + \dots] \quad (2.15)$$

and further by introducing one (or more) correction function  $f_{\mathcal{O}}^{(C)}$  and correction exponent  $w_{\mathcal{O}} > 0$  and repeat the discussion as above.

### 2.2.3 Fermions On The Lattice

To end this section, we will add two additional remarks that mainly apply to the simulation of fermions. These will be the existence of so-called doublers and the infamous *sign problem* (SP).

Already WILSON [25] in 1977 knew that simulating fermions on a lattice does not show the expected particle content. With a naive discretization of the derivative in one spacetime dimension, there are exactly twice as much fermions on the lattice as in the original theory [26]. These additional particles are called doublers. The reason for this was found by NIELSEN and NINOMIYA [24, 27]. The famous NIELSEN-NINOMIYA *theorem* (NNT) states as formulated in [17]:

**Theorem 2.1.** *There exists no translational invariant formulation of fermions on a lattice that is*

1. *local, i.e. has a smooth fourier transform (FT),*
2. *chiral, i.e. preserves the full chiral symmetry in the free theory,*
3. *free of doublers and*
4. *has the correct continuum limit for lattice spacing  $a \rightarrow 0$ .*

<sup>9</sup>In formula Eq. (2.14)  $L$  should be seen as dimensionless quantity. More formally, one would use a reference length  $L_0$  and formulate this with the variable  $b$  such that  $L = bL_0$ .

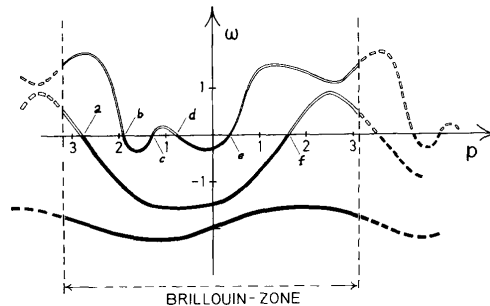


Fig. 2.1: Arbitrary one-dimensional dispersion relations as they could arise on a lattice with periodic boundary conditions from [24].

## 2 General Preliminaries

We will not give the rigorous proof here (see the original papers for that [24, 27]) but sketch an intuitive argument: Consider any smooth dispersion relation on a one-dimensional, periodic lattice (with continuous time, e.g. Fig. 2.1). Then, its zeros correspond to particles of the theory. But due to smoothness and periodicity there is always an even number of zeros, i.e. an even number of particles. For example, the naive derivative yields a sinusoidal dispersion relation with two nodes.

Although all the “mild assumptions” – as it is called in the original work [27] – are desirable properties of a theory, the obvious workaround is dropping at least one of them. For  $N_f = 1$ , which we will investigate in Sec. 5, dropping the freedom of doublers is not an option and for the observation of chiral symmetry (breaking) one is tempted not to drop the chirality, too. Thus, dropping the locality is the way to go in this work. This is e.g. done by the so-called SLAC-derivative. It was introduced in [28, 29] and implements the exact DIRAC cone dispersion relation  $-i\partial^\mu = p^\mu$  which corresponds to

$$\partial_\mu^{\text{SLAC}}(x, y) = \begin{cases} 0 & \text{for } x^\mu = y^\mu \\ \frac{\pi}{L^\mu} \frac{(-1)^{x^\mu - y^\mu}}{\sin\left(\frac{\pi}{L^\mu}(x^\mu - y^\mu)\right)} & \text{else} \end{cases} \quad (2.16)$$

in real space where  $L^\mu$  is the number of lattice points in direction  $\mu$ .<sup>10</sup>

The term *sign problem* (SP) is used for the following problem arising in MC simulations: If the action is not real, the term  $\frac{1}{Z}e^{-S}$  cannot be interpreted as a probability density which was crucial for the MC importance sampling to work properly. At first glance, there is a simple workaround called reweighting; any observable  $\mathcal{O}$  obeys

$$\langle \mathcal{O} \rangle = \frac{1}{Z} \int \mathcal{D}\phi \mathcal{O}[\phi] e^{-S[\phi]} = \frac{\int \mathcal{D}\phi \mathcal{O}[\phi] e^{-i\Im S[\phi]} e^{-\Re S[\phi]}}{\int \mathcal{D}\phi e^{-i\Im S[\phi]} e^{-\Re S[\phi]}} = \frac{\langle \mathcal{O} e^{-i\Im S[\phi]} \rangle_{\Re S}}{\langle e^{-i\Im S[\phi]} \rangle_{\Re S}} \quad (2.17)$$

where  $\langle \cdot \rangle_{\Re S}$  denotes the expectation value with respect to probability density  $\frac{1}{Z_{\Re S}} e^{-\Re S}$  and thus can be calculated via expectation values from real actions. The remaining problem is a numerical one: Since  $\langle e^{-i\Im S[\phi]} \rangle_{\Re S}$  might be a pretty small number, the division on the right hand side of Eq. (2.17) must be carried out with a high precision and thus the expectation values – approximated by means over the configurations – must have high precision. This results in an exponential scaling of the uncertainty of a quantity derived by reweighting with the lattice volume [32, 33] and usually spoils all attempts to work with large lattice sizes making the extrapolation to the thermodynamic limit infeasible. The SP does not exclusively

<sup>10</sup>In other contexts, particularly gauge theories, dropping locality does not work [30] and the SLAC-derivative was abandoned from that part of the lattice community. Since there are only global symmetries in our case, we do not run into such problems [31].

occur within fermionic theories but is particularly often encountered there. It then arises from the term  $\ln \det D$  after integrating over the fermions (cf. Eq. (3.30), [17]).

### 3 Four Fermion Theories

After the general setup is defined and the physical notions as well as the means to compute physical quantities are explained, we will use this section to introduce spinors, describing the fermionic degrees of freedom in a system, and a particular class of theories involving them, the so-called *four fermion theories* (4FT). It will also include a further discussion of their properties and the usual reformulation via a HUBBARD-STRATONOVICH (HS) transformation that will bring them into a form more suitable for analytical as well as numerical calculations.

#### 3.1 Spinors And Representations

The most fundamental principle in defining our theories is the spacetime symmetry, particularly the LORENTZ symmetry. Every physical object should have a well-defined transformation behavior under such transformations and must therefore transform via a representation of the corresponding symmetry group which is, to include particles with half-integer spin, the universal (double) cover of the LORENTZ group, the so-called spin group. That is why the fermionic degrees of freedom we want to describe here are held in *spinors*, i.e. objects transforming under representations of the spin group that are no representations of the LORENTZ group [34]. In  $D$  dimensions, the irreducible representations<sup>11</sup> are  $2^{\lfloor \frac{D}{2} \rfloor}$  dimensional and hence spinors can be seen as column vectors with  $2^{\lfloor \frac{D}{2} \rfloor}$  GRASSMANN-valued<sup>12</sup> entries, called DIRAC *spinors*, where  $\lfloor q \rfloor$  denotes the largest integer smaller than  $q$ . To form quantities invariant under LORENTZ transformation, we introduce the (EUCLIDEAN) DIRAC *conjugate*<sup>13</sup>  $\bar{\psi} = \psi^\dagger$  such that (the spinor part of) terms involving  $\bar{\psi}\psi$  does not change during a transformation.

Beside the irreducible representation, one can also form *reducible* representations acting on higher dimensional objects. This might cause some confusion since the same physical properties can be encoded in very different mathematical statements depending on the representation in use, as will be seen in Sec. 3.3 and Sec. 3.4. For example in  $D = 3$ , the above paragraph states that the irreducible spinors are two-component objects. Nevertheless, most of the literature on the topic is concerned with four-component DIRAC spinors, and thus a reducible representation. This is the natural setup in the application to graphene [8, 9] as well as in QED<sub>3</sub> [10]. The

<sup>11</sup>A subtlety occurs in odd dimensions: While the irreducible representation is unique (modulo unitary transformations) in even dimensions, there are two inequivalent irreducible representations in odd dimensions [35].

<sup>12</sup>More mathematically, they are elements of the exterior algebra, but from a physical point of view this just ensures the anti-commutation property desired for fermions.

<sup>13</sup>The reader may be more familiar with the MINKOWSKI version  $\bar{\psi} = \psi^\dagger \gamma_0$  but this does not lead to invariant quantities in EUCLIDEAN spacetime [17].



three-dimensionality can then be obtained from neglecting the dependence on one coordinate or equivalently using only three out of the four available  $\gamma$ -matrices<sup>14</sup>. When dealing with an even number  $N_f$  of copies of two-component spinors, so-called *flavors*, one can combine always two of them into a four-component spinor while at the same time directly summing the corresponding  $2 \times 2$   $\gamma$ -matrices into  $4 \times 4$  matrices. More precisely, one has to combine one flavor from one irreducible representation and one from the other, which particularly implies that naively plugging in two-component spinors for reducible four-component spinors and vice versa will not yield the same theory in general. Nevertheless, carefully evaluated there is a relation between the irreducible representation for even flavor numbers  $N_f$  and the reducible formulations. There is no such equivalence between odd flavor irreducible models and reducible models.

### 3.2 General Four Fermion Theories

The theoretical models of interest in this work are *four fermion theories* (4FT) given by Lagrangians of the form

$$\mathcal{L} = \mathcal{L}_K + \mathcal{L}_I = \sum_{a=1}^{N_f} \bar{\psi}_a (i\cancel{\partial} - im) \psi_a - \frac{g^2}{2N_f} \sum_{a,b=1}^{N_f} (\bar{\psi}_a M_1 \psi_a) (\bar{\psi}_b M_2 \psi_b). \quad (3.1)$$

The fundamental degrees of freedom are held by DIRAC spinors  $\psi, \bar{\psi}$  in the irreducible representation describing the fermions that come in  $N_f$  different copies, the *flavors*. The mass  $m$  as well as the four-fermion coupling  $g$  are scalar parameters of the theory and  $M_1, M_2$  matrices acting in spinor space. The slash notation means contraction with the  $\gamma$ -matrices, i.e.  $\cancel{\partial} = \gamma^\mu \partial_\mu$ , which are elements of the CLIFFORD algebra defined via

$$\{\gamma_\mu, \gamma_\nu\} = 2\eta_{\mu\nu} \quad (3.2)$$

where  $\eta$  is the spacetime metric<sup>15</sup> and  $\{\cdot, \cdot\}$  denotes the anti-commutator. We will usually imply a summation over corresponding flavor indices and sometimes even omit flavor indices by the identifications  $\psi = (\psi_1, \dots, \psi_{N_f})^\top$  and  $\bar{\psi} = (\bar{\psi}_1^\top, \dots, \bar{\psi}_{N_f}^\top)$ .

The first term  $\mathcal{L}_K$  of Eq. (3.1) is the usual kinetic term of fermionic theories. The second term  $\mathcal{L}_I$  is the eponymous interaction term coupling four (anti-)fermionic fields to each other. The various choices possible for  $M_1$  and  $M_2$  correspond to different 4FT. Frequently discussed examples are<sup>16</sup>

<sup>14</sup>See Eq. (3.2) and context for a definition.

<sup>15</sup>Since we are working in the EUCLIDEAN formulation, we have  $\eta_{\mu\nu} = \delta_{\mu\nu}$ .

<sup>16</sup>A detailed investigation of the 4FT space in dimension  $2 < D < 4$  is e.g. done in [15].

### 3 Four Fermion Theories

#### 1. GROSS-NEVEU (GN) [11]

$$\mathcal{L}_I = -\frac{g^2}{2N_f} \sum_{a=1}^{N_f} (\bar{\psi}_a \psi_a)^2 =: -\frac{g^2}{2N_f} (\bar{\psi}\psi)^2, \quad (3.3a)$$

$$\text{i.e. } M_1 = \mathbf{1} = M_2, \quad (3.3b)$$

#### 2. THIRRING (TH) [36]

$$\mathcal{L}_I = -\frac{g^2}{2N_f} \sum_{a,b=1}^{N_f} (\bar{\psi}_a \gamma^\mu \psi_a) (\bar{\psi}_b \gamma_\mu \psi_b) =: -\frac{g^2}{2N_f} (\bar{\psi} \gamma^\mu \psi)^2, \quad (3.4a)$$

$$\text{i.e. } M_1 = \gamma_\mu, \quad M_2 = \gamma^\mu \quad (\text{sum convention}), \quad (3.4b)$$

#### 3. NAMBU-JONA-LASINIO (NJL) [5, 6]

$$\mathcal{L}_I = -\frac{g^2}{2N_f} \sum_{a=1}^{N_f} [(\bar{\psi}_a \psi_a)^2 - (\bar{\psi}_a \gamma^5 \psi_a)^2] =: -\frac{g^2}{2N_f} [(\bar{\psi}\psi)^2 - (\bar{\psi}\gamma^5\psi)^2], \quad (3.5a)$$

$$\text{i.e. } M_1^{(1)} = \mathbf{1} = M_2^{(1)}, \quad M_1^{(2)} = \gamma^5 = M_2^{(2)} \quad (3.5b)$$

which can only be defined (reasonably) if there exists a non-trivial

$$\gamma^5 = i^{\frac{D}{2}} \prod_{\mu=0}^d \gamma_\mu \quad (3.6)$$

matrix in  $D$  dimensions which is only true for even numbers of dimensions.

For fixed spacetime dimension  $D$  there is only a fixed number of linearly independent theories since  $M_1$  and  $M_2$  can always be expanded into a basis of the corresponding matrix space yielding a linear combination of basis theories. Additionally, though the setting of Eq. (3.1) might seem to prohibit interactions between the various flavors, i.e. terms like

$$\bar{\psi}_a M \psi_b, \quad (3.7)$$

those can be rewritten as linear combinations of the allowed flavor-singlet terms by the use of FIERZ *identities* as e.g. done in [15]. The only restrictive assumption (besides LORENTZ invariance) in Eq. (3.1) is therefore the explicit flavor symmetry introduced by the fact that every flavor is treated equally.

In this thesis, we will only work in the irreducible representation with  $D = 3$ . However, the reducible representation admits a slightly larger class of 4FT to be defined: While they would formally be exactly of the form of Eq. (3.1) (but  $\bar{\psi}, \psi$  would be four-component spinors), half the irreducible flavors could then have a minus sign in front of the interaction term. Irreducibly, this would be achieved by allowing a slightly non-trivial flavor structure  $(M_1)_{ab} = (-1)^a M_1 \delta_{ab}$ .

### 3.3 Symmetries Of Four Fermion Theories

4FT exhibit a rich pool of global symmetries. The maximally symmetric fermionic theory is the free massless theory given by  $\mathcal{L}_K$  for  $m = 0$ . Its symmetries are:<sup>17</sup>

#### External Symmetries.

1. POINCARÉ symmetry: A general LORENTZ transformation is given by

$$x^\mu \rightarrow x'^\nu = \Lambda^\nu{}_\mu x^\mu \quad (3.8)$$

for any  $\Lambda \in SO(D)$ .<sup>18</sup> Though we are using a EUCLIDEAN spacetime, we will stick to this term to describe the corresponding spacetime symmetry. If not stated else, a EUCLIDEAN metric is always implied. It acts on spinors via

$$\psi_a(x) \rightarrow e^{-\frac{i}{4}\omega_{\mu\nu}[\gamma^\mu, \gamma^\nu]} \psi_a(x'), \quad \bar{\psi}_a(x) \rightarrow \bar{\psi}_a(x') e^{\frac{i}{4}\omega_{\mu\nu}[\gamma^\mu, \gamma^\nu]} \quad (3.9)$$

where  $\omega$  denotes an anti-symmetric tensor of transformation parameters. To get the full spacetime symmetry, the POINCARÉ *symmetry*, LORENTZ invariance is augmented by translational symmetry  $x \rightarrow x' = x + c$  for some constant vector  $c$  which is

$$\psi_a(x) \rightarrow e^{ic^\mu p_\mu} \psi_a(x'), \quad \bar{\psi}_a(x) \rightarrow \bar{\psi}_a(x') e^{-ic^\mu p_\mu} \quad (3.10)$$

in spinor space with the momentum operator  $p^\mu$ . On the lattice, the POINCARÉ symmetry is broken to a discrete subgroup depending on the lattice in use.

2. Parity: The usual parity transformation is given by a sign flip in all spatial coordinates. But in odd dimensions, the described transformation has determinant one corresponding to just a rotation. Thus a more general way to define the parity transformation is

$$x = (x_0, x_1, \dots, x_{d-1}, x_d) \rightarrow x' = (x_0, x_1, \dots, x_{d-1}, -x_d) \quad (3.11)$$

which can be combined with spatial rotations to get the conventional form in even dimensions. It acts on the spinors via

$$\psi_a(x) \rightarrow \gamma^0 \cdots \gamma^{d-1} \psi_a(x'), \quad \bar{\psi}_a(x) \rightarrow (-1)^D \bar{\psi}_a(x') \gamma^{d-1} \cdots \gamma^0. \quad (3.12)$$

<sup>17</sup>The following discussion follows [15, 16].

<sup>18</sup>The MINKOWSKI version is  $\Lambda \in SO(1, d)$  for  $d = D - 1$ .

### 3 Four Fermion Theories

3. Time Reversal: The time reversal transformation is given by inversion ( $\mathbb{Z}_2$ ) of the time coordinate, i.e.

$$x = (x_0, x_1, \dots, x_d) \rightarrow x' = (-x_0, x_1, \dots, x_d). \quad (3.13)$$

This acts on the spinors via

$$\psi_a(x) \rightarrow \gamma^d \cdots \gamma^1 \psi_a(x'), \quad \bar{\psi}_a(x) \rightarrow (-1)^D \bar{\psi}_a(x') \gamma^1 \cdots \gamma^d. \quad (3.14)$$

4. Charge Conjugation: Charge conjugation transforms the spinors via

$$\psi_a \rightarrow \psi_a^c = \mathcal{C} \psi_a^*, \quad \psi_a \rightarrow \bar{\psi}_a^c = \psi_a^\top \mathcal{C}^\dagger \quad (3.15)$$

which is again a  $\mathbb{Z}_2$  transformation.

### Internal Symmetries.

1. Flavor Symmetry: As already mentioned, every flavor is treated equally in the Lagrangian Eq. (3.1). Thus, a unitary transformation  $U \in U(N_f)$  acting in flavor space does not change the Lagrangian

$$\psi_a \rightarrow U_{ab} \psi_b, \quad \bar{\psi}_a \rightarrow \bar{\psi}_b (U^\dagger)_{ba}. \quad (3.16)$$

2. Chiral Symmetry: If there exists a non-trivial  $\gamma^5$ -matrix (as defined in Eq. (3.6)) in  $D$  dimensions, the kinetic term in the massless case is invariant under **continuous chiral symmetry** transformations ( $U(N_f)$ )

$$\psi_a \rightarrow (e^{i\alpha\gamma^5})_{ab} \psi_b, \quad \bar{\psi}_a \rightarrow \bar{\psi}_b (e^{i\alpha\gamma^5})_{ba} \quad (3.17)$$

with an hermitian parameter matrix  $\alpha_{ab}$  in flavor space due to the anti-commutation of  $\gamma^5$  with  $\gamma^\mu$ . A special case of this is the **discrete chiral symmetry** ( $\mathbb{Z}_2$ )

$$\psi_a \rightarrow \gamma^5 \psi_a, \quad \bar{\psi}_a \rightarrow -\bar{\psi}_a \gamma^5, \quad (3.18)$$

which can be intact even if the continuous version is broken.

We see that in odd dimensions  $D$  there is no way of defining chirality and the internal symmetry group is the  $U(N_f)$  flavor symmetry. In even dimensions, the maximal internal symmetry is a  $U(N_f) \times U(N_f)$  of flavor and chiral symmetry. The external symmetry group is the same for both.

### 3.3 Symmetries Of Four Fermion Theories

At first glance, there seems to be a discrepancy between the reducible and the irreducible formulation of GN that arise naturally<sup>19</sup> in odd dimensions (cf. Sec. 3.1): The internal symmetry group of the latter is  $U(N_f)$  with  $N_f^2$  degrees of freedom while the former admits seemingly only for  $U(N_f^{\text{red}}) \times U(N_f^{\text{red}})$  transformations with  $2(N_f^{\text{red}})^2 = \frac{1}{2}N_f^2$  degrees of freedom. The missing  $2(N_f^{\text{red}})^2$  degrees of freedom are hidden in the discarded one of the  $\gamma$ -matrices, say  $\gamma_3$ . Since  $\gamma_3$  anti-commutes with all  $\gamma$ -matrices there is an additional symmetry of the kind of Eq. (3.17) with  $\gamma_3$  instead of  $\gamma_5$ . Furthermore, there is a non-trivial matrix commuting with each of the  $\gamma$ -matrices in use, i.e.  $\gamma_{35} = i\gamma_3\gamma_5$ , yielding a  $U(N_f^{\text{red}})$  symmetry similar to Eq. (3.16) with  $U^{ab} = (e^{i\alpha\gamma_{35}})_{ab}$ . Thus, the degrees of freedom are exactly the same and the actual symmetry group of the reducible model is  $U(2N_f^{\text{red}})$ . In a proper basis the reducible formulation decouples the two (irreducible) flavors combined in one four-component spinor [16]. In this basis the additional symmetries resolve to just the  $U(N_f)$  symmetry of irreducible flavors.

Finally, one should be aware that if there are continuous symmetries there is a conserved current. In the classical case, this is the famous theorem by NOETHER [37, 38]. In quantum physics, this is true for the expectation values as can be seen by the use of TAKAHASHI-WARD *identities* [19, 39, 40]

**Theorem 3.1.** *Given a continuous symmetry transformation of the action, such that  $\phi \rightarrow \phi + \delta\phi$  infinitesimally, that changes the Lagrangian by  $\delta\mathcal{L} = \partial_\mu K^\mu$  there exists a conserved four-current*

$$J^\mu = \frac{\partial\mathcal{L}}{\partial(\partial_\mu\phi)}\delta\phi - K^\mu \quad \text{such that} \quad \langle\partial_\mu J^\mu\rangle = 0. \quad (3.19)$$

The corresponding Noether charge

$$\langle Q\rangle = \int d^d x \langle J^0\rangle \quad (3.20)$$

is constant in time if  $\langle J^\mu\rangle$  vanishes sufficiently fast at the spatial boundaries.

For internal symmetries, one always finds  $K^\mu = 0$ . Thus the flavor symmetry's conserved current is

$$J^\mu = \bar{\psi}_a \gamma^\mu (\alpha_{ab} + \alpha_{ab}^\dagger) \psi_b \quad (3.21)$$

and the chiral symmetry's conserved current is

$$J^\mu = \bar{\psi}_a \gamma^\mu \gamma^5 (\alpha_{ab} - \alpha_{ab}^\dagger) \psi_b \quad (3.22)$$

---

<sup>19</sup>In principle, one could use arbitrarily high dimensional reducible representations but we restrict this discussion to the case described in Sec. 3.1.

### 3 Four Fermion Theories

if  $\alpha_{ab}$  is the matrix parametrizing the transformation (cf. Eq. (3.17)).

After specializing to  $D = 3$  there will be no chiral symmetry. But the flavor symmetry, more specific its  $U(1)$  part of simultaneous phase transformations, corresponds to fermion number conservation and the conserved Noether charge is the fermion number

$$N = \int d^d x \bar{\psi} \gamma^0 \psi. \quad (3.23)$$

If one wants to study a nonzero net number of fermions in the theory, one has to use the grand canonical partition function

$$Z = \text{tr} e^{-\beta(H - \mu N)}$$

where we coupled the particle number to a chemical potential  $\mu$ . In the continuum, this corresponds to changing the kinetic part of the Lagrangian to

$$\mathcal{L}_K = i\bar{\psi} (\not{\partial} - m + \mu\gamma^0) \psi. \quad (3.24)$$

This does in general not apply to the lattice. Instead a careful evaluation of the discretized currents leads to the correct implementation there (see [7, 41, 42] for details).

### 3.4 Symmetry Breaking In Four Fermion Theories

Including additional terms in the Lagrangian might break some of the symmetries. For example a mass term breaks parity in odd dimensions and chiral symmetry in even dimensions. We will therefore not allow for an explicit mass term in the following. Nevertheless, there are occasions when a mass is generated dynamically (see below) and this dynamical symmetry breaking is one of the most interesting features of the theory.

Adding interaction terms like those defined in Sec. 3.2 potentially breaks symmetries, too. This is not the case for the TH and NJL interactions defined by Eq. (3.4) and Eq. (3.5), respectively, but GN (defined in Eq. (3.3)) breaks the continuous chiral symmetry down to the discrete one in even dimensions.

Again, one can see that the relation between irreducible and reducible formulation of a model is non-trivial: In case of the GN, it was already discussed that the irreducible formulation in  $D = 3$  admits for  $U(N_f)$  transformations corresponding to the four  $U(N_f^{\text{red}})$  (flavor, chiral,  $\gamma_3$  and  $\gamma_3\gamma_5$ ) symmetries which can be combined into  $U(2N_f^{\text{red}})$ . Since the reducible representation is defined in  $D = 4$  even, the chiral symmetry is broken. Thus, GN cannot be equivalent in the reducible and

irreducible representation. Instead GN in the irreducible representation is equivalent to an interaction<sup>20</sup>  $(\bar{\psi}\gamma_3\gamma_5\psi)^2$  in the reducible representation which admits the full  $U(2N_f^{\text{red}})$  symmetry.

Beside the explicit breaking of symmetries by inclusion of terms that do so, there exists another possibility of breaking a symmetry called *spontaneous symmetry breaking* (SSB). When spontaneously broken, the symmetry is preserved on the level of the action but a non-vanishing vacuum expectation value breaks the symmetry if one considers only small excitations above the vacuum [19]. If such a non-vanishing vacuum expectation value is present in the theory, it might depend on external parameters like coupling constant, temperature or chemical potential and in that case the theory can show a transition from the symmetry preserving to a spontaneously broken phase. In our fermionic theories, a typical breaking mechanism is the formation of a non-vanishing condensate like

$$\Sigma = \langle \bar{\psi}\psi \rangle \quad \text{or} \quad \Pi = \langle \bar{\psi}\gamma_5\psi \rangle \quad (3.25)$$

acting like a scalar, resp. pseudo-scalar, mass term and therefore breaking the symmetries as described above.

### 3.5 Bosonization Of Four Fermion Theories

While the fermion bilinears can be handled analytically, the quartic interaction terms cannot be evaluated directly. The usual workaround is application of the so-called HUBBARD-STRATONOVICH (HS) transformation. We demonstrate this for the simplest model, the GN as defined compactly in Eq. (4.1). By introduction of a bosonic auxiliary field  $\sigma$  one can rewrite the quartic exponential as

$$\exp\left(-\frac{g^2}{2N_f}(\bar{\psi}\psi)^2\right) = \int \mathcal{D}\sigma \exp\left(-N_f\lambda\sigma^2 - i\sigma\bar{\psi}\psi\right) \quad (3.26)$$

where a factor  $\left(\sqrt{\frac{\pi}{\lambda}}\right)^V$  with spacetime volume  $V$  has been included into the measure and we introduced

$$\lambda = \frac{1}{2g^2}. \quad (3.27)$$

By use of Eq. (3.26), the partition function Eq. (2.4) for Lagrangian Eq. (4.1) can be reformulated to

$$Z = \int \mathcal{D}\bar{\psi}\mathcal{D}\psi e^{-S[\bar{\psi},\psi]} = \int \mathcal{D}\sigma\mathcal{D}\bar{\psi}\mathcal{D}\psi e^{-\int d^Dx \left(\bar{\psi}(x)D(x)\psi(x) + \frac{N_f}{2g^2}\sigma(x)^2\right)} \quad (3.28)$$

<sup>20</sup>The  $\gamma_3\gamma_5$  matrix explicitly takes care of the fact that the irreducible spinors must belong to the different representations as described in Sec. 3.1.

### 3 Four Fermion Theories

with a fermion operator depending on the bosonic auxiliary field

$$D(x) =: \left( i\cancel{\partial}(x) - i(m - \sigma(x)) + i\mu\gamma^0 \right). \quad (3.29)$$

Now, the well-known formula for the fermionic GAUSSIAN integral (e.g. [17]) can be applied yielding

$$Z = \int \mathcal{D}\sigma \det(D) e^{-N_f \lambda \int d^D x \sigma(x)^2}. \quad (3.30)$$

Similar transformations by introduction of a vector field  $v^\mu$  for TH or a scalar  $\sigma$  and a pseudo-scalar  $\pi$  for NJL can be performed in the other models.



## 4 Large- $N_f$ Limit

After the general discussion of *four fermion theories* (4FT) in the previous section, we now specify the model under investigation: The GN interaction will serve as a prototypical model for the study of spontaneous symmetry breaking. Hence, putting together Eq. (3.1), Eq. (3.3) and Eq. (3.30) from now on we study

$$\mathcal{L} = \bar{\psi} \left( i\cancel{\partial} - im + i\mu\gamma^0 \right) \psi - \frac{g^2}{2N_f} \left( \bar{\psi}\psi \right)^2, \quad (4.1a)$$

$$\text{or } \mathcal{L} = \bar{\psi} \left( i\cancel{\partial} - im + i\mu\gamma^0 + i\sigma \right) \psi + N_f\lambda\sigma^2 \quad (4.1b)$$

with potentially vanishing chemical potential  $\mu$ .

In this section, we will follow a line of approximations leading to analytical results for GN. Those are mainly two-fold:

1. We will consider the limit of large flavor numbers  $N_f$ . This is called the 't Hooft *limit*<sup>21</sup> [43]. After the limiting procedure semi-classical approximations become exact. Concretely, we will use a saddle point approximation of the path integral to investigate the critical behavior and thermodynamic quantities analytically.
2. Our starting point will be the assumption that the auxiliary field  $\sigma$  is constant in the thermodynamic equilibrium. This seems reasonable from the physical point of view since in thermodynamical equilibrium there should be no distinguished length scale [13]. Nevertheless, this is not mathematically necessary: Particularly for GN and related models in two dimensions, the 't Hooft limit allows a complete analytical treatment of the theory [44] revealing an inhomogeneous crystalline phase for certain parameter settings [45, 46]. Our method will be incapable of finding such phases. However, it is yet unknown if such phases exist in any other dimension (since the solitonic theory used is restricted to the two-dimensional setting) or even for large (but not infinite) flavor numbers.

From the results of this section, we will be able to build up a physical intuition and expectation for the less easily treatable case of  $N_f = 1$  though a comparison has to be handled with care since the both assumptions above are very restrictive and particularly the first cannot be expected to be reasonable then. A similar calculation with another focus can be found in [47].

---

<sup>21</sup>The 't Hooft limit is usually defined as  $N_f \rightarrow \infty$  while  $\tilde{g}^2 N_f = \text{const.}$ , but since we already normalized the interaction term by the definition of the coupling as  $\frac{g^2}{2N_f} = \frac{\tilde{g}^2}{2}$ , this additional condition is not necessary here.

## 4.1 Calculation Of The Partition Function

We start from the GN partition function in HS formulation (Eq. (3.30))

$$Z = \int \mathcal{D}\sigma (\det D)^{N_f} e^{-N_f \lambda \int dx \sigma^2(x)} \quad (4.2)$$

where  $D$  means the single-flavor version of Eq. (3.29) because the full determinant factorizes. If  $\sigma = \text{const.}$  as we assume in this part, the spacetime integration yields a factor  $V$  in the exponent and the inclusion of  $\sigma$  into  $D$  results in a shift of the eigenvalues to

$$\lambda_{\pm} = -i(m - \sigma) \pm \sqrt{(k_0 - i\mu)^2 + \vec{k}_{\perp}^2} \quad (4.3)$$

where  $\vec{k} = (k_0, \vec{k}_{\perp})$  is the wave vector of the corresponding eigenstate. If we impose anti-periodic boundary conditions in time direction, the possible frequencies  $k_0$  are the so-called *fermionic Matsubara frequencies*

$$k_0 = \omega_n = \frac{\pi}{\beta} (2n + 1), \quad n \in \mathbb{Z}. \quad (4.4)$$

Now, the determinant of  $D$  is given by

$$\det D = \prod_{\lambda, i=\pm} \lambda_i = \prod_{\lambda} \lambda_+ \lambda_- = \prod_{\vec{k}} -(k_0 - i\mu)^2 - M^2 \quad (4.5)$$

defining

$$M^2 = \vec{k}_{\perp}^2 + (m - \sigma)^2. \quad (4.6)$$

This determinant is positive and real since with  $k_0$  there is also  $-k_0$  in the product yielding terms such as

$$\left[ -(k_0 - i\mu)^2 - M^2 \right] \left[ -(-k_0 - i\mu)^2 - M^2 \right] = M^4 - M^2 \mu^2 + \mu^4 + \dots > 0 \quad (4.7)$$

where some positive terms have been omitted. Thus, we have

$$\ln \det D = L^2 \int \frac{d^2 \vec{k}_{\perp}}{(2\pi)^2} v(M(k_{\perp})), \quad v(M) = \sum_{n=-\infty}^{\infty} \ln \left[ -(\omega_n - i\mu)^2 - M^2 \right]. \quad (4.8)$$

This sum obviously diverges. But, as used for example in [48], we can extract a non-divergent relative expression by a convenient choice of the integration constant in

$$v(M) = \int dM \frac{\partial v}{\partial M}. \quad (4.9)$$

In the following, we will shift the HS field  $\sigma$  to be  $\sigma \rightarrow \sigma - m$

**Derivation of  $v$ .** To extract the relevant parts of  $v$  via Eq. (4.9) we make use of

$$\tanh y = \coth \left( y \pm i \frac{\pi}{2} \right) = \sum_{n=-\infty}^{\infty} \frac{\left( y \pm i \frac{\pi}{2} \right)}{\pi^2 n^2 + \left( y \pm i \frac{\pi}{2} \right)}. \quad (4.10)$$

First, we have

$$\frac{\partial v}{\partial M} = \sum_{n=-\infty}^{\infty} \frac{2M}{(\omega_n - i\mu)^2 + M^2} = \beta \sum_{n=-\infty}^{\infty} \frac{x}{[i\pi n + (x + i\pi\alpha)][-i\pi n + (x - i\pi\alpha)]} \quad (4.11)$$

with the shorthand notations

$$\alpha = \frac{1}{2} - i \frac{\beta\mu}{2\pi}, \quad x = \frac{\beta M}{2}. \quad (4.12)$$

We use a partial fraction decomposition to get

$$\frac{2}{\beta} \frac{\partial v}{\partial M} = \sum_{n=-\infty}^{\infty} \left( \frac{-i\pi n + (x + i\pi\alpha)}{\pi^2 n^2 + (x + i\pi\alpha)^2} + \frac{i\pi n + (x - i\pi\alpha)}{\pi^2 n^2 + (x - i\pi\alpha)^2} \right). \quad (4.13)$$

The parts  $\sim n$  are not absolutely convergent but converge to 0 if the sum is evaluated in an alternating fashion. Thus, they are discarded here. It remains

$$\begin{aligned} \frac{2}{\beta} \frac{\partial v}{\partial M} &= \sum_{n=-\infty}^{\infty} \frac{(x + i\pi\alpha)}{\pi^2 n^2 + (x + i\pi\alpha)^2} + \sum_{n=-\infty}^{\infty} \frac{(x - i\pi\alpha)}{\pi^2 n^2 + (x - i\pi\alpha)^2} \\ &= \coth(x + i\pi\alpha) + \coth(x - i\pi\alpha) \\ &= \tanh\left(\frac{\beta M + \beta\mu}{2}\right) + \tanh\left(\frac{\beta M - \beta\mu}{2}\right) \end{aligned} \quad (4.14)$$

where we plugged in Eq. (4.10) and Eq. (4.12). This can be integrated easily to arrive at

$$v(M) = \int dM \frac{\partial v}{\partial M} = \beta M + \ln\left(1 + e^{-\beta M + \beta\mu}\right) + \ln\left(1 + e^{-\beta M - \beta\mu}\right) + \text{const}. \quad (4.15)$$

**Performing the integrations.** Next, we perform the integration in Eq. (4.8). The integral consists of two parts ( $\sim M$  and  $\sim \ln(1 + e^{-\beta M \pm \beta\mu})$ ). Since the first part diverges we introduce a momentum cutoff  $\Lambda$ . Then this part of the integral yields

$$\int_0^\Lambda \frac{d^2 \vec{k}_\perp}{2\pi} M = \frac{|\sigma|^3}{3} \left[ \left( \sqrt{\frac{\Lambda^2}{\sigma^2} + 1} \right)^3 - 1 \right] = -\frac{|\sigma|^3}{3} + \frac{\Lambda^3}{3} + \frac{\Lambda}{2} \sigma^2 + \mathcal{O}\left(\frac{\sigma}{\Lambda}\right). \quad (4.16)$$

#### 4 Large- $N_f$ Limit

Finally, we integrate

$$\int_0^\infty dk k \ln \left( 1 + e^{-\beta M \pm \beta \mu} \right) \quad (4.17)$$

with the aid of

$$M dM = M \frac{2k}{2\sqrt{k^2 + (m - \sigma)^2}} dk = k dk. \quad (4.18)$$

To do so, for  $s \in \mathbb{Z}$  we define the polylogarithm  $\text{Li}_s : \mathbb{C} \rightarrow \mathbb{C}$  [49] via

$$\text{Li}_{s+1}(x) = \int_0^x dt \frac{\text{Li}_s(t)}{t} \quad \text{with} \quad \text{Li}_1(x) = -\ln(1-x). \quad (4.19)$$

Then, the above integral yields

$$\int_0^\infty dk k \ln \left[ \left( 1 + e^{-\beta M + \beta \mu} \right) \left( 1 + e^{-\beta M - \beta \mu} \right) \right] = -\frac{|\sigma| f_2^+(\sigma, \mu, \beta)}{\beta} - \frac{f_3^+(\sigma, \mu, \beta)}{\beta^2} \quad (4.20)$$

where we used

$$f_s^\pm(\sigma, \mu, \beta) = \text{Li}_s \left( -e^{-\beta|\sigma| + \beta\mu} \right) \pm \text{Li}_s \left( -e^{-\beta|\sigma| - \beta\mu} \right). \quad (4.21)$$

For later use, we remark

$$\partial_\sigma f_{k+1}^\pm = -\text{sgn}(\sigma) \beta f_k^\pm, \quad \partial_\mu f_{k+1}^\pm = \beta f_k^\mp, \quad \partial_\beta f_{k+1}^\pm = -\left( |\sigma| f_k^\pm - \mu f_k^\mp \right) \quad (4.22)$$

as well as

$$f_1^+(\sigma, \mu, \beta) = -\ln \left[ 2 \cosh \beta |\sigma| + 2 \cosh \beta \mu \right] + \beta |\sigma|, \quad (4.23)$$

$$f_1^-(\sigma, \mu, \beta) = -\ln \left[ \frac{\cosh \left[ \frac{\beta}{2} (|\sigma| - \mu) \right]}{\cosh \left[ \frac{\beta}{2} (|\sigma| + \mu) \right]} \right] - \beta \mu. \quad (4.24)$$

## 4.2 Chiral Condensate And Critical Behavior

In the previous subsection we found the partition function to be

$$Z(\mu, m, g) = \int \mathcal{D}\sigma \exp \left[ N_f \ln \det D - \frac{N_f}{2g^2} V_\beta \sigma^2 \right] \quad (4.25)$$

## 4.2 Chiral Condensate And Critical Behavior

with the spacetime volume  $V_\beta = \beta L^2$ . After introducing the renormalized coupling  $\lambda_R = \frac{2\pi}{g^2} - \Lambda$  we find from Eq. (4.16) and Eq. (4.20)

$$Z = \int \mathcal{D}\sigma \exp \left[ - \frac{V_\beta N_f}{2\pi} \underbrace{\left( \frac{|\sigma|^3}{3} + \frac{\lambda_R}{2} \sigma^2 + \frac{|\sigma|}{\beta^2} f_2^+(\sigma, \mu, \beta) + \frac{1}{\beta^3} f_3^+(\sigma, \mu, \beta) \right)}_{=U} \right] \quad (4.26)$$

where a (cutoff dependent) constant offset has been included into the measure. As one can see, the terms calculated in the previous subsection form a potential for  $\sigma$ . For a given temperature and chemical potential, spontaneous symmetry breaking manifests in a non-trivial global minimum of  $\sigma$ .

**Calculation of the condensate.** The condensate is given by the global minimum of the potential  $U$  which will be found at one of the points with

$$0 = \partial_\sigma U = \lambda_R \sigma + \frac{\sigma}{\beta} \ln [2 \cosh \beta \sigma + 2 \cosh \beta \mu] \quad (4.27)$$

derived by use of Eq. (4.22) and Eq. (4.23). Solutions to this equation are either  $\sigma = 0$  or

$$\sigma = \pm \frac{1}{\beta} \operatorname{arcosh} \left( \frac{1}{2} e^{-\lambda_R \beta} - \cosh \beta \mu \right) \quad (4.28)$$

which exists only if

$$e^{-\lambda_R \beta} \geq 2 (\cosh \beta \mu + 1) \quad \Leftrightarrow \quad |\mu| \leq \frac{1}{\beta} \operatorname{arcosh} \left( \frac{1}{2} e^{-\lambda_R \beta} - 1 \right) = \mu_c(\beta). \quad (4.29)$$

In particular, we have to choose a negative renormalized coupling  $\lambda_R$  to get any non-trivial candidate. A second differentiation at  $\sigma = 0$  shows

$$\partial_\sigma^2 U \Big|_{\sigma=0} = \lambda_R + \frac{1}{\beta} \ln [2 + 2 \cosh \beta \mu]. \quad (4.30)$$

Since we have chosen  $\lambda_R$  to be negative, we see that whenever the non-trivial candidate exists (i.e. Eq. (4.29) holds)  $\sigma = 0$  is a maximum and by  $U(\pm\sigma) \rightarrow \infty$  for  $\sigma \rightarrow \infty$  the non-trivial solutions must be minima. Thus, we find the condensate to be

$$\Sigma = |\sigma_{\min}(\mu, \beta)| = \begin{cases} \frac{1}{\beta} \operatorname{arcosh} \left( \frac{1}{2} e^{-\lambda_R \beta} - \cosh \beta \mu \right) & \text{for } |\mu| \leq \mu_c(\beta), \\ 0 & \text{else.} \end{cases} \quad (4.31)$$

#### 4 Large- $N_f$ Limit

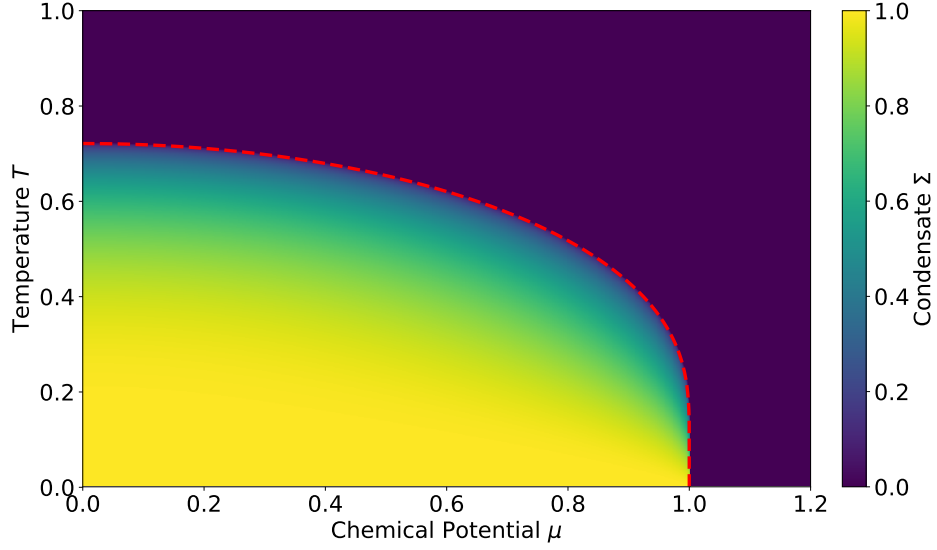


Fig. 4.1: Phase diagram in the  $T$ - $\mu$  plane of the GN in the limit of large flavor number  $N_f$  and in units of  $-\lambda_R$  as derived in Eq. (4.31). The dashed line indicates the critical line given by equality in Eq. (4.29).

We see that there is a broken phase with non-vanishing condensate as well as a phase with restored symmetry separated by the critical line of equality in Eq. (4.29). The phase diagram is shown in Fig. 4.1.

Next, we investigate the critical exponents of the phase transition. We start with the temperature dependence, i.e. we want to find  $\beta$  such that

$$\Sigma(\tau) \sim \tau^\beta \quad (4.32)$$

for  $\tau = \frac{T-T_c}{T_c} \rightarrow 0$ .<sup>22</sup> This can be explicitly solved for  $\beta$

$$\beta = \lim_{\tau \rightarrow 0} \frac{\ln \Sigma}{\ln |\tau|} = \frac{1}{2} \quad (4.33)$$

by extensive use of L'HOSPITAL's formula. In fact, one does not make use of  $\tau$  parametrizing the temperature dependence. Thus, defining a  $\tau_\mu = \frac{\mu - \mu_c}{\mu_c}$  or  $\tau_{\lambda_R} = \frac{\lambda_R - \lambda_{R,c}}{\lambda_{R,c}}$  the same calculation holds such that

$$\Sigma(T, \mu) \sim \left( \frac{T - T_c}{T_c} \frac{\mu - \mu_c}{\mu_c} \frac{\lambda_R - \lambda_{R,c}}{\lambda_{R,c}} \right)^{\frac{1}{2}} \quad (4.34)$$

<sup>22</sup>We assume to be in the broken phase, i.e.  $\tau < 0$ , because the condensate vanishes otherwise.

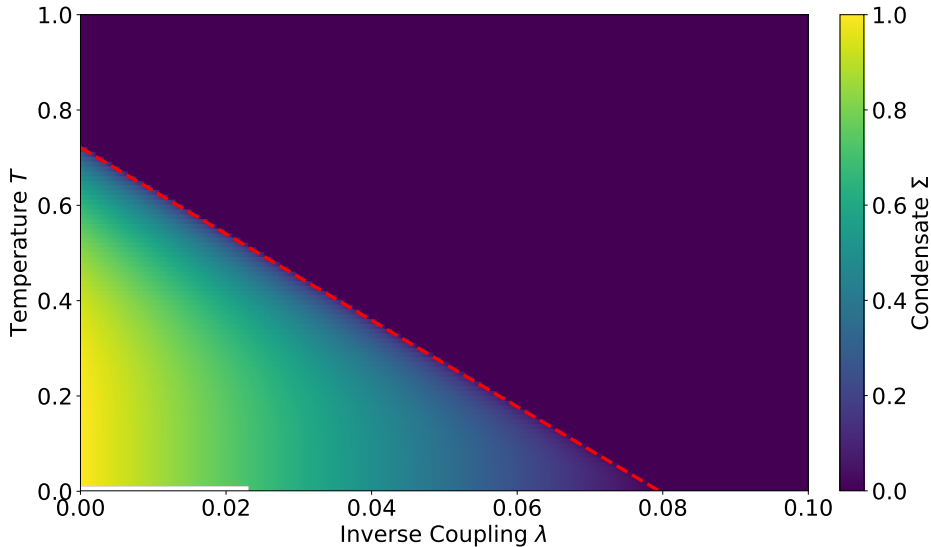


Fig. 4.2: Phase diagram in the  $T$ - $\lambda$  plane of the GN model in the limit of large flavor number  $N_f$  with  $\Lambda = 10$  as derived in Eq. (4.36). The dashed line indicates the critical line given by equality in Eq. (4.35).

close to a triple of corresponding  $T_c, \mu_c, \lambda_{R,c}$ . This result could have been anticipated from the fact that we work in a mean field approximation in this section. It is well-known that the critical exponents for such an approximation are always the same, particularly  $\beta = \frac{1}{2}$  [17]. For the rest of this subsection, we will derive analytical expressions for either  $\mu = 0$  or  $T = 0$ .

**The special case  $\mu = 0$ .** For this special case, Eq. (4.29) can be solved explicitly for  $\beta$  yielding

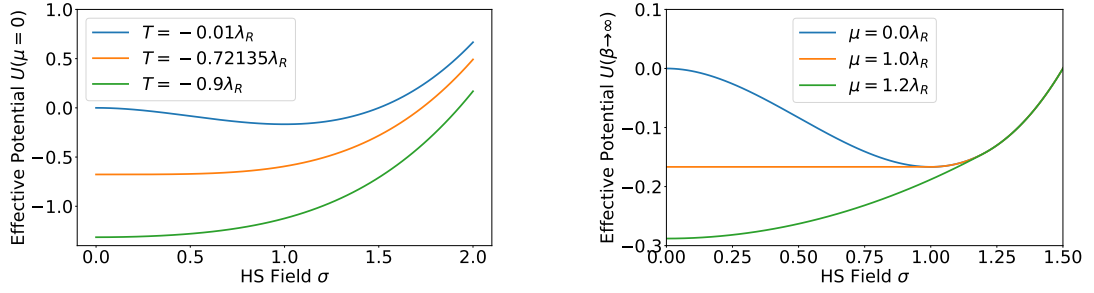
$$\frac{1}{\beta_c} = T_{c,\max} = -\frac{\lambda_R}{\ln 4} \quad (4.35)$$

where the subscript max is introduced to mark it as the maximal temperature with a phase transition in  $\mu$  (actually at  $\mu = 0$ ). Furthermore, from Eq. (4.31) we find

$$\Sigma(\mu = 0, \beta) = \frac{1}{\beta} \operatorname{arcosh} \left( \frac{1}{2} e^{-\lambda_R \beta} - 1 \right) \quad (4.36)$$

in the broken phase ( $\beta \geq \beta_c$ ). The potential  $U(\sigma)$  can be seen in Fig. 4.3(a). For comparison with the lattice results later on, the phase diagram in the  $\lambda$ - $T$  plane is also shown in Fig. 4.2.

#### 4 Large- $N_f$ Limit



(a) Potential  $U(\sigma)$  for vanishing chemical potential  $\mu = 0$  and three real values of the temperature  $T$  in units of  $\lambda_R$ .

(b) Potential  $U(\sigma)$  for vanishing temperature  $T = 0$  and three real values of the chemical potential  $\mu$  in units of  $\lambda_R$ .

Fig. 4.3: The effective potential  $U(\sigma)$  for  $\mu = 0$ , resp.  $T = 0$ .

**The special case  $T = 0$ .** This time, by  $T \rightarrow 0$  we have  $\beta \rightarrow \infty$  and can therefore discard all but the highest order terms in  $\beta$  (exactly those which are hidden in the volume factor). This is best done directly in the potential. Since it fulfills  $U(-\sigma) = U(\sigma)$  and  $U(-\mu) = U(\mu)$ , we restrict ourselves to  $\mu, \sigma \geq 0$  and generalize the result afterwards. In particular, we have to evaluate the functions  $f_2$  and  $f_3$  in the limit of large  $\beta$ . We make use of

$$\lim_{\beta \rightarrow \infty} \frac{\text{Li}_s(-e^{-\beta(\sigma-\mu)})}{\beta^s} = \begin{cases} 0 & \text{for } \mu \leq \sigma \\ -\frac{(\mu-\sigma)^s}{s!} & \text{else} \end{cases} \quad (4.37)$$

as derived in [49]. Now, the potential simplifies to

$$U(T = 0) = \begin{cases} \frac{\sigma^3}{3} + \frac{\lambda_R}{2}\sigma^2 & \text{for } \mu \leq \sigma \\ \frac{\mu + \lambda_R}{2}\sigma^2 - \frac{\mu^3}{6} & \text{else} \end{cases} \quad (4.38)$$

with

$$0 = \partial_\sigma U = \begin{cases} \sigma^2 + \lambda_R \sigma & \text{for } \mu \leq \sigma \\ (\mu + \lambda_R) \sigma & \text{else} \end{cases} \quad (4.39)$$

as the necessary condition for extrema which is solved by  $\sigma = 0$  in both cases and additionally  $\sigma = -\lambda_R$  for  $\mu \leq \sigma$ . It is easily seen that the latter is a minimum if  $\lambda_R < 0$ . To resolve the case distinction, we assume  $\sigma$  in Eq. (4.39) to be the minimizing one. Then, we see that

$$\Sigma(\mu, \beta \rightarrow \infty) = \begin{cases} -\lambda_R & \text{for } |\Re \mu| < -\lambda_R \\ 0 & \text{for } |\Re \mu| > -\lambda_R \end{cases} \quad \text{and} \quad \Sigma \in [0, -\lambda_R] \text{ if } |\Re \mu| = -\lambda_R. \quad (4.40)$$



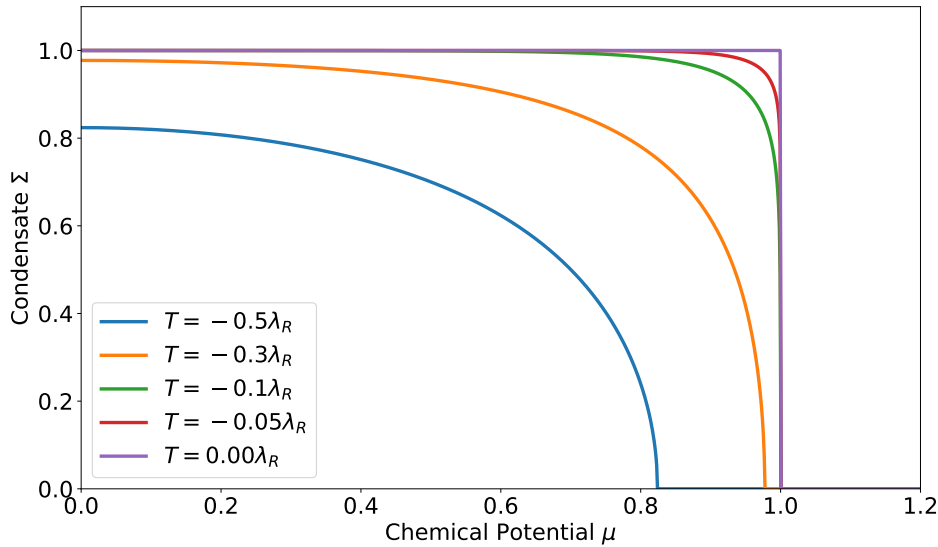


Fig. 4.4: The condensate  $\Sigma$  for various temperatures  $T$  in units of  $\lambda_R$  including the limiting case of  $T \rightarrow 0$ .

Exactly at the critical point, we find that the potential gets flat (see Fig. 4.3(b)) for all  $|\sigma| \leq -\lambda_R$ . This unusual critical behavior can be seen as the limiting case from the small temperature regime (see Fig. 4.4). Only at temperature  $T = 0$ , the phase transition in  $\mu$  is of first order admitting coexistence of a continuum of phases. This interpretation is underpinned by investigation of the susceptibility

$$\chi = \partial_m^2 U = \begin{cases} -\lambda_R & \text{for } |\Re\mu| < -\lambda_R \\ \mu + \lambda_R & \text{for } |\Re\mu| > -\lambda_R. \end{cases} \quad (4.41)$$

For its definition, we shortly reintroduced an explicit mass and excluded the critical point where it would be ill-defined. One can clearly see that there is no power law singularity in Eq. (4.41) as we would expect for a second order phase transition which strengthens the evidence for it to be of first order.

### 4.3 Thermodynamics

With the used independent variables, the corresponding thermodynamic potential is the grand canonical potential  $J(T, \mu, V)$  given by

$$J = -\frac{\ln Z}{\beta} \quad (4.42)$$

#### 4 Large- $N_f$ Limit

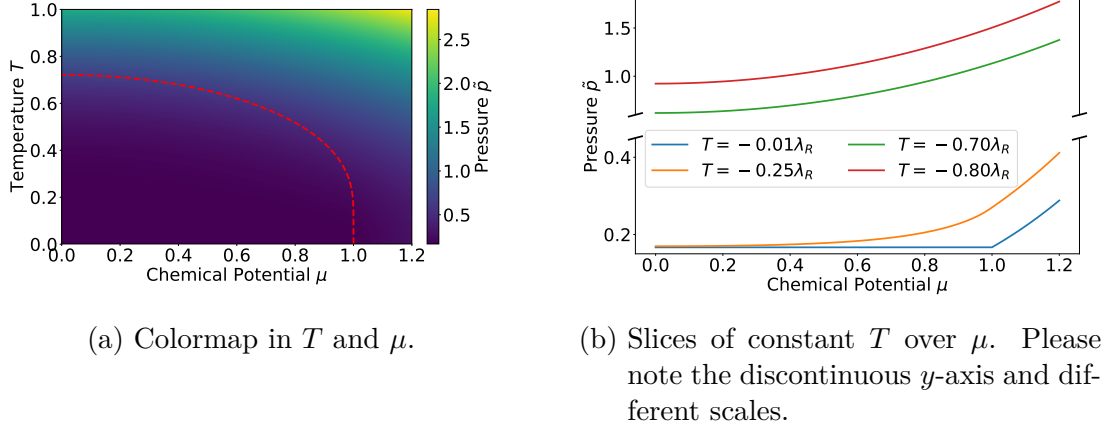


Fig. 4.5: Pressure  $\tilde{p}$  according to Eq. (4.45) in dependence of temperature  $T$  and chemical potential  $\mu$  for  $\lambda_R = -1$ .

where  $V = L^2 = \frac{V_\beta}{\beta}$  is the physical volume. First, we see that this is easily evaluated in a saddle point approximation where  $\ln Z$  takes the form

$$\ln Z = -\frac{V\beta N_f}{2\pi} U(\mu, \beta, \Sigma(\mu, \beta)) + \mathcal{O}(N_f^{-1/2}) \quad (4.43)$$

and  $\Sigma$  is the (non-negative)  $\sigma$ -value where  $U$  takes the minimum for the given parameters  $\mu, \beta$ . To exploit this, we always consider  $T$  (or  $\beta$ ),  $\mu$ ,  $V$  as independent variables if not stated else and introduce the notation

$$\tilde{a} = \frac{2\pi a}{N_f V} \quad (4.44)$$

for any suitable quantity  $a$ , i.e.  $\tilde{a}$  is an intensive (per Volume) quantity per number of flavors. With the above conventions we can compute thermodynamic quantities like<sup>23</sup> the pressure (which is the same as the grand canonical potential)

$$\tilde{p} = -\frac{2\pi}{N_f V} J = -U = -\frac{\Sigma^3}{3} - \frac{\lambda_R \Sigma^2}{2} - \frac{\Sigma f_2^+}{\beta^2} - \frac{f_3^+}{\beta^3}, \quad (4.45)$$

the entropy density

$$\tilde{s} = -\frac{2\pi}{N_f V} \partial_T J = \beta^2 \partial_\beta U = -f_1^+ \Sigma^2 - \left( \frac{3f_2^+}{\beta} - \mu f_1^- \right) \Sigma - \frac{3f_3^+}{\beta^2} + \frac{\mu f_2^-}{\beta}, \quad (4.46)$$

the particle density

$$\tilde{n} = -\frac{2\pi}{N_f V} \partial_\mu J = -\partial_\mu U = -\frac{\Sigma f_1^-}{\beta} - \frac{f_2^-}{\beta^2} \quad (4.47)$$

<sup>23</sup>The following formulae can be found for example in [13].

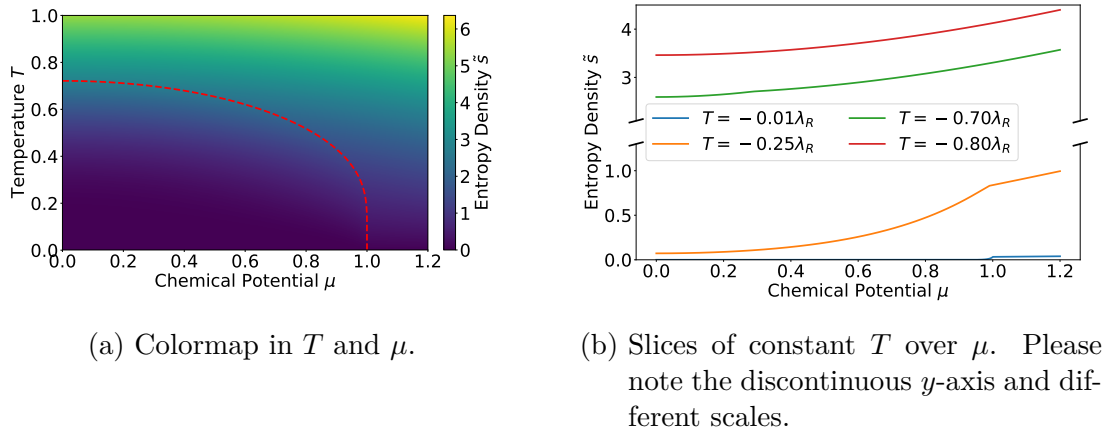


Fig. 4.6: Entropy density  $\tilde{s}$  according to Eq. (4.46) in dependence of temperature  $T$  and chemical potential  $\mu$  for  $\lambda_R = -1$ .

or the specific heat

$$\tilde{c}_V = T (\partial_T \tilde{s})_{V,n} = T \partial_T \tilde{s} - \frac{T (\partial_T \tilde{n})^2}{\partial_\mu \tilde{n}} \quad (4.48)$$

where the analytical result of the latter is far too large to fit the page and does not yield much additional insight. Instead, Fig. 4.5 to Fig. 4.8 show the results as colormaps and slices of constant  $T$ . The temperature slices are chosen such that the lowest is a good approximation to<sup>24</sup>  $T \rightarrow 0$  while the highest shows the behavior without any transition (above  $T_c(\mu = 0) \approx -0.72\lambda_R$ ). In between, there is one moderate temperature and one close to the maximal critical temperature. The former's transition point is still  $\mu_c \approx 1$  while the latter's is  $\mu_c \approx 0.3$  as can be read off conveniently from the specific heat (Fig. 4.8(b)). Please note that some graphics have a discontinuous  $y$ -axis and different scales in the upper and lower part.

In Fig. 4.5 we see that the potential (resp. pressure) is continuous everywhere and differentiable for all  $T > 0$  as we already discussed as the defining behavior at a second order phase transition (cf. Sec. 2.1.1). In fact, raising the temperature has the effect of smoothening the transition. While there is a pronounced kink for low temperatures (becoming sharp for  $T \rightarrow 0$ ), even for moderate temperature the transition is already not exactly locatable in the slices. Nevertheless, the further discussion of its derivatives shows that it is not a smooth function of the thermodynamical variables.

<sup>24</sup>The case  $T = 0$  would have required an additional limiting procedure. This was neither numerically nor analytically possible for  $\tilde{c}_V$ . For the sake of comparability, it was decided to always use a small but non-vanishing value for  $T$ .

#### 4 Large- $N_f$ Limit

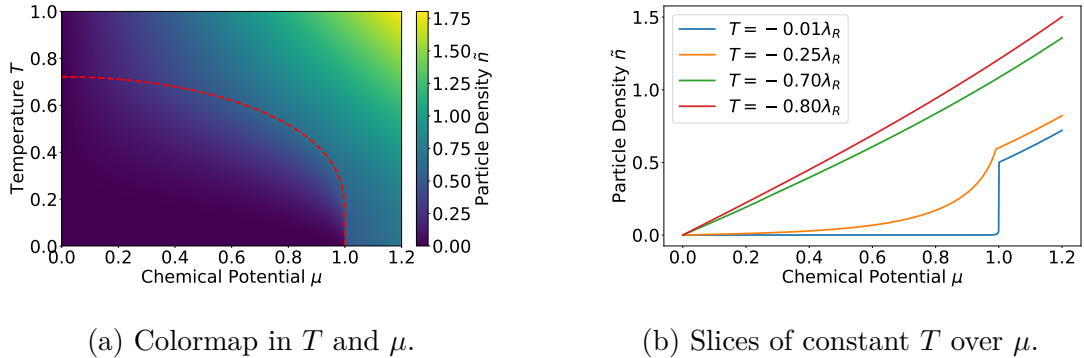


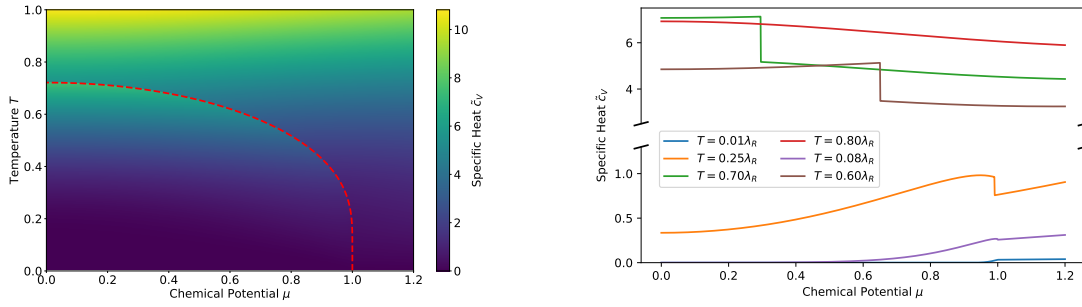
Fig. 4.7: Particle density  $\tilde{n}$  according to Eq. (4.47) in dependence of temperature  $T$  and chemical potential  $\mu$  for  $\lambda_R = -1$ .

The entropy density (Fig. 4.6) in general rises with rising temperature. This is a well-known fact [50]. Furthermore, it is continuous but shows a kink for all temperatures that have a phase transition in  $\mu$  as we expect for a second order phase transition. This kink becomes arbitrarily weak with rising temperature and vanishes at  $\mu_c = 0$  at the maximal critical temperature.<sup>25</sup> Above, the entropy density is smooth. As for the pressure, the critical line is not recognizable in the colormap due to continuity.

This is different in the particle density for low temperatures (Fig. 4.7). For low temperatures, there is a steep ascent close to the transition that can be seen to be a smoothed version of an actual jump at  $T = 0$ . This jumping behavior is related to the so-called *Silver Blaze* property. In [32], it is explained for the massive free fermion case: The chemical potential is the amount of free energy needed to increase the particle number. If this is smaller than the particle's mass there will be no excitation and the particle number does not change. Otherwise, particle creation is possible and sets in as soon as  $\mu$  exceeds  $m$ . In our case, the non-vanishing condensate  $\Sigma$  also serves as a mass term because we assumed it to be homogeneous. At  $T \rightarrow 0$ , we have  $\Sigma \rightarrow -\lambda_R = \text{const.}$  in the broken phase such that the same argumentation holds as long as  $\mu < -\lambda_R$ . The discontinuity in the particle density then occurs because with the onset of particle creation (right at the transition) the mass-like  $\Sigma$  jumps to zero and one can see the free massless particle's behavior. For non-zero temperatures this jump is smoothed by the smoothing of the FERMI-DIRAC distribution [32] and in our case additionally by the fact that  $\Sigma$  goes to zero continuously.

The most complicated behavior is shown by the specific heat (cf. Fig. 4.8). To get a more complete picture of the changes in  $T$ , we added some more temperature

<sup>25</sup>It is already hardly noticeable for  $T = -0.7\lambda_R$  in Fig. 4.6(b) but after proper rescaling it can still be made out.



(a) Colormap in  $T$  and  $\mu$  with the critical line (dashed).

(b) Slices of constant  $T$  over  $\mu$ . Please note the discontinuous  $y$ -axis and different scales.

Fig. 4.8: Specific heat  $\tilde{c}_V$  according to Eq. (4.48) in dependence of temperature  $T$  and chemical potential  $\mu$  for  $\lambda_R = -1$ .

slices to Fig. 4.8(b). There we see the following behavior: For high temperatures without a phase transition it is a smooth, rising function in  $\mu$ . Lowering the temperature below  $T_{c,\max}$ , the specific heat jumps between the broken and the restored phase. This is the expected behavior at a second order phase transition and can be seen as a clear cut in the colormap Fig. 4.8(a). This jump becomes smaller for smaller temperatures but for every finite temperature the limit from the left is larger than the limit from the right. Also, the overall magnitude of  $\tilde{c}_V$  decreases when lowering the temperature.

## 5 Lattice Results for $N_f = 1$

This section contains the main results of the thesis. We will present lattice results for the critical coupling constant and critical exponents at zero temperature and the lattice phase diagram in the temperature-coupling plane for a single irreducible flavor (without chemical potential). To the best of our knowledge, this thesis is the first to present such findings from *Monte Carlo* (MC) lattice simulations. Before we can start the discussion of the results, we first work out the concrete formulation and observables in use.

### 5.1 Dualization Of Gross-Neveu

From now on we consider a single flavor only. Accordingly, the index on a spinor field denotes the spinor components. As was observed in [51], the  $N_f = 1$  GN model suffers a severe *sign problem* (SP). It is therefore not feasible to simulate it within the standard approaches. For this thesis, we will instead reformulate the model in terms of a dual variable  $k$  – an approach that is similar to ideas in [52]. It was originally introduced in [16, 51]. This will not completely cure the SP but at least make it much more tractable (see [51] and Sec. 5.4). Furthermore, the possibility of exact reweighting (see Sec. 2.2.3) arises since the reweighting factor can be calculated easily during the simulation.

We consider the generating functional, i.e. the partition function Eq. (3.28) with classical sources  $\bar{\eta}, \eta$ , given by

$$Z_{\eta, \bar{\eta}} = \int \mathcal{D}\sigma \mathcal{D}\bar{\psi} \mathcal{D}\psi \exp\left(-\bar{\psi} D \psi - \lambda \sigma^2 + \bar{\eta} \psi - \bar{\psi} \eta\right). \quad (5.1)$$

We define the fermionic part to be

$$W = \int \mathcal{D}\bar{\psi} \mathcal{D}\psi \exp\left(-\bar{\psi} i (\not{\partial} + m) \psi - \bar{\psi} i \sigma \psi + \bar{\eta} \psi - \bar{\psi} \eta\right) \quad (5.2)$$

and expand the exponential of the interaction part yielding

$$W = \int \mathcal{D}\bar{\psi} \mathcal{D}\psi \exp\left(-\bar{\psi} i (\not{\partial} + m) \psi + \bar{\eta} \psi - \bar{\psi} \eta\right) \prod_{x,i} \left(1 - \bar{\psi}_i(x) i \sigma(x) \psi_i(x)\right) \quad (5.3)$$

which is exact due to the Grassmann properties of the spinor fields. For every tuple  $(x, i)$ , this can be written via a number  $k_{x,i} \in \{0, 1\}$  as

$$W = \int \mathcal{D}\bar{\psi} \mathcal{D}\psi \exp\left(-\bar{\psi} i (\not{\partial} + m) \psi + \bar{\eta} \psi - \bar{\psi} \eta\right) \prod_{x,i} \sum_{k_{x,i}=0}^1 \left(-\bar{\psi}_i(x) i \sigma(x) \psi_i(x)\right)^{k_{x,i}}. \quad (5.4)$$

Next, we can rearrange the finite sum and product as a sum over all configurations  $K = (k_{x,i} \in \{0, 1\} : x \in \Lambda, i \in \{0, 1\}) \in \{0, 1\}^{2|\Lambda|}$  and obtain from that

$$W = \sum_{K \in \{0,1\}^{2|\Lambda|}} \int \mathcal{D}\bar{\psi} \mathcal{D}\psi \exp\left(-\bar{\psi}i(\not{\partial} + m)\psi + \bar{\eta}\psi - \bar{\psi}\eta\right) \prod_{x,i} \left(-\bar{\psi}_i(x)i\sigma(x)\psi_i(x)\right)^{k_{x,i}}. \quad (5.5)$$

For any fixed configuration, we perform the integration over all spinor fields with  $k_{x,i} = 1$ . What remains is the following integral where the integration includes only those spinors where  $k_{x,i} = 0$

$$W = \sum_{K \in \{0,1\}^{2|\Lambda|}} \int \mathcal{D}\bar{\psi} \mathcal{D}\psi \exp\left(-\bar{\psi}i(\not{\partial} + m)\psi + \bar{\eta}\psi - \bar{\psi}\eta\right) (-i)^k \prod_{x,i} \sigma(x)^{k_{x,i}} \quad (5.6)$$

defining  $k_x = k_{x,0} + k_{x,1}$  and  $k = \sum_{x,i \in K} k_{x,i}$ . By a variable transformation

$$-\bar{\psi}i(\not{\partial} + m)\psi + \bar{\eta}\psi - \bar{\psi}\eta = -\bar{\psi}'i(\not{\partial} + m)\psi' - \bar{\eta}(i(\not{\partial} + m))^{-1}\eta \quad (5.7)$$

in the remaining spinor fields we can perform the integrations (including the  $\sigma$  integration) yielding

$$Z_{\bar{\eta},\eta} = C \sum_{K \in \mathcal{K}} \det(iD[K]) \exp\left(-\bar{\eta}(iD[K])^{-1}\eta\right) w(K) \quad (5.8)$$

where  $C = \left(\frac{\sqrt{\pi}}{\sqrt{\lambda}}\right)^V$ ,  $D[K]$  denotes the reduced fermionic operator  $(\not{\partial} + m)$  with every  $I = \{xi\}$ -th row and column removed when  $k_{x,i} = 1$  and the weight of the configuration  $w(K)$  is

$$w(K) = \frac{1}{C} (-i)^k \int \mathcal{D}\sigma \prod_{x,i} \sigma(x)^{k_{x,i}} \exp\left(-\lambda\sigma(x)^2\right) = \left(\frac{-1}{2\lambda}\right)^{\frac{k}{2}} \quad (5.9)$$

if for every  $x \in \Lambda$  we have  $k_{x,0} = k_{x,1}$  and vanishes otherwise. From that, we see that the set  $\mathcal{K} \subset \{0, 1\}^{2|\Lambda|}$  to sample from consists only of those configurations where  $k_{x,0} = k_{x,1}$ . The partition function of the theory without sources is then given by

$$Z = C \sum_{K \in \mathcal{K}} \det(iD[K]) w(K) \quad (5.10)$$

such that we can sample  $K$ -configurations in our Monte-Carlo simulations.

## 5.2 Observables In Dual Formulation

Now, that we have a formulation ready for simulation, we need to know what correspondence there is to physical quantities. An intuitive starting point would be the chiral condensate<sup>26</sup>

$$\langle \bar{\psi}\psi \rangle = -(2\lambda) \langle \sigma \rangle \quad (5.11)$$

because it serves as an order parameter for the symmetry breaking in GN. Unfortunately, in MC simulation there is no spontaneous symmetry breaking in a strict sense due to the *detailed balance* condition<sup>27</sup>: Since the symmetry is not explicitly broken, the probability density of any observable obeys this symmetry. By detailed balance, we know that every configuration can be reached within the simulations and from the symmetry it is further clear that configurations that are identical modulo this symmetry appear with same probability in equilibrium. Thus, we know by symmetry that

$$\langle \sigma \rangle = 0. \quad (5.12)$$

Only in the infinite volume limit, the small transition probability between the positive and negative configurations is suppressed to zero, hence yielding actual spontaneous symmetry breaking. The usual fix for this well-known problem is to consider the absolute value's expectation which is invariant under the transformation. This would indeed work but we do not have direct access to  $\sigma$  for a given configuration and hence cannot calculate this. Yet, there is another way to derive an expectation value of the chiral condensate, namely, by the same means as in Sec. 4.2 via the minimum of the effective potential. We will call this the *local condensate* since it is the expectation value of  $\sigma$  at every point on the lattice independently and becomes a global expectation value only after employing translational invariance. In the finite  $N_f$  case there is no analytical expression for the effective potential known but it can be calculated from observables measurable in our simulations (see [51] for details). For  $N_f = 1$ , its minimum<sup>28</sup> is given by

$$\Sigma_{\text{loc}} = \begin{cases} \sqrt{2\lambda} \sqrt{\frac{\langle n \rangle - \frac{1}{3}}{\langle n \rangle}} & \langle n \rangle \geq \frac{1}{3} \\ 0 & \text{else} \end{cases} \quad (5.13)$$

---

<sup>26</sup>We will call this the *chiral* condensate although there is no concept like chirality in  $D = 3$ .

This is a convention in the literature with its origin in the reducible representation.

<sup>27</sup>This is also argued in [23]. More on the detailed balance condition can be found in [17].

<sup>28</sup>By symmetry, there is an additional minimum  $-\Sigma_{\text{loc}}$  but if we would include this, averaging would again yield the above problem.



with the  $k$ -density

$$n = \frac{k}{2V}. \quad (5.14)$$

A detailed derivation of the corresponding effective potential can be found in [51] and the minimization can then be carried out analytically. The local condensate has the great advantage that it will be exactly zero as soon as the broken phase is left while any global quantity would assume a small but non-vanishing value due to fluctuations. This makes it easy to precisely detect the phase transition in the local condensate. However, there is nothing known about its FSS behavior because the arguments from Sec. 2.2.2 do not apply any longer. Even derivation from the assumption of FSS behavior for  $\langle n \rangle$  is not applicable because we will see in Sec. 5.5.2 that the physically relevant parameter region is far away from the *lattice artifact phase* (LAP) transition where FSS arguments concerning  $\langle n \rangle$  would hold.

Another typical approach to find a phase transition is via the peak of the susceptibility which is the first derivative of the order parameter. Since the latter is continuous but not differentiable at a second order phase transition, its susceptibility should be sharply peaked at the transition smoothed only by finite size effects. If one defines the susceptibility from the local condensate via

$$\chi_{\text{loc}} = \begin{cases} \frac{\Sigma_{\text{loc}}}{2\lambda} + \frac{V}{2\Sigma_{\text{loc}}} \frac{\langle n^2 \rangle - \langle n \rangle^2}{(1 - \langle n \rangle)^2} & \langle n \rangle \geq \frac{1}{3} \\ 0 & \text{else,} \end{cases} \quad (5.15)$$

at least for the chirally broken phase, one obviously gets a peak where the local condensate tends to zero. Since this is a local quantity, again FSS theory does not apply and no smoothing effect of the finite lattice will be present. Particularly, one can see that near the transition small statistical fluctuations of  $\Sigma_{\text{loc}}$  will gain importance making the precise determination more and more computationally expensive.

A completely different starting point for the investigation of the simulation results is the native variable  $n$  (Eq. (5.14)). For example, the  $n$ -susceptibility

$$\chi_n = \langle n^2 \rangle - \langle n \rangle^2 \quad (5.16)$$

and the fourth-order BINDER cumulant (in  $n$ )

$$U_n = 1 - \frac{\langle n^4 \rangle}{3 \langle n^2 \rangle^2} \quad (5.17)$$

are straightforwardly defined. As one can see from its definition, Eq. (5.14),  $n$  is the density of the local interactions on the lattice. From the local condensate

## 5 Lattice Results for $N_f = 1$

Eq. (5.13), we know that the phase transition occurs at  $\langle n \rangle = \frac{1}{3}$  but it is unclear if this is a distinguished point in the definitions of the  $n$ -susceptibility Eq. (5.16) and the  $n$ -BINDER cumulant Eq. (5.17). However, those have the advantage of being global observables such that the FSS behavior is known. In fact, we will see in Sec. 5.5.2 that they will be of no use for investigation of the expected phase transition but indicate the set-in of a LAP.

Finally, higher order expectation values in  $\bar{\psi}\psi$ , resp.  $\sigma$ , are not flawed by the symmetry restrictions and can be defined as usual. This implies, for example, the four-fermion term

$$\frac{g^2}{V} \left\langle (\bar{\psi}\psi)^2 \right\rangle = -\frac{(2\lambda)}{V} \langle \sigma^2 \rangle = 1 + \langle n \rangle \quad (5.18)$$

and the fourth-order BINDER cumulant in  $\sigma$

$$U_\sigma = 1 - \frac{\langle \sigma^4 \rangle}{3 \langle \sigma^2 \rangle^2} = \frac{4}{3} - \frac{2}{3(1 + \langle n \rangle)} - \frac{\langle n^2 \rangle - \langle n \rangle^2}{3(1 + \langle n \rangle)^2}. \quad (5.19)$$

By the symmetry restriction  $\langle \bar{\psi}\psi \rangle = 0$ , Eq. (5.12), we see that the four-fermion term also equals the conventionally defined susceptibility

$$\chi = \frac{d^2 \ln Z}{dm^2} = \left\langle (\bar{\psi}\psi)^2 \right\rangle - \underbrace{\langle \bar{\psi}\psi \rangle^2}_{=0} \quad (5.20)$$

but as we know from  $\langle n \rangle \in [0, 1]$  that this will not be peaked at any point.<sup>29</sup>

### 5.3 Evaluation Details

In this subsection we give some technical details of the simulation and evaluation. As already announced in Sec. 2.2.1, the simulations were performed with a simple local Metropolis update algorithm. More details about the implementation can be found in [16]. Since the such generated Markov chain is usually strongly correlated [14] only every 100-th configuration was stored for evaluation. Possible further autocorrelations are taken care of later in the evaluation. Depending on the lattice size, 200 to 20,000 configurations have been generated and the (Markov chain) time series for  $n$  (Eq. (5.14)) were used for the computation of the observables from Sec. 5.2.

<sup>29</sup>Actually, it would be peaked if we performed the infinite volume limit *before* integrating out the fermions. But as explained above, on every finite lattice the latter term vanishes exactly because we integrate positive and negative contributions symmetrically. Only in the infinite volume limit the measure becomes spontaneously asymmetric and a peak could be found.

In detail, the thermalization phase was self-consistently determined as follows: From the starting configuration  $D[K] = \mathbb{1}$  corresponding to  $n = 1$ , the time series drops to (fluctuations around) the expectation value  $\langle n \rangle \leq 1$ . Therefore, the equilibrium can be defined as the time  $t_0$  where the time series firstly drops below the average. To avoid underestimation, this approximation was repeated after removing all configurations with  $t \leq t_0$ . If  $t_0$  does not change anymore between two iterations, it was considered to be the relaxation time. It should be stressed here that this dynamical determination of the thermalization intrinsically excludes a time series if it did not reach stationarity yet. The beginning of a time series is shown in Fig. 5.1. For sufficiently large time series, the thermalization period usually does not influence the average over the ensemble significantly and thus the typical number of iterations is one.

From the thermalized time series, estimators for the observables were calculated via the corresponding functional relation to  $n$  where the expectation value was approximated by the mean average. The statistical uncertainty (given by the standard deviation) of such estimators was estimated via a Jackknife analysis [14] with bin size  $b = 50$ . Nevertheless, the integrated autocorrelation time  $\tau_{\text{int}}$  was computed for some ensembles to get a notion of the possible impact. This was done as suggested in [14] via a self-consistent truncation  $\delta_{\text{max}}$  of the series

$$\tau_{\text{int}}(\delta_{\text{max}}) = \frac{1}{2} + \sum_{\delta=1}^{\delta_{\text{max}}} \frac{\overline{n_t n_{t+\delta}} - \overline{n_t} \overline{n_{t+\delta}}}{\overline{n_t^2} - \overline{n_t}^2} \quad (5.21)$$

such that  $\delta_{\text{max}} \geq 6\tau_{\text{int}}(\delta_{\text{max}})$  where the overscore means averaging in  $t$ . The relative uncertainty of such an estimate is then approximated [14] by

$$\frac{\Delta\tau_{\text{int}}}{\tau_{\text{int}}} \approx \sqrt{\frac{24\tau_{\text{int}}}{N}} \quad (5.22)$$

if  $N$  is the number of configurations used for the estimate. The effect of autocorrelation can be seen in Fig. 5.1 and some autocorrelation times are given in Fig. 5.2. Both indicate that a bin size  $b = 50$  as used in the Jackknife method will surely capture all autocorrelations. However, the autocorrelation time depends on  $\lambda$  significantly. This will be discussed in Sec. 5.5.2.

Finally, the estimates for the crossing of the BINDER parameters Eq. (5.17) used in Sec. 5.5.2 are obtained as follows. A small region  $I$  around the roughly estimated crossing is fitted with least squares to a linear function  $U(\lambda) = A\lambda + B$ . This can be done analytically from  $\{\lambda_i, U(\lambda_i)\}$  with  $\lambda_1, \dots, \lambda_n \in I$  and yields

$$A = \frac{n \sum_{i=1}^n \lambda_i U(\lambda_i) - \sum_{i,j=1}^n \lambda_i U(\lambda_j)}{n \sum_{i=1}^n \lambda_i^2 - (\sum_{i=1}^n \lambda_i)^2}, \quad (5.23a)$$

$$B = \frac{1}{n} \sum_{i=1}^n U(\lambda_i) - \frac{A}{n} \sum_{i=1}^n \lambda_i. \quad (5.23b)$$

## 5 Lattice Results for $N_f = 1$

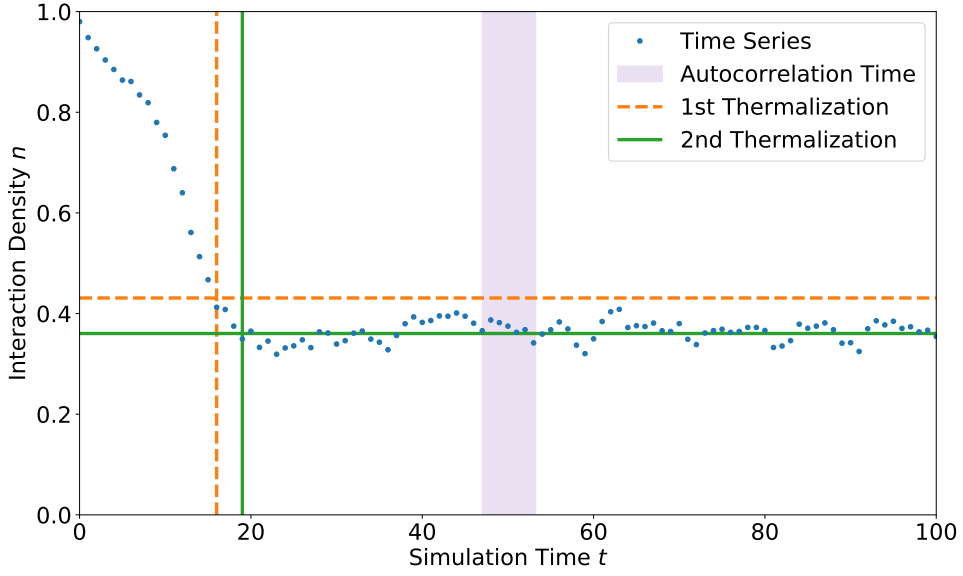


Fig. 5.1: The (simulation) time series in  $n$  for  $L = 16$  and  $\lambda = 0.1257$  truncated to the first 100 entries. The dashed lines indicate the average over the whole ensemble and the first derived thermalization period. The solid lines indicate the next (and final) iteration step. Finally, one window of correlated measurements computed via Eq. (5.21) from the untruncated series is drawn as shaded blue area.

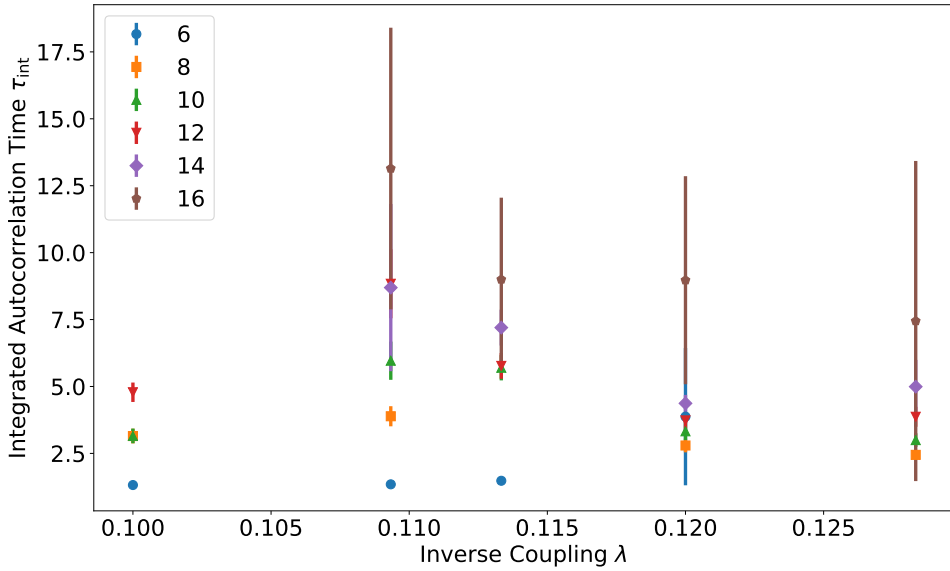


Fig. 5.2: Integrated autocorrelation times according to Eq. (5.21) and Eq. (5.22) over the inverse coupling  $\lambda$ . One observes a significant dependence on both,  $V$  and  $\lambda$ , which is discussed in Sec. 5.5.2.

After having these linear approximations the crossing point of  $U^{(L_0)}$  and  $U^{(bL_0)}$  is simply

$$\lambda_c^{(L_0)}(b) = \frac{B_{bL_0} - B_{L_0}}{A_{L_0} - A_{bL_0}}. \quad (5.24)$$

This final formula with the plugged in expressions Eq. (5.23) is then directly used to obtain the crossing points. The statistical uncertainty can now be estimated by nearly straightforward jackknifing: One estimator for  $U(\lambda_i)$  is obtained by excluding one bin of data. From that the corresponding estimator for  $\lambda_c^{(L_0)}$  is computed. Since the number of bins might vary between the values of  $\lambda_i$  and  $L$  the choice of bins is done independently and randomly, generating only as many estimators as the smallest number of bins in the data series.

## 5.4 Remarks On The Sign Problem

As already discussed, the *sign problem* (SP) can be a severe problem in lattice simulations (cf. Sec. 2.2.3). After reformulation of the partition function in the dual variables, we observe that it is appreciably eased though it is not yet fully understood why. This subsection presents the current state of knowledge about the SP.

First, the determinant is real for all configurations  $K$  such that  $e^{i\Im S} = \pm 1$ . Furthermore, it is exactly known which configuration contributes which sign. This can be proven as follows: From Sec. 3.3, we know that in the original formulation the theory is invariant under charge conjugation. After choosing a concrete realization of the  $\gamma$ -matrices as the PAULI matrices, we can use

$$\mathcal{C} = \begin{pmatrix} 0 & 1 \\ -1 & 0 \end{pmatrix} \quad (5.25)$$

as charge conjugation matrix. Now, we decompose the complex fermion fields into real MAJORANA-like [35] spinors  $\eta_1, \eta_2$  via

$$\psi = \eta_1 + i\eta_2, \quad \bar{\psi} = -(\eta_1^\top - i\eta_2^\top) \mathcal{C}. \quad (5.26)$$

The partition function can then be written in terms of these new spinors (implicitly assuming the spacetime integration, which is a sum on the lattice, in the exponent)

$$Z = \int \mathcal{D}\sigma \left( \prod_{r=1}^2 \mathcal{D}\eta_r \right) \exp \left( -\eta_r^\top (i\mathcal{C}\not{\partial} - i\sigma) \eta_r - \lambda\sigma^2 \right). \quad (5.27)$$

## 5 Lattice Results for $N_f = 1$

Now, we can proceed exactly as in the derivation of the dual formulation to arrive at

$$Z = \sum_{K \in \mathcal{K}} \int \mathcal{D}\sigma \left( \prod_{r=1}^2 \mathcal{D}\eta_r \right) \exp \left( -\eta_r^\top \left( i\mathcal{C}\phi[K] \right) \eta_r - \lambda\sigma^2 \right) \quad (5.28)$$

where we reformulated the partition function in terms of interaction point configurations  $K$  and introduced the reduced operator  $\phi[K]$  with removed rows and columns as above (cf. Eq. (5.8)). But now we see that the path integral factorizes because for both MAJORANA flavors we had to remove the same rows and columns. Thus, we see

$$Z = \sum_{K \in \mathcal{K}} \left[ \int \mathcal{D}\eta \exp \left( -\eta^\top \left( i\mathcal{C}\phi[K] \right) \eta \right) \right]^2 w(K) \quad (5.29)$$

and conclude by comparison with Eq. (5.10) that

$$\det iD[K] = \left[ \int \mathcal{D}\eta \exp \left( \eta^\top \left( -i\mathcal{C}\phi[K] \right) \eta \right) \right]^2. \quad (5.30)$$

For the following steps we introduce the short-hand notations  $U = -i\mathcal{C}\phi[K]$ ,  $\eta(x_i) = \eta_i$ ,  $l = (i, j)$  and expand the exponential

$$\sqrt{\det iD[K]} = \int \prod_{i=1}^V d\eta_i \sum_{j=1}^V \sum_{n_{i,j}=0}^1 \left( \eta_i^\top U_{ij} \eta_j \right)^{n_{i,j}} = \sum_{\mathcal{N}} \int \prod_{l_1=1}^V d\eta_{l_1} \left( \eta_{l_1}^\top U_l \eta_{l_2} \right)^{n_l} \quad (5.31)$$

where we exchanged summation and multiplication by summing over possible linking configurations  $\mathcal{N}$ . Now, the integrations factorize into closed loops  $\mathcal{L}$  because the integration at the end points of an open path will vanish. Hence, we can write

$$\sqrt{\det iD[K]} = \sum_{\mathcal{N}} \prod_{\mathcal{L} \in \mathcal{N}} W(\mathcal{L}) \quad (5.32)$$

with<sup>30</sup>

$$W(\mathcal{L}) = \int \left( \prod_{l=1}^L d\eta_l \right) \eta_1^\top U_1 \prod_{l=2}^L \left( \eta_l \eta_l^\top U_l \right) \eta_1 = -\text{tr} \prod_{l=1}^L \mathcal{C}U_l = -i^L \text{tr} \prod_{l=1}^L \phi[K]_l. \quad (5.33)$$

Now, there will be  $n_\nu$  links in direction  $\nu = 0, 1, 2$ . Every link in direction  $\nu$  contributes a factor  $\gamma_\nu$  to the product. Now, we can always reorder the  $\gamma$ -matrices

<sup>30</sup>Some words on the notation may be appropriate here: In Eq. (5.33), we enumerated the links from the loop  $\mathcal{L}$  to be  $l = 1, \dots, L$  such that  $l$  can be counted through. As an index  $l$  still means the tuple  $(i, j)$  for  $U$  and its first, resp. second, entry on the (transposed) spinor.

such that we have  $\gamma_\nu^{n_\nu}$  but every swap of two  $\gamma$ -matrices introduces a minus sign. After combining the product of swapping sign into  $\text{sgn}(\mathcal{L})$  we can write

$$W(\mathcal{L}) = -i^L \text{sgn}(\mathcal{L}) \left( \prod_{l=1}^L \partial[K]_l \right) \text{tr}(\gamma_0^{n_0} \gamma_1^{n_1} \gamma_2^{n_2}) \quad (5.34)$$

where  $\partial[K]_l$  means the  $l = (i, j)$  element of the reduced discrete partial derivative in use, i.e. the SLAC-derivative with the corresponding rows and columns removed<sup>31</sup>. Because  $\gamma_\nu^2 = \mathbb{1}$  we just have to consider  $n_\nu$  modulo two which yields only two non-vanishing cases

$$W(\mathcal{L}) = -2 \text{sgn}(\mathcal{L}) \left( \prod_{l=1}^L \partial[K]_l \right) \begin{cases} (-1)^{\frac{L}{2}} & n_0 = n_1 = n_2 = 0 \\ (-1)^{\frac{L-1}{2}} & n_0 = n_1 = n_2 = 1. \end{cases} \quad (5.35)$$

By  $L = n_0 + n_1 + n_2$  (not modulo two), we see that the exponent is integer-valued in both cases. We finally conclude that the determinant of  $iD[K]$  is the square of a real number and therefore positive. Hence, the partition function can be formulated as follows

$$Z = C \sum_{K \in \mathcal{K}} (-1)^{Vn} \det iD[K] \left( \frac{1}{2\lambda} \right)^{Vn} = C \sum_{Vn=1}^V (-1)^{Vn} \left( \frac{1}{2\lambda} \right)^{Vn} Z_n \quad (5.36)$$

using the interaction density  $n$  from Eq. (5.14) and grouping the configurations  $K$  into  $K(n)$ , denoting those with exactly  $k = 2Vn$  ones in it, and introduced

$$Z_n = \sum_{K(n)} \det(iD[K]). \quad (5.37)$$

In Eq. (5.36) we see that every configuration with an odd number of interaction points contributes a minus sign while every even configuration yields a positive contribution.

After the above discussion, we now know the, in general hard to determine, sign of each configuration. By this knowledge, it is now particularly easy to obtain the reweighting factor  $\langle e^{i\Im S} \rangle_{\Re S}$  from the relation

$$1 = \langle n_0 + n_1 \rangle = \frac{1}{\langle e^{i\Im S} \rangle_{\Re S}} \left( \langle n_0 e^{i\Im S} \rangle_{\Re S} + \langle n_1 e^{i\Im S} \rangle_{\Re S} \right) \quad (5.38)$$

(for a properly normalized partition function) where we have used the reweighting formulation from Eq. (2.17) in the last equation. Since  $e^{i\Im S}$  is known exactly on

<sup>31</sup>In this context, the removal is done by replacing the row/column by the corresponding row/column of  $\mathbb{1}$ .

every configuration, an exact reweighting hence requires just a simple normalization of  $\langle n_0 e^{i\mathfrak{S}S} \rangle_{\mathfrak{RS}} + \langle n_1 e^{i\mathfrak{S}S} \rangle_{\mathfrak{RS}}$ . This is no cure of the SP because it persists, hidden in the possibility that the expression in parentheses might be close to zero making the normalization numerically instable. However, we observed that the reweighting procedure actually does not affect any observable we used. We therefore suspect that there is a further argument why the SP could be more mild in this formulation. After all, we have an easy way to determine the reweighting factor and the reweighting procedure does not enlarge the statistical uncertainty significantly. Thus, the SP has no significant effect on the simulation results.

## 5.5 Results For Vanishing Temperature

We start with the results for vanishing temperature. Here, the only external parameter is the coupling  $g^2$  or equivalently  $\lambda$ . Though we will use mostly  $\lambda$  during the discussion, in accordance to the physical background we will stick to the term “strong coupling” for large  $g^2$  meaning small values of  $\lambda$ . It will turn out that the lattice model under investigation actually features two phase transitions, first the expected parity breaking “chiral” condensation and second a transition into a phase of strong lattice artifacts. They will be discussed successively starting with the expected one. The lattice simulations were performed as parameter scans in  $\lambda$  for all lattice sizes<sup>32</sup>  $V = L(L - 1)^2$  with  $L = 6, 8, \dots, 16$ .

### 5.5.1 Investigation Of The Physical Phase Transition

**The Local Chiral Condensate.** Fig. 5.3 shows the local condensate according to Eq. (5.13). One can clearly see that there is a non-vanishing condensate for strong couplings that vanishes continuously but not smoothly at a critical coupling  $\lambda_c$ . By these properties it fulfils all expectations about an order parameter for a second order phase transition. From the discussion of second order phase transitions in Sec. 2.1.1 we know that it then has a critical behavior

$$\Sigma_{\text{loc}} = \text{const.} \left( \frac{\lambda - \lambda_c}{\lambda_c} \right)^\beta + \dots \quad (5.39)$$

(cf. Eq. (2.1)). Thus, a fit of this form to a region close enough to the phase transition yields a good estimation of the critical coupling  $\lambda_c$  as well as the order parameter’s critical exponent  $\beta$ . The results from least squares fits can be seen in Fig. 5.7, resp. Fig. 5.4.

As expected, the usage of a finite lattice introduces deviations. Unfortunately, for the local quantities there is no FSS theory available to describe their behavior.

<sup>32</sup>As discussed in [16], the correct boundary conditions need an even number of lattice points in temporal direction and odd number of points in spatial directions.



However, under the assumption that the overall scaling behavior is sufficiently monitored by these 6 lattice sizes, the smoothness of the values for the critical coupling admits a naive fit via an ansatz

$$\lambda_c(L) = \frac{\text{const.}}{L^\kappa} + \lambda_c(L \rightarrow \infty) \quad (5.40)$$

where  $\kappa$  is some exponent and the offset  $\lambda_c(L \rightarrow \infty)$  is an extrapolation to the infinite lattice. Even without the exact FSS arguments, this should be at least reasonable as an expansion to lowest order. The extracted critical coupling is then given by

$$\lambda_c^{(\Sigma_{\text{loc}})} = 0.1268(1). \quad (5.41)$$

To the best of our knowledge, the only other published value of this coupling is a MC result on a  $16 \times 15 \times 15$  lattice from [51] with<sup>33</sup> 0.130(3). This is consistent, though less precise, with our estimates.

The critical exponents (Fig. 5.4) do not show such a monotonic behavior. Instead, it seems that they are fluctuating around their exact value. This shows that the local variables capture important physical aspects much better than typical for global quantities. Presumably, this is the case because the order parameter exactly vanishes at the (finite lattice) critical coupling and can therefore monitor the behavior close to the critical point much better.<sup>34</sup> As a rough estimate from Fig. 5.4 one could use the mean of the extracted exponents

$$\beta = 0.406(8). \quad (5.42)$$

To the best of our knowledge there is only one other publication including values for the critical exponents in  $N_f = 1$ : NOWAK et al. [53] use functional renormalization group methods to derive the flow equations and calculate critical exponents from that. Since they use a variety of methods differing in technical details they find four values  $\beta = 0.406, 0.407, 0.411, 0.420$ . Our findings agree almost perfectly with their lower values.

**The Local Susceptibility.** A similar evaluation can be done for the local susceptibility (Eq. (5.15)) shown in Fig. 5.5. It is only reasonably defined for couplings

<sup>33</sup>For comparison, one has to switch from the TH inverse coupling  $\lambda_{\text{TH}} = 3\lambda$  to the GN inverse coupling as used in this thesis.

<sup>34</sup>The estimates for this critical exponent should be compared to the results for  $\beta_n$  from the global quantity  $n$  (cf. Fig. 5.8(b)) which are far off from the conjectured correct value for small lattices and show a clearly monotonic behavior. The latter estimates were also obtained from direct fits to an order parameter which, in contrast, did not vanish exactly in one of the phases.

5 Lattice Results for  $N_f = 1$

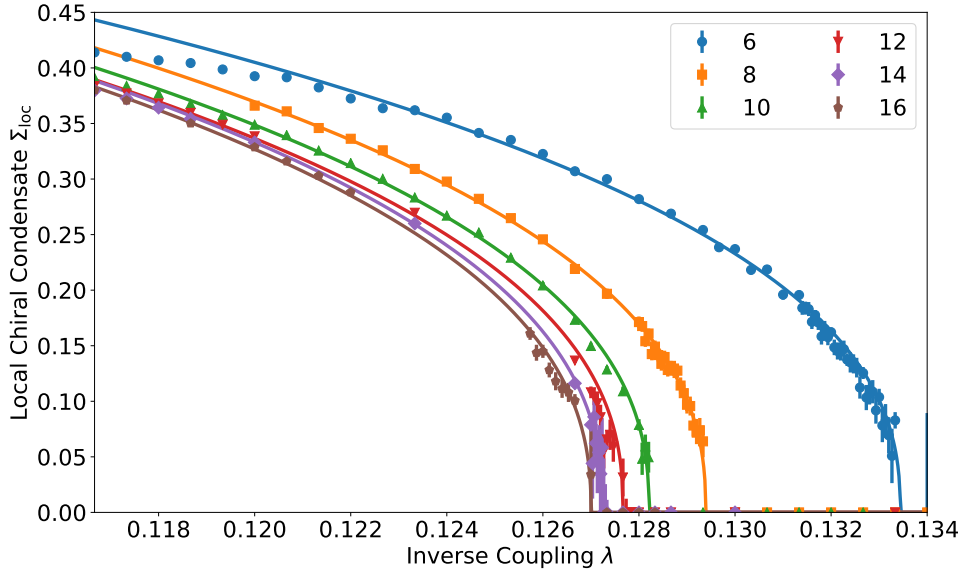


Fig. 5.3: Local condensate according to Eq. (5.13) for various linear lattice sizes  $L$  over the inverse coupling  $\lambda$  with fits (solid lines) according to Eq. (5.39).

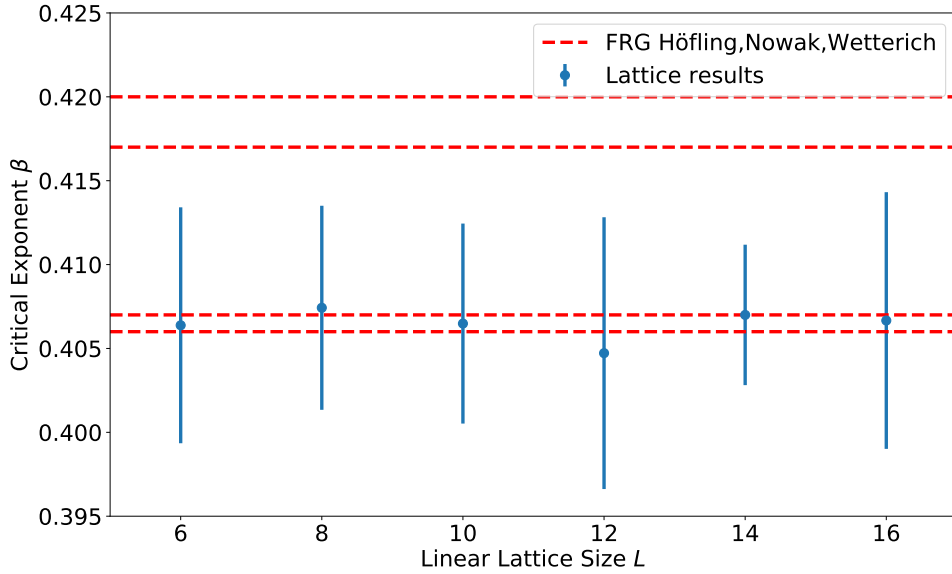
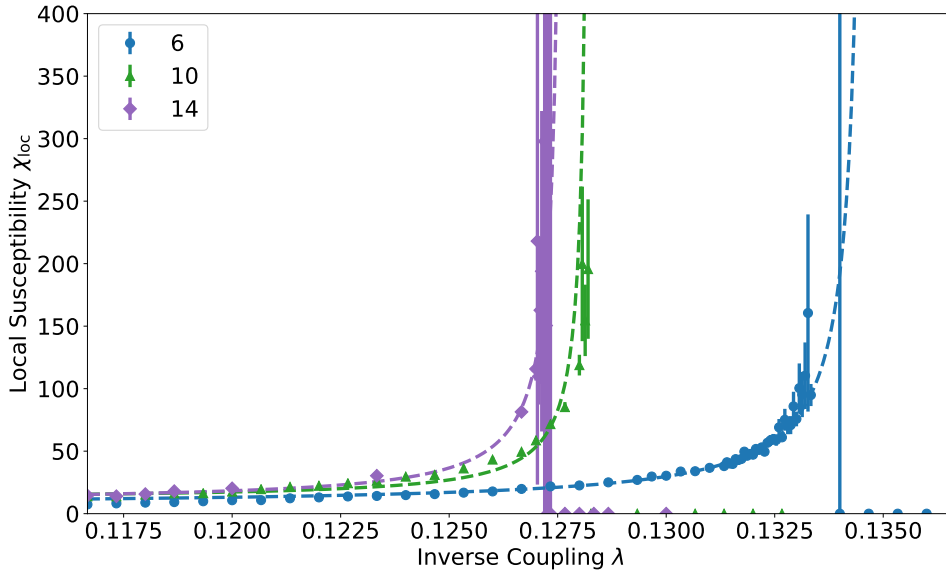
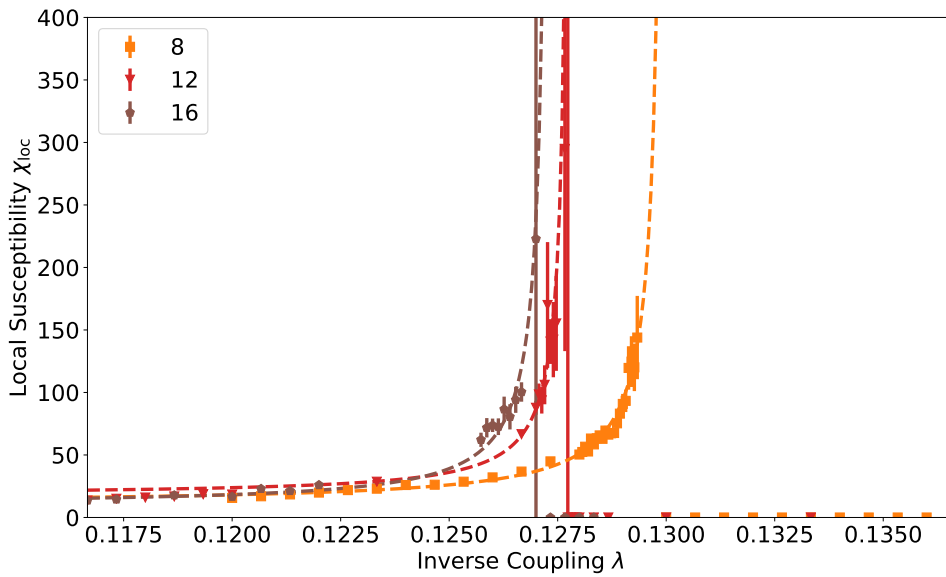


Fig. 5.4: Critical exponent  $\beta$  from the local condensate (Eq. (5.13)) as a result of the fits according to Eq. (5.39) in Fig. 5.3. In dashed lines, the values from [53] are given (cf. text).

## 5.5 Results For Vanishing Temperature



(a) Linear lattice sizes 6, 10, 14.



(b) Linear lattice sizes 8, 12, 16.

Fig. 5.5: Local susceptibility for various linear lattice sizes  $L$  over the inverse coupling  $\lambda$  with fits (dashed lines) according to Eq. (5.43). For the sake of readability, the data has been split into two subfigures. As discussed in Sec. 5.2, the uncertainty in the data becomes huge close to criticality.

## 5 Lattice Results for $N_f = 1$

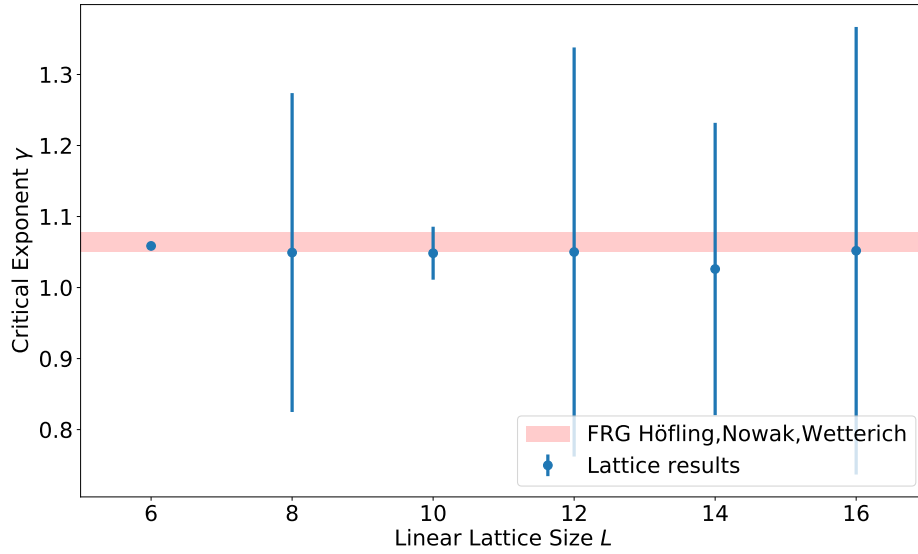


Fig. 5.6: Critical exponent  $\gamma$  from the local susceptibility as a result of the fits according to Eq. (5.39) in Fig. 5.5. The shaded area indicates the range of the values from [53] (cf. text). It must be stressed here, that the fits were very unstable and that the results should not be trusted more than the errorbars indicate (despite the seemingly better agreement).

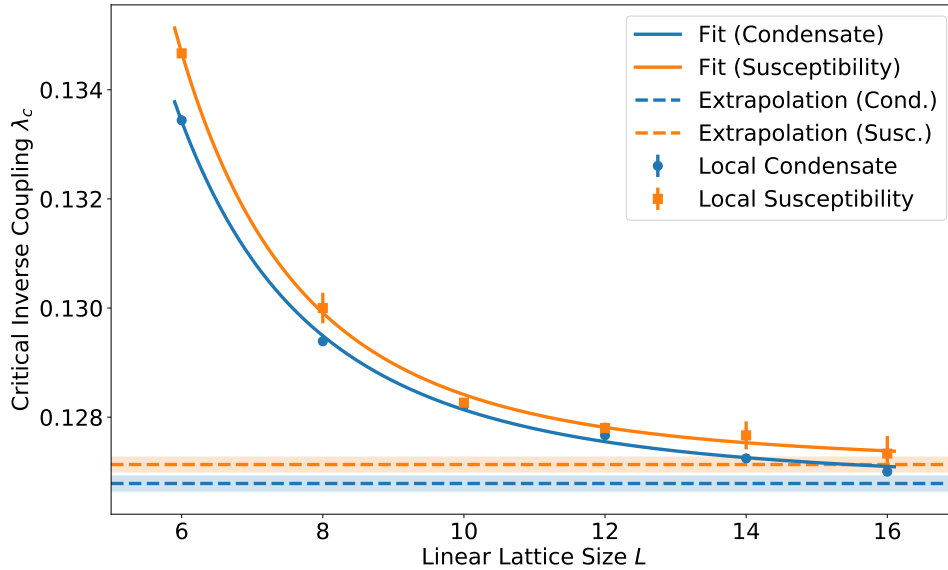


Fig. 5.7: Critical coupling  $\lambda_c$  over the linear lattice size  $L$  from the fits in Fig. 5.3 and Fig. 5.5.

lower than the ( $L$ -specific) critical value and divergences when approaching it from the left. To the right, we set it to zero as follows from Eq. (5.13). Its critical behavior can therefore be fitted as

$$\chi_{\text{loc}} = \text{const.} \left( \frac{\lambda - \lambda_c}{\lambda} \right)^{-\gamma} \quad (5.43)$$

from which we again extract an estimation for the critical coupling  $\lambda_c$  and its critical exponent  $\gamma$ . This behavior is qualitatively well fulfilled by the data of Fig. 5.5. However, as discussed during its introduction, statistical fluctuations gain importance in the region close to the critical coupling making the data very noisy in this region. Nevertheless, the fitting of Eq. (5.43) to the data yields results very consistent with the available sources for comparison (cf. Fig. 5.7 and Fig. 5.6).

The critical coupling derived from the local susceptibility is also depicted in Fig. 5.7. By the same means as above, we find

$$\lambda_c^{(\chi_{\text{loc}})} = 0.1271(1). \quad (5.44)$$

This is very close to the result from the local condensate though the uncertainties do not overlap.

The susceptibility's critical exponent  $\gamma$  is shown in Fig. 5.6. For this parameter, the fits were particularly instable which results in large errorbars. Apart from this instability, the extracted exponents show a similar behavior to those from the local condensate, i.e. fluctuations around the exact value. A rough estimate from Fig. 5.6 yields<sup>35</sup>

$$\gamma = 1.05(30). \quad (5.45)$$

Again, there are values for comparison only from [53]. In fact, for  $\gamma$  they find tiny deviations comparing the limiting from the symmetry broken, resp. restored, phase. But by general arguments [14] they should agree on both sides yielding now 6 values<sup>36</sup> in the range 1.050...1.077 to compare to. As before, the results almost perfectly agree. If one would neglect the large uncertainty of this value, one could again argue that the results are in favor of the lower values from [53]. However, from the particularly noisy data this conclusion cannot be stated reliably.

**The Global Quantities.** Results from the global quantities defined in Eq. (5.16) to Eq. (5.20) are shown in the next subsection (see Fig. 5.8(a) to Fig. 5.11). In fact, it seems that none of them shows distinguished behavior at the parity breaking

<sup>35</sup>Here, we included a second significant digit into the result for better comparison with the literature.

<sup>36</sup>Actually, they find 8 values of which two pairs agree.

phase transition that is indicated by the local quantities. Nevertheless, they all point to a second order phase transition that will be discussed in the following subsection.

There is the remote possibility that the extrapolations for estimating the location of the parity breaking phase transition (Eq. (5.41) and Eq. (5.44)) are far from reality because the lattice sizes  $L = 6, \dots, 16$  hide some important behavior. But in regards to the excellent agreement with the findings from [53], it seems highly unlikely that significant finite size effects are concealed from this discussion.

### 5.5.2 Investigation Of The Lattice Artifact Phase Transition

As discussed above, the global observables defined in Eq. (5.16) to Eq. (5.20) do not respond to the parity breaking transition expected in the model. Nevertheless, they do show interesting behavior: Both BINDER parameters  $U_n$  (Eq. (5.17)) and  $U_\sigma$  (Eq. (5.19)) as well as the  $n$ -susceptibility  $\chi_n$  (Eq. (5.16)) exhibit the typical forms indicating a second order phase transition [14]; namely, these are a unique, (up to higher orders)  $L$ -independent crossing point of the BINDER cumulants and a – with increasing  $L$  rising and sharpening – peak of the susceptibility. This is clear evidence for another phase transition. Since two of the three discussed observables are directly related to  $\langle n \rangle$ , it seems natural to assume that this could be an order parameter for this transition.

This additional phase transition occurring only in the lattice formulation of the theory is already known in the literature [54] and called *lattice artifact phase* (LAP). The latest interpretation of this is given by [16, 51]. It makes use of the *lattice filling factor*  $k$  – as they call it – resp. its density  $n$  (cf. Eq. (5.14)). There it is argued that the additional phase occurs when the coupling becomes so strong that the interactions on the lattice outnumber the points with free dynamics. In this subsection, we will go into more detail about this and determine the locality of this transition.

**Mathematical Discussion.** The dual formulation used in this thesis provides already a lot of insight on this problem. To get started, we recover some basic properties of the model: It is intuitively clear that for  $g^2 \rightarrow 0$  we will recover free fermions and for  $g^2 \rightarrow \infty$  the lattice will get filled up with interactions and the free dynamics will be further and further suppressed. In the dual formulation (Eq. (5.10)) this can be stated as follows. For  $g^2 \rightarrow \infty$  we have, by  $w(K) = (-1)^{Vn} g^{2Vn}$  (Eq. (5.9)),

$$Z(g^2) = C \sum_n (-1)^{Vn} g^{2Vn} Z_n \rightarrow C (-1)^V g^{2V} Z_1 \quad (5.46)$$

with  $Z_n$  from Eq. (5.37). It should be stressed here that  $Z_n$  will strongly depend on  $V$  but does not depend on  $g^2$  at all. For arbitrarily strong coupling, all but

## 5.5 Results For Vanishing Temperature

the highest order in  $g$  are suppressed justifying the last limit in Eq. (5.46). Thus,  $\langle n \rangle \rightarrow 1$  for  $g \rightarrow \infty$ . Furthermore,  $Z_1 = 1$  and no fermion dynamics take place. This can be interpreted as the whole lattice being blocked by interactions. A similar argument for  $g^2 \rightarrow 0$  leads to completely free dynamics, i.e.  $\langle n \rangle \rightarrow 0$  and  $Z(g^2) \rightarrow CZ_0$ , as expected. This could have been also seen from the original formulation.

Now, consider the second limiting case  $V \rightarrow \infty$  at fixed  $g^2 > 1$ . We always know that the completely filled lattice has  $Z_1 = 1$ . For partial filling, there are two possibilities: First, there might be an  $n < 1$  such that  $Z_n$  can compensate the suppression by  $g^{2V(n-1)}$ . Such terms lead to significantly contributing configurations with  $n < 1$  and hence  $\langle n \rangle < 1$ . Second, if for no  $n < 1$  the terms  $Z_n$  compensate the suppression, we have  $\langle n \rangle = 1$  for all couplings larger than  $g^2$ . The second case will be called LAP and we know that

$$\lim_{V \rightarrow \infty} Z_n g^{2V(1-n)} = 0 \quad (5.47)$$

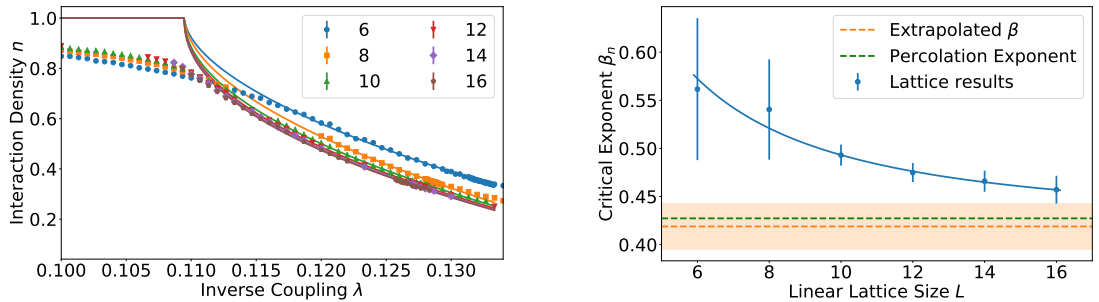
for all  $n < 1$  there. What scenario we are in, may depend on the concrete value of  $g^2$  and there could be a critical  $g^2$  where a transition may happen. A similar result can also be obtained from a strong coupling expansion as done in [51]: In the region of validity of such an expansion it can be shown that observables – particularly  $\langle n \rangle$  in our case – does not depend on  $\lambda$  in the infinite volume limit. From the first discussion, one can then conclude that  $\langle n \rangle = 1$  in the region of validity. Unfortunately, there is no reasoning in [51] nor known to us that the strong coupling expansion should be valid for any finite  $g^2$ .

Since we do not see any (feasible) method to compute  $Z_n$  analytically, lattice simulations are in need to explore which scenario holds. Since only after the limiting procedure the above discussion applies strictly, the lattice results will not show exactly  $\langle n \rangle = 1$  in the LAP but a slightly smaller value where the corrections from the  $n$ -term are suppressed by  $g^{2V(n-1)}$  which is finite before limiting.

**Lattice Results.** In Fig. 5.8(a) the interaction density  $n$  is shown. One could conjecture that it approaches 1 in the strong coupling limit for all lattice sizes which was argued in the previous paragraph. Additionally, there are two distinct regions where  $\langle n \rangle$  is increasing, resp. decreasing, with growing volume. This suggests that there is indeed a finite critical coupling at which the transition to the LAP happens. This transition should then be the (up to higher orders)  $L$ -independent crossing point of all  $U_n(L)$  and the point of divergence of  $\chi_n$  in the infinite volume limit. These quantities are shown in Fig. 5.9(a) and Fig. 5.10, respectively.

The first question to ask is of what order the phase transition is. In [55], an exemplary discussion of the form of BINDER cumulants for first and second order

## 5 Lattice Results for $N_f = 1$



(a) Interaction density  $n$  over the inverse coupling  $\lambda$  for various linear lattice sizes  $L$  with fits (solid lines) according to Eq. (5.50).

(b) Critical exponent  $\beta_n$  of the LAP transition as obtained from the fits to Fig. 5.8(a).

Fig. 5.8: Lattice results concerning the interaction density  $n$  (Eq. (5.14)).

transitions can be found. By comparison with the data from Fig. 5.9(a) we conclude that this must be a second order phase transition, since we already know that  $\langle n \rangle$  is the order parameter of the transition. Its susceptibility Fig. 5.10 also shows the typical behavior as to be compared e.g. with [21]. Nevertheless, we will focus the discussion on the BINDER parameter because a detailed analysis from the poor resolution and statistics obtained for the susceptibility would not be very conclusive.

After the order of the transition is known, we can use the techniques from FSS, particularly the fact that the BINDER parameter exactly at the critical point is (up to higher orders) independent of the lattice size<sup>37</sup>. In Fig. 5.9(a) this behavior is clearly seen to happen around  $\lambda \approx 0.11$ . To get a more precise estimate, we include higher orders into the discussion. As stated in [16], the scaling of the BINDER cumulant's crossing points  $\lambda_c(b)$  should then obey

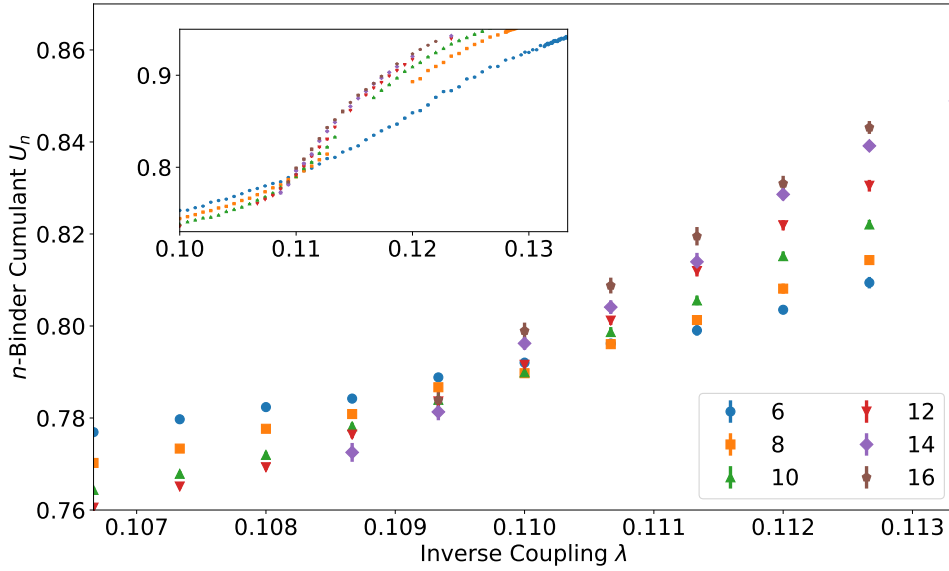
$$\lambda_c^{-1}(b) \approx \lambda_c^{-1}(L \rightarrow \infty) + \frac{\text{const.}}{\ln b} \quad (5.48)$$

if we compare the BINDER crossing points between results from  $L_0$  and  $L = bL_0$ . This analysis is carried out in Fig. 5.9(b) by the means described in Sec. 5.3 where we use  $I = [0.1093, 0.1126]$ . The points for  $L_0 = 6$  still show some higher orders' influence, particularly for  $L = 8$ , i.e. the rightmost point (which is therefore omitted in the fit). But all other points can almost perfectly be extrapolated via

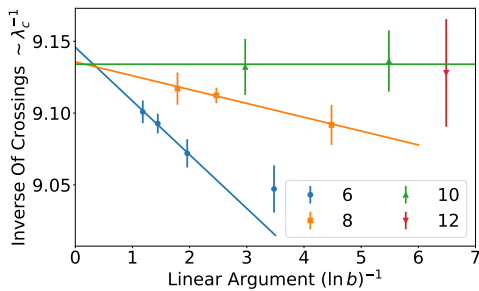
<sup>37</sup>A subtlety arises here: Due to the different lattice sizes in temporal and spatial direction, it is unclear which value to use for  $L$  in the formulae. But [16] finds that the actual choice does not matter and we checked this statement carefully. Since we also found that this does not affect the result, we will stick to the naive definition as used above.



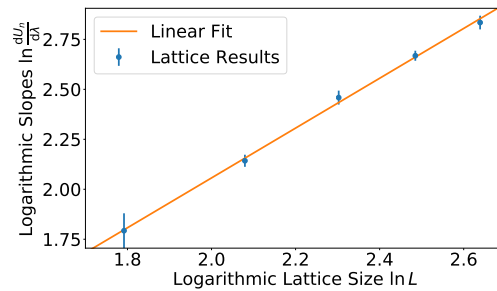
## 5.5 Results For Vanishing Temperature



(a) The  $n$ -BINDER cumulant over the inverse coupling  $\lambda$ . The inset shows a broad scan while the main graphic is zoomed into the crossing.



(b) The inverse  $n$ -BINDER crossing points over the linear argument  $(\ln b)^{-1}$  according to Eq. (5.48). For various reference lengths  $L_0$  the crossing points with all results from larger lattices have been taken and fitted linearly (solid lines).



(c) The logarithmic slopes of the  $n$ -BINDER cumulant over the logarithmic lattice size  $\ln L$ . According to Eq. (5.52), the slope of the linear fit corresponds to  $\frac{1}{\nu}$ .

Fig. 5.9: Lattice results concerning the BINDER cumulant in  $n$  according to Eq. (5.17).

## 5 Lattice Results for $N_f = 1$

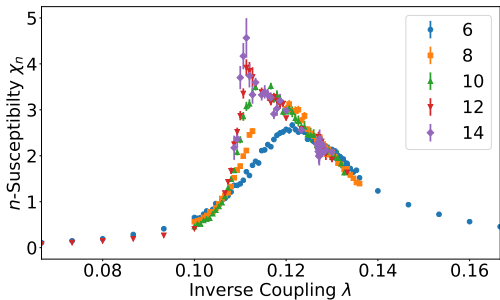


Fig. 5.10: The  $n$ -susceptibility over the inverse coupling  $\lambda$  for various linear lattice sizes  $L$ .

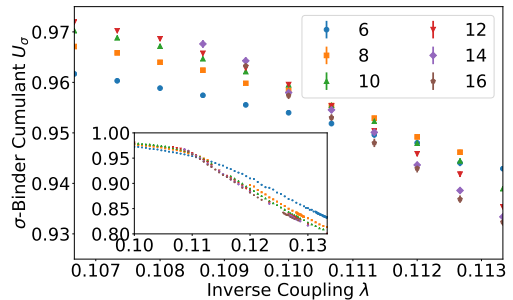


Fig. 5.11: The  $\sigma$ -BINDER parameter over the inverse coupling  $\lambda$  for various linear lattice sizes  $L$ . Unexpectedly, its crossing is at the LAP transition and not at the parity breaking transition.

Eq. (5.48) yielding<sup>38</sup>

$$\lambda_c^{(\text{artifact})} = 0.10946(3). \quad (5.49)$$

This is also estimated in [51] on an  $8 \times 7 \times 7$  lattice where  $0.116(3)$  was found. In fact, this result could have also been anticipated from the autocorrelation times discussed in Sec. 5.3 (cf. Fig. 5.2). As [14] states, for a second order phase transition the autocorrelation time of simple local algorithms, like the Metropolis in use here, scales according to  $\tau^{-\nu z}$  for some  $z$  usually  $\sim 2$ . Thus, the strongest autocorrelations appear close to the critical point. By the same reasoning as for the FSS theory of observables, this translates also to a behavior like  $L^z$  if  $L \ll \xi$ , explaining also the dependence on the lattice size  $L$ .

Finally, from the data we can extract various critical exponents. Since the LAP transition's order parameter is  $n$ , we will denote all exponents for this transition with a subscript  $n$  to be distinguishable from the results for the parity breaking transition. These can then be used to identify the universality class of the phase transition and give a hint on the continuum model that will be obtained from the continuum limit at this critical point. First, from a naive fit

$$\langle n \rangle = 1 - \text{const.} (\lambda - \lambda_c)^{\beta_n} \quad (5.50)$$

to the finite- $L$  data we can extract

$$\beta_n = 0.42(2) \quad (5.51)$$

<sup>38</sup>This is the result of  $L_0 = 8$  because for  $L_0 = 6$  the finite size effects seem comparably large and for  $L_0 = 10$  a fit between two points does not yield reliable uncertainties.

(cf. Fig. 5.8(b)). In this formula we fixed  $\lambda_c$  to its value from the BINDER crossing point analysis above and extrapolated naively to infinite volume.<sup>39</sup> Second, the correlation length critical exponent  $\nu$  can be obtained via the scaling behavior of

$$\ln \frac{\partial U}{\partial \lambda}(L) = \frac{1}{\nu_n} \ln L + \text{const.} \quad (5.52)$$

as stated in [16].<sup>40</sup> To obtain the slope of  $U$ , we again use Eq. (5.23). The results can be seen in Fig. 5.9(c) and the linear fit yields

$$\nu_n = 0.80(4). \quad (5.53)$$

The last question to answer is if a universality class with these critical exponents is known. Since the above analysis was only of moderate precision, we do not expect to find a perfect match. Nevertheless, the results are in good agreement with the  $D = 3$  percolation universality class with its exponents [56]

$$\beta_{\text{Perc.}} = 0.4273, \quad \nu_{\text{Perc.}} = 0.8960. \quad (5.54a)$$

Percolation theory is concerned with the dynamics of stochastic clusters [57] which seems reasonable from the point of view that we indeed describe the dynamics of stochastically distributed interaction points in the dual formulation. But an investigation if these form clusters such that there could be a direct interpretation as percolation is out of the scope of this thesis. Nevertheless, it should be mentioned that a connection to percolation theory can also be observed in other lattice models like  $SU(3)$  gauge theory [58] or the ISING model [59].

## 5.6 The Phase Diagram Of Gross-Neveu

In this subsection, we will present first results about the phase diagram in the  $T$ - $\lambda$  plane. This is still work in progress and mainly intended to document the current state. Therefore, the data might be noisier and sparser as desirable and the results and interpretations a little less conclusive than the scientific standard requires. Nevertheless, we will gain some interesting insights here to build on in further research.

### 5.6.1 Preliminary Discussion

As already mentioned when introducing the EUCLIDEAN formulation, temperature is varied by compressing the (imaginary) time direction of the lattice, usually via

<sup>39</sup>This is done as in the analysis of  $\lambda_c$  for the other transition.

<sup>40</sup>As before, we use  $L$  as dimensionless quantity. If  $L$  means a physical length, one should change  $L \rightarrow \frac{L}{L_0}$  for some reference length  $L_0$ .

## 5 Lattice Results for $N_f = 1$

changing the number of points  $L_t$  in this direction. Unfortunately, there is not much freedom to do this for us because the computational cost of the algorithm restricts us to small lattices up to  $L = 16$ . Additionally, a parameter scan in two parameters needs much more data points.

Instead, we will restrict ourselves to medium sized lattices but introduce an asymmetry that further compresses the temporal direction. Concretely, we use  $L \in \{9, 11, 13\}$  spatial lattice points and  $L_t \in \{2, 4, 6, 8\}$  temporal points and vary  $c_T = \frac{a}{a_t}$  where  $a$  is the spatial lattice spacing (set to one as always) and  $a_t$  is the temporal lattice spacing. Thus, we find that the physical temperature is given by

$$\tilde{T}(L_t, \lambda) = \tau(L_t, \lambda) \frac{c_T}{L_t} \quad (5.55)$$

where the fraction is the inverse temporal extent (in units of  $a$ ) and  $\tau$  denotes the a priori unknown relation between lattice units and physical units. Typical means of investigating this relation are measuring masses (and relating them to physical ones) or the peak of the susceptibility. Unfortunately, for the physical phase transition we only have the local susceptibility that has no finite peak height and in a short investigation no (in both phases) non-vanishing masses were found. Thus, an independent determination of  $\tau$  was not possible during the restricted period of work for this thesis. For starters, we set  $\tau = 1$  keeping in mind that the such defined temperature

$$T = \frac{c_T}{L_t} \quad (5.56)$$

is no physical quantity and the same value of  $T$  does not necessarily imply the same physical temperature on different lattices. Furthermore, by introducing an explicit asymmetry the spacetime integration measure is changed. This can be compensated by including a factor<sup>41</sup>  $\sqrt{aa_t}$  into the fermion fields but implies a rescaling of the inverse coupling by<sup>42</sup>  $c_T a$ .

It should be stressed particularly that the above approximation via an asymmetric lattice is only reliable in the medium and high temperature regime because in the low temperature regime we have  $a_t = \frac{a}{c_T} \rightarrow \infty$ . This tells us that the discretization errors will become huge in the limit  $c_T \rightarrow 0$ . It is actually more appropriate to think about this limit as simulating  $L_t$  independent slices of a 2-dimensional model with periodic boundary conditions in both directions.

For technical reasons it was more convenient to scan small rectangles in  $c_T$  and the *unscaled*  $\lambda$ . Thus, the resolution in  $\lambda$  becomes higher with decreasing temperature but this was taken care of by additional finer scans in the high temperature

<sup>41</sup>This is true for dimensionful fermion fields. If a factor of  $a$  was already included to get dimensionless fields, the factor is  $\sqrt{\frac{aa_t}{a}} = \sqrt{c_T}$ .

<sup>42</sup>As before, this would only be  $c_T$  if the fermion fields are already dimensionless.

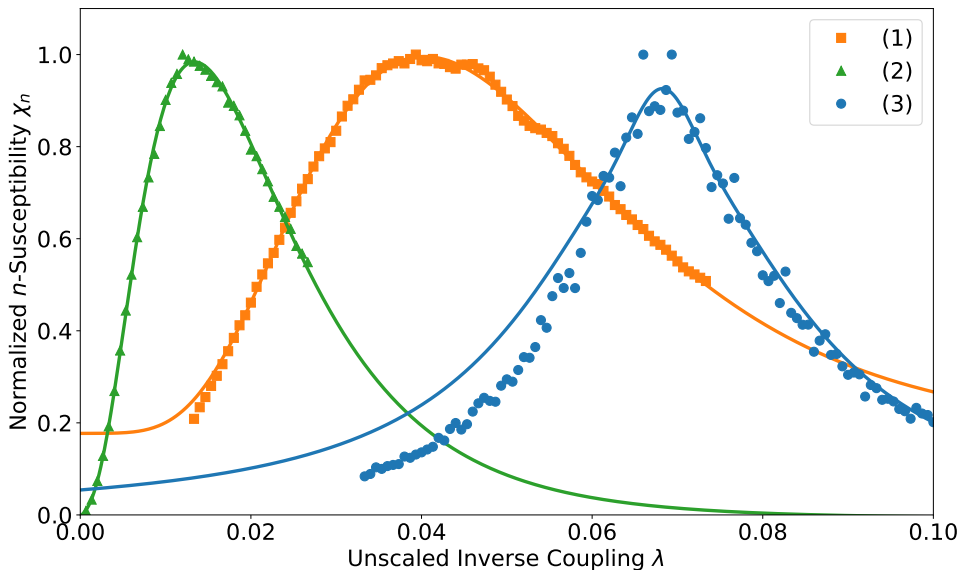


Fig. 5.12: Three examples of fits (solid lines) to determine the maximum of the susceptibility at fixed temperature in the unscaled  $\lambda$ . Since the purpose of this procedure was to determine precisely the peak position, some deviations between fit and data away from the peak were accepted. (1)  $c_T = 2.8$  on a  $2 \times 9 \times 9$  lattice fitted with a linear combination of Eq. (5.58) and Lorentzian shape. (2)  $c_T = 5.4$  on the same lattice fitted only with Eq. (5.58). (3)  $c_T = 2.0$  on a  $4 \times 9 \times 9$  lattice fitted with a linear combination of GAUSSIAN and LORENTZIAN function.

regime. Afterwards, the critical coupling at fixed  $T$  was estimated as the mean between the first vanishing condensate and the last non-vanishing condensate. The error bars given in Fig. 5.13 indicate the range between these two points of measurement.

Additionally, one should keep in mind that the physically relevant quantity is actually not the lattice parameter  $\lambda_c$ . As shown in [60], the renormalized coupling becomes zero at (and negative beyond) the LAP transition. It is thus more appropriate to think in terms of

$$\tilde{\lambda} = \lambda_c - \lambda_c^{(\text{artifact})} \quad (5.57)$$

to describe physics that could be related to continuum physics. That, combined with the possibility that the critical line might run into the LAP during our simulations, is why we will also scan for the LAP transition to get at least some notion about the relation of the two. On a finite lattice, this transition is indicated by the maximum of the  $n$ -susceptibility (Eq. (5.16)). As already found in

the  $T = 0$  analysis, this can be clearly made out if the resolution is large enough and provides means for locating the transition with a single lattice (as opposed to the more precise but also much more time-consuming BINDER analysis). At fixed  $T$ , we then extract the position of the maximum by one of the following methods:<sup>43</sup> The method of choice was fitting a medium sized region  $R$  around the maximal point  $\lambda_{\max}$  by a function  $f(\lambda)$ . Its details strongly depended on the shape of the peak and all the fits were faithfully adjusted by hand to give the most precise and reliable result. Some examples of data and fits are shown in Fig. 5.12. Generally, we varied the following parameters: The fit region was chosen to be  $[\lambda_{\max} - \Delta\lambda, \lambda_{\max} + \Delta\lambda]$  with the width  $\Delta\lambda$  chosen to include the upper approximately 20-40% of the peak. Various fit functions were used, including a linear combination of GAUSSIAN and LORENTZIAN shaped functions (with shared peak location) and for the more asymmetric peaks a shape proposed in [61] (in the form given in [62])

$$f(\lambda) = A \exp \left[ -\frac{\ln 4}{2 (\ln z)^2} \left( \ln \frac{x_m - \lambda}{x_m - \lambda_0} \right)^2 \right] + \text{const.} \quad (5.58)$$

$$x_m = \lambda_0 - \frac{z + z^{-1}}{2\Delta}, \quad z = \sqrt{h|\Delta| + \sqrt{h^2\Delta^2 + 1}}$$

with constant offset  $\text{const.}$ , full width at half maximum  $h$ , asymmetry parameter  $\Delta$  and peak location  $\lambda_0$  (in some cases linearly combined with a Lorentzian shape with shared peak at  $\lambda_0$ ). If a successful combination of initial guess, functional dependence and fit range was found, this usually gave a precise and reliable estimate. Otherwise, we fell back to a method similar to the determination of the physical critical line, i.e. the maximal point was chosen as critical one and its distance to the second highest point as uncertainty. This last methods yields just a rough estimate and was avoided where possible. Particularly, it introduces characteristic artifacts that will also be seen for the parity breaking critical line at poor resolution: If the unscaled  $\lambda_c(c_T)$  varies only slowly in  $c_T$  the such determined critical line will be parallel to the  $T$ -axis. Thus, in the correctly scaled critical coupling will have a saw-tooth shape where the artifact parts all point to the origin (see e.g. the high temperature regime of  $2 \times 11 \times 11$  in Fig. 5.14(a)). In Fig. 5.12, one can also see another problem with this method: While it needs relatively few statistics to determine whether or not the chiral condensate is zero, fluctuations in the maximum make it hard to determine the precise location with such a naive approach. The example (3) shows two nearly equal maxima in the data while none of them seems to be at the center of the peak as estimated by eye. In contrast,

<sup>43</sup>The choice of the method was done by hand for every temperature slice and the appropriateness of the result was checked by eye for every point.

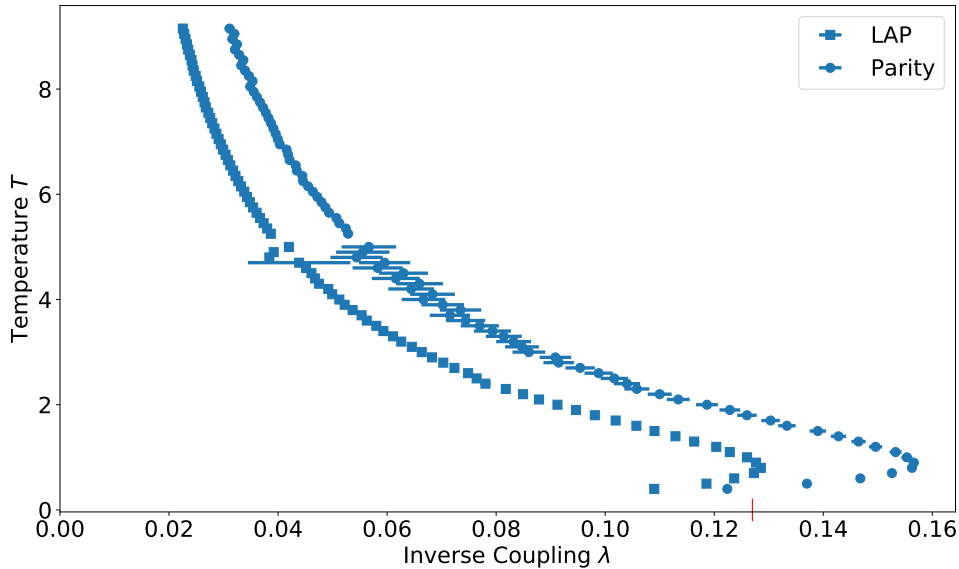


Fig. 5.13: Phase diagram in the  $T$ - $\lambda$  plane with the critical line of the parity breaking transition and the critical line of LAP transition on a  $2 \times 9 \times 9$  lattice. The leftmost region is the LAP, the rightmost region is the phase of restored symmetry. In between, the physical phase with broken symmetry is found. The red extra tick on the  $x$ -axis indicates the  $\lambda_c(T = 0)$  from Eq. (5.41).

the fit finds the center pretty well though it is only a rough approximation at the wings.

### 5.6.2 Results

The critical lines obtained from a scan in  $\lambda$  and  $c_T$  on a  $2 \times 9 \times 9$  lattice can be seen in Fig. 5.13. For all lattices the critical line is qualitatively the same (cf. Fig. 5.14, 5.15 and 5.16). For  $c_T \rightarrow 0$ , the curves all go to  $\lambda_c = 0$ . As already discussed, this is not the limit  $T \rightarrow 0$ . In fact, from the first lattice results (Sec. 5.5) we already know that there should be a finite critical coupling  $\lambda_c(T = 0) \approx 0.127$ . Instead, one finds that the unscaled critical coupling becomes roughly constant for sufficiently small  $c_T$  and therefore the correctly scaled critical lines approach the origin in an almost linear fashion. However, we see that a larger temporal extent reduces this artifact in  $T$ .<sup>44</sup> As a side remark we note that the hypothetical theoretical model on the decoupled spatial slices at  $c_T \rightarrow 0$  seems to have both phase transitions (LAP and parity breaking) at finite coupling.

<sup>44</sup>This is clearly expected because the unreliable region of  $c_T$  should stay approximately constant while the denominator in Eq. (5.55) becomes larger.

## 5 Lattice Results for $N_f = 1$

Above this obviously unphysical region, one observes a bump in the critical line that (at least for the small to medium lattice sizes in use) extends beyond the  $T = 0$  critical coupling. If this would hold for all lattice sizes this would imply that the critical line approaches the limit  $T \rightarrow 0$  from high  $\lambda$  and the maximal critical coupling  $\lambda_c(T)$  would not be observed for  $T \rightarrow 0$ . Alternatively, one could imagine that this is a finite size and discretization artifact that vanishes for sufficiently large lattices. In this case, the critical coupling would become constant or even slightly increasing with decreasing temperature. As can be seen in Fig. 5.16<sup>45</sup> this bump reduces its extent for a larger number of temporal points. This could be seen as evidence for the latter scenario. However, the currently available data does not allow any final conclusion on this.

In the high temperature regime, the situation is clearer: For every probed temperature, we found a phase transition in  $\lambda$ . For increasing temperature the critical line approaches  $\lambda = 0$ . This is physically plausible when compared to the typical toy models for symmetry breaking, e.g. the ISING model where maintaining an order at higher temperature also needs a stronger coupling [17]. As an open question, it remains whether or not there is a maximal critical temperature as in the large- $N_f$  case. However, to answer this question (at least negatively) lattice simulations might not be the way to go because with this method one can only probe discrete temperatures in a finite range and from this it is never possible to exclude a crossing of  $\lambda = 0$  for *all* temperatures. One should again stress at this point that for all probed temperatures a phase transition at finite coupling was found. This implies that there is a small coupling regime where no broken phase exists at any temperature.

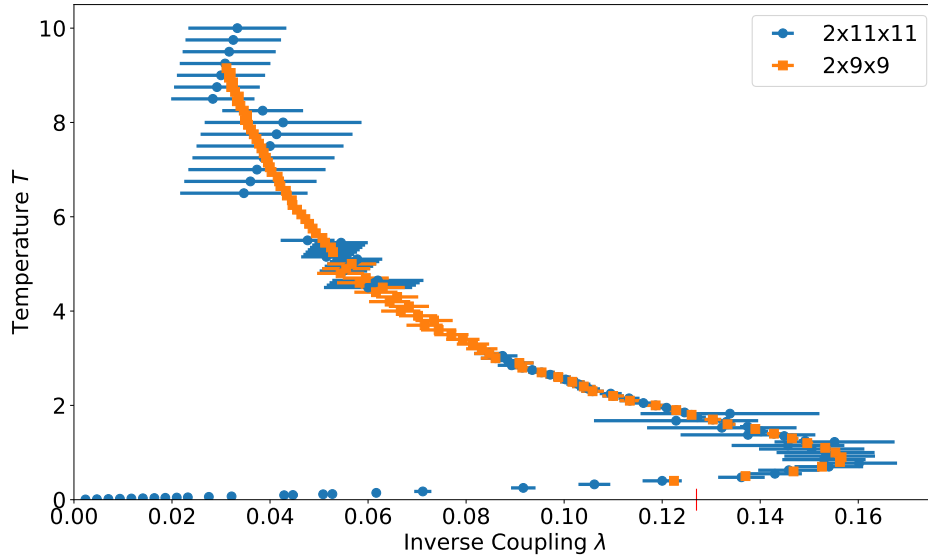
After this discussion of the similarities, we will now focus on the differences between the various lattice sizes. In Fig. 5.14 the critical lines for fixed temporal extent are shown. It can be seen clearly that the extracted critical lines are identical within the given resolution (which is admittedly poor for the larger lattices). We thus conclude that the spatial extent is chosen large enough to capture the qualitative and quantitative behavior according to the given resolution. Concerning the temporal extent, this cannot be said. With increasing number of temporal points the critical line is significantly moved towards smaller temperatures as can be seen in Fig. 5.15 and Fig. 5.16. This is well understandable in the low temperature regime because the decoupling artifacts for low  $c_T$  set in later if we are already at larger temporal extent. For high temperature, this might be a finite size artifact. As stated in [7], finite size effects should be mainly expected from the spatial extent which we found to be large enough to be used with  $L_t \in \{2, 4\}$ . However, it should also be chosen in relation to  $L_t$ . Thus, one expects the finite

---

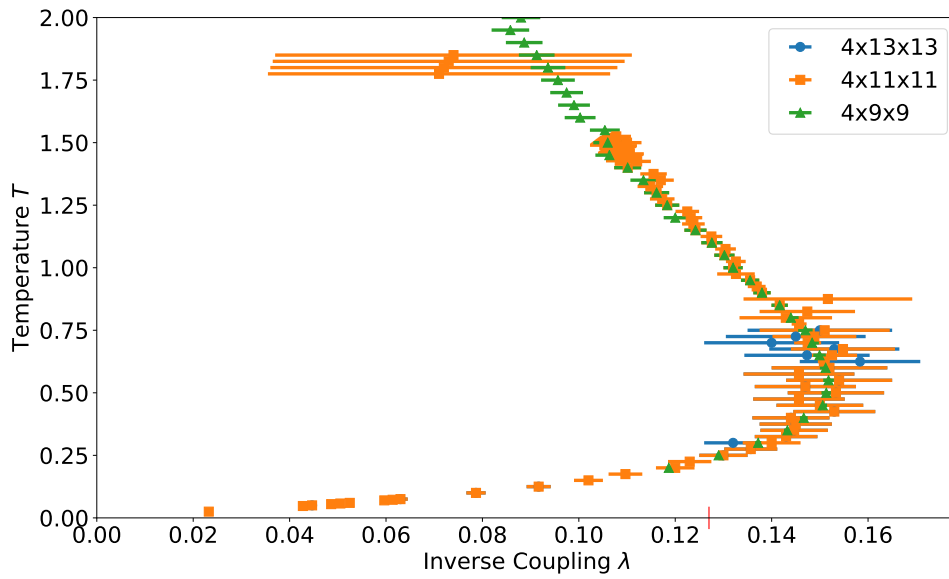
<sup>45</sup>This can also be conjectured about the data in Fig. 5.15 but there it is much too noisy claim something about this region.



## 5.6 The Phase Diagram Of GROSS-NEVEU



(a)  $L_t = 2$ .



(b)  $L_t = 4$ .

Fig. 5.14: The critical lines of the parity breaking phase transition in the  $T$ - $\lambda$  plane for various spatial extents at fixed temporal extent. The red extra tick on the  $x$ -axis indicates the  $\lambda_c(T = 0)$  from Eq. (5.41). Please note the different  $y$ -axes.

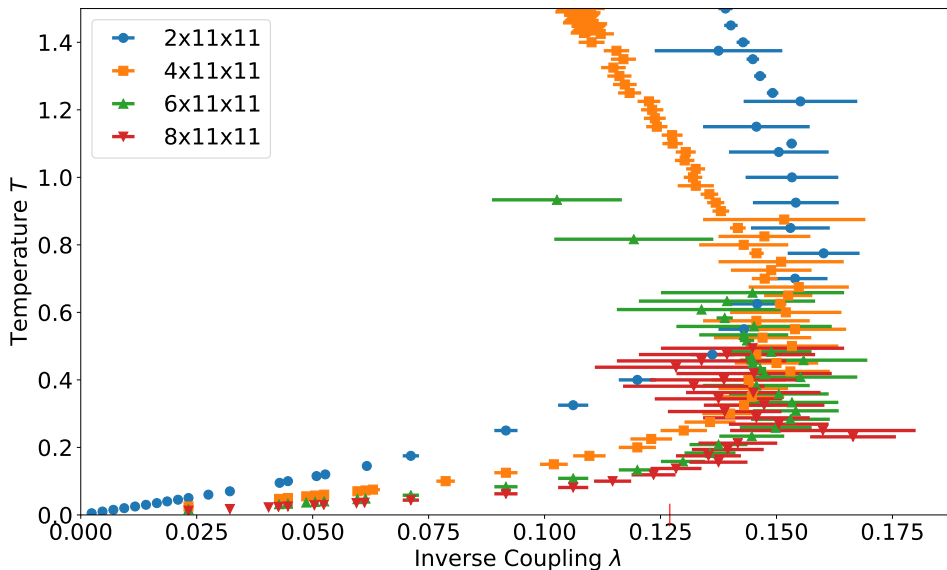


Fig. 5.15: The critical lines of the parity breaking phase transition in the  $T$ - $\lambda$  plane for various temporal extents at fixed  $L = 11$ . The red extra tick on the  $x$ -axis indicates the  $\lambda_c(T = 0)$  from Eq. (5.41).

size effects to increase significantly whenever the ratio  $\frac{L}{L_t}$  is enlarged appreciably. In our case, this ratio is increased by a factor of 2...4 which could be a reason for these huge effects. In this case, the critical line should converge after increasing both, the spatial and the temporal extent, further. Another thing to keep in mind is the fact that there is still the unknown relation to physical temperatures involved. It is hence not clear if the temperature definition in use here (with  $\tau = 1$ ) yields temperatures that can be compared between the various lattice sizes. This will be explored further in the future. The second effect to be seen was already discussed: The bump in the critical line moves to the left slightly. This is best be seen in Fig. 5.16 and could be an explanation for the relatively large difference between the peak of the bump and the critical coupling at  $T = 0$ .

Concerning the LAP transition line, one can note three things: First, the general temperature dependence of this transition is similar to the physical one. It goes to zero for  $c_T \rightarrow 0$ , exhibits a bump around  $c_T \approx 2$  and approaches  $\lambda = 0$  for large temperatures. Second, the artifact line and the critical line never cross (inside the scanned range). Thus, the results about the physical transition are not spoiled by the strong artifacts expected in this phase. Finally, as already discussed the renormalized  $\tilde{\lambda}$  should be physically more relevant and hence the exact separation of both lines is of particular interest. However, one can directly see in Fig. 5.16 (and also in Fig. 5.17) that this separation actually behaves pretty much the same

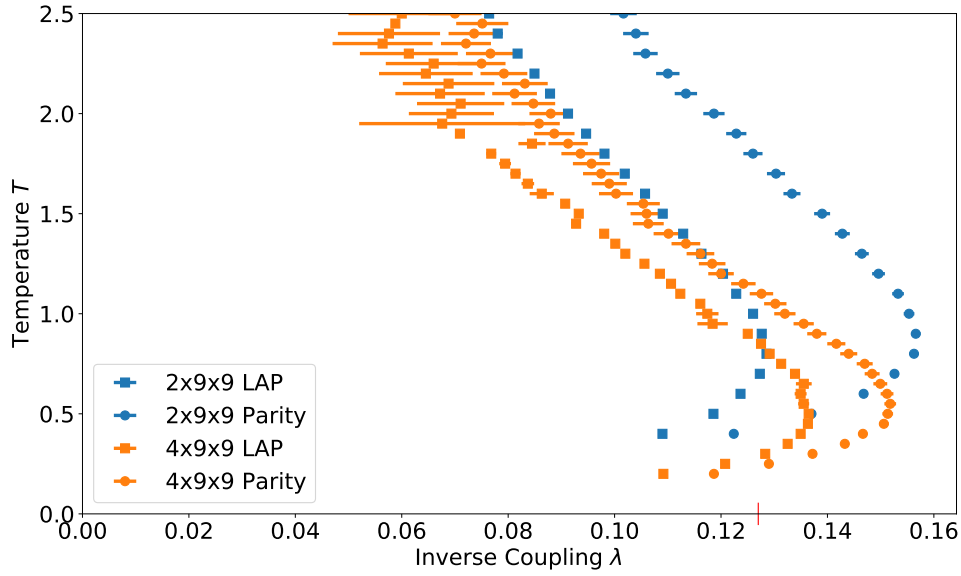


Fig. 5.16: Comparison of the LAP and the parity breaking phase transition for two temporal extents at fixed spatial extent  $L = 9$ . The red extra tick on the  $x$ -axis indicates the  $\lambda_c(T = 0)$  from Eq. (5.41).

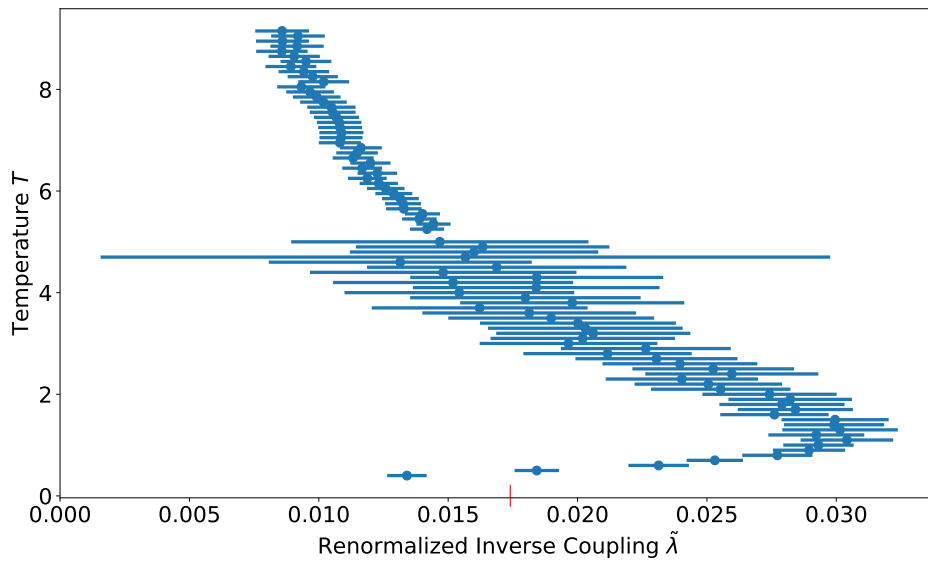


Fig. 5.17: Phase diagram in the  $T$ - $\tilde{\lambda}$  plane where  $\tilde{\lambda}$  denotes the separation between the inverse coupling of the lattice model and the LAP transition (cf. Eq. (5.57)) on a  $2 \times 9 \times 9$  lattice. The red extra tick on the  $x$ -axis indicates the  $\tilde{\lambda}_c(T = 0)$  from Eq. (5.41) and Eq. (5.49).

as the two individual lines. Particularly, it exhibits a bump that exceeds the critical  $\tilde{\lambda} = 0.0174(1)$  at  $T = 0$  and approaches  $\tilde{\lambda} = 0$  at high temperatures. Furthermore, Fig. 5.16 could be interpreted as evidence that the bump in the separation decreases even faster than the bump of the individual lines. If this extends to a substantial trend at larger lattices, this could be the final argument in favor of a close to zero or even negative slope of the critical line at all temperatures. However, it must be stressed again that the results in the current state are not conclusive, particularly concerning the finite size effects.

### 5.6.3 Comparisons

After the general behavior is presented as good as possible from the data, we will attempt a first comparison to related results. For starters, an internal comparison with the results from Sec. 4.2 and Sec. 5.5 was already touched in the previous subsection. There it was found that the  $T \rightarrow 0$  limit is not yet conclusively monitored but does not contradict the previous results beyond what could be explainable by finite size effects. A comparison to the large- $N_f$  scenario could then focus on three aspects: First, the simple shape of the critical line will presumably not be conserved when going from  $N_f = \infty$  to  $N_f = 1$ . This is comprehensible because infinity is in most cases considered a pretty bad approximation of the value one. One should, however, note that an expansion in  $N_f^{-1}$  still yields a good approximation at  $N_f \sim 4 \dots 8$  as found in [16]. On the other hand, it was found in [47] that this approximation is already not reasonable any longer in the  $N_f^{\text{red}} = 1$  case. Second, the presented lattice results are not conclusive about the question whether or not there is a maximal critical temperature. If so, this could be a similarity but as discussed above the data seems to be more in favor of the second scenario where the  $\lambda = 0$  axis is approached asymptotically. Finally, the large- $N_f$  approximation also predicts a maximal inverse critical coupling. As discussed above, this is also expected from the lattice data though the decoupling artifacts for  $c_T \rightarrow 0$  forbid to see it. Additionally, in a medium sized region above the bump the lattice critical line is almost linear which is similar to the large- $N_f$  case. One could imagine that the reduction of finite size effects could lead to a low temperature behavior similar to the analytic result while the high temperature receives unpredicted corrections in the finite  $N_f$  regime (or maybe not even this). Again, we can only refer to the in-progress state of the results and omit a final conclusion.

Concerning the literature, there are to the best of our knowledge only two publications (both by the same team) that present related results [63, 64]. However, even for those it is not clear if they are applicable here because it is nowhere stated in which representation they work. As we know from the general discussion (Sec. 3), this crucially changes the model. On the other hand, it could be irrele-

vant in their calculation or could at least be some approximation like the large- $N_f$  limit. We will thus attempt a comparison but keep in mind that discrepancies may occur without any mistakes on either side just by incompatibility.

In [63], the temperature dependent critical inverse coupling  $\lambda_c$  is computed in the massive case from a one-loop calculation. They find<sup>46</sup>

$$\lambda_c = 16 \left( T \ln \left( 1 + e^{-\frac{m}{T}} \right) - \frac{\pi}{1 + e^{\frac{m}{T}}} \right)^{-1} \xrightarrow{m \rightarrow 0} \frac{16}{\ln 2} \frac{1}{T} \quad (5.59)$$

which simplifies in the massless case. While the high temperature behavior is qualitatively similar to the findings of this thesis, the low temperature prediction, namely a symmetry broken phase for all couplings, contradicts our results. This is presumably an artifact of the massive calculation. Though we had no problems to obtain the limit from the final formulae, there might be a problem of well-definedness within their derivation and its applicability is not established in the massless case without further investigation. Particularly, with a mass term included parity symmetry is explicitly broken such that for sufficiently small temperatures the system is always in the broken phase. This is a crucial difference to the intrinsically massless case where a finite critical coupling exists at  $T = 0$  and explains the discrepancy.

In a follow up investigation [64], the same team did a similar calculation with one spatial direction compactified to a length  $L$ . One could image that this might shed a light on the finite size effects one will encounter in further research about the lattice phase diagram. Their result is then not as easily written down as Eq. (5.59) but is shown in Fig. 5.18. For all finite lengths, the compactification implies a finite critical coupling at  $T = 0$  and deviations from the uncompactified result in the low temperature regime. At larger spatial extent the results more and more resemble the uncompactified version. After all, this would again contradict the expectations from this thesis. We finally see that the setting of [63, 64] is not comparable to the one of this section.

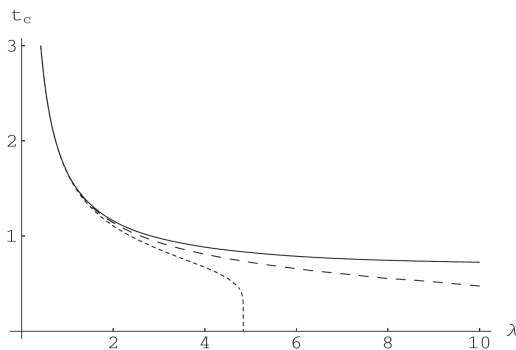


Fig. 5.18: The critical line for one to length  $L$  compactified spatial direction in units of the finite mass  $m$  (i.e.  $t = \frac{T}{m}, \dots$ ) from [64]. The solid line corresponds to the infinite  $L$  case (cf. Eq. (5.59)), the dashed, resp. dotted, line to shrinking  $L$ .

<sup>46</sup>This follows from formula Eq. (37) in [63] after plugging in the corresponding expressions and using the formula  $K_{\pm\frac{1}{2}}(z) = \sqrt{\frac{\pi}{2z}} e^{-z}$ , Eq. (15) from [64].

## 6 Conclusions And Outlook

The present thesis investigated *spontaneous symmetry breaking* (SSB) in *four fermion theories* (4FT). To get concrete results from this broad field of theories, the focus was put on GROSS-NEVEU (GN) models in three spacetime dimensions.

From the well-known large- $N_f$  approximation a first glance on SSB was possible. In this approximation, the critical exponents were found to be the mean field critical exponents and various thermodynamical quantities were calculated and analyzed. In particular, a light was shed on their behavior around the phase transition and on the silver blaze property of the particle density.

Afterwards, the model was further specified to one irreducible flavor. The *Monte Carlo* (MC) results obtained are (to the best of our knowledge) the first of their kind. This is due to technical difficulties in this setting that could be circumvented within a dual formulation that was only recently proposed in [16, 51]. Concretely, for vanishing temperature the generally accepted phase structure with a *lattice artifact phase* (LAP), a chirally/parity broken phase and a symmetry restored phase was confirmed. For both transitions, a precise estimate for the critical coupling and various critical exponents could be obtained from a *finite size scaling* (FSS) analysis. For the physical transition, the former was in good agreement with another estimate from MC simulations [51]; the latter confirmed a functional renormalization group result [53]. The LAP transition was found to be in the 3-dimensional percolation universality class and the estimate for its location was a refinement of the previous MC result in [51].

Finally, the current status of an investigation of the finite temperature phase diagram was documented. As work in progress, the results were not fully conclusive but a general notion was obtained. The best established result was the fact that for every probed temperature a phase transition at finite critical coupling was observed. Particularly, it was conjectured that the critical line would approach  $\lambda = 0$  asymptotically in the high temperature regime while for low temperatures the critical value for  $T \rightarrow 0$  would match the previously found critical coupling at  $T = 0$  after finite size effects become negligible. For the shape of the critical line in between several scenarios were discussed. After all, the general trends seem well-established and the results for small lattices very reliable, while the in-progress state of the research mainly affected the analysis of the scaling behavior.

As a next step in the understanding of SSB in 4FT, we will try to answer the open questions concerning the phase diagram of the GN. To do so, it might be necessary to further improve the algorithmic properties such that the necessarily large parameter scans become feasible on larger lattices. This would also positively affect the precision of the  $T = 0$  estimates. After this structure is finally established, one could turn to study the influence of chemical potential as already done in the large- $N_f$  limit. There are interesting results in two dimensions where the ground

state of the theory was found to be not homogeneous but periodic [22, 45, 46, 65]. Until now, it is not known whether this is an artifact of the limiting procedure or a physical phenomenon also present at finite flavor numbers. If this would be physical, a lot of new questions arise, e.g. if there is a minimal flavor number at which it occurs for the first time.

## References

- [1] ISING, Ernst: Beitrag zur Theorie des Ferromagnetismus. In: *Zeitschrift für Physik* 31 (1925), Nr. 1, S. 253–258
- [2] HIGGS, P. W.: Broken Symmetries and the Masses of Gauge Bosons. In: *Physical Review Letters* 13 (1964), S. 508–509. <http://dx.doi.org/10.1103/PhysRevLett.13.508>. – DOI 10.1103/PhysRevLett.13.508
- [3] GURALNIK, G. S. ; HAGEN, C. R. ; KIBBLE, T. W.: Global Conservation Laws and Massless Particles. In: *Physical Review Letters* 13 (1964), S. 585–587. <http://dx.doi.org/10.1103/PhysRevLett.13.585>. – DOI 10.1103/PhysRevLett.13.585
- [4] ENGLERT, F. ; BROUT, R.: Broken Symmetry and the Mass of Gauge Vector Mesons. In: *Physical Review Letters* 13 (1964), S. 321–323. <http://dx.doi.org/10.1103/PhysRevLett.13.321>. – DOI 10.1103/PhysRevLett.13.321
- [5] NAMBU, Y. ; JONA-LASINIO, G.: Dynamical Model of Elementary Particles Based on an Analogy with Superconductivity. I. In: *Physical Review* 122 (1961), S. 345–358. <http://dx.doi.org/10.1103/PhysRev.122.345>. – DOI 10.1103/PhysRev.122.345
- [6] NAMBU, Y. ; JONA-LASINIO, G.: Dynamical Model of Elementary Particles Based on an Analogy with Superconductivity. II. In: *Phys. Rev.* 124 (1961), 246–254. <https://link.aps.org/doi/10.1103/PhysRev.124.246>
- [7] GATTRINGER, Christof ; LANG, Christian: *Quantum chromodynamics on the lattice: an introductory presentation*. Bd. 788. Springer Science & Business Media, 2009
- [8] NETO, AH C. ; GUINEA, Francisco ; PERES, Nuno M. ; NOVOSELOV, Kostya S. ; GEIM, Andre K.: The electronic properties of graphene. In: *Reviews of modern physics* 81 (2009), Nr. 1, S. 109
- [9] HERBUT, Igor F. ; JURIČIĆ, Vladimir ; ROY, Bitan: Theory of interacting electrons on the honeycomb lattice. In: *Physical Review B* 79 (2009), Nr. 8, S. 085116
- [10] ITOH, Taichi ; KIM, Yoonbai ; SUGIURA, Masaki ; YAMAWAKI, Koichi: Thirring model as a gauge theory. In: *Progress of theoretical physics* 93 (1995), Nr. 2, S. 417–439
- [11] GROSS, D. J. ; NEVEU, A.: Dynamical symmetry breaking in asymptotically free field theories. In: *PRD* 10 (1974), S. 3235–3253. <http://dx.doi.org/10.1103/PhysRevD.10.3235>. – DOI 10.1103/PhysRevD.10.3235
- [12] BRAUN, Jens ; GIES, Holger ; SCHERER, Daniel D.: Asymptotic safety: A simple example. In: *Phys. Rev. D* 83 (2011), 085012. <https://link.aps.org/doi/10.1103/PhysRevD.83.085012>
- [13] BARTELMANN, Matthias ; FEUERBACHER, Björn ; KRÜGER, Timm ; LÜST, Dieter ; REBHAN, Anton ; WIPF, Andreas: *Theoretische Physik*. Springer-Verlag, 2014
- [14] JANKE, Wolfhard: Monte Carlo Methods in Classical Statistical Physics. In: FEHSKE, H. (Hrsg.) ; SCHNEIDER, R. (Hrsg.) ; WEISSE, A. (Hrsg.): *Computational Many-Particle Physics*. Berlin, Heidelberg : Springer Berlin Heidelberg, 2008, S. 79–140



- [15] GEHRING, Friedrich ; GIES, Holger ; JANSSEN, Lukas: Fixed-point structure of low-dimensional relativistic fermion field theories: Universality classes and emergent symmetry. In: *Phys. Rev. D* 92 (2015), 085046. <https://link.aps.org/doi/10.1103/PhysRevD.92.085046>
- [16] SCHMIDT, Daniel: *Three-dimensional four-fermion theories with exact chiral symmetry on the lattice*. Jena, Diss., 2018. <http://dx.doi.org/10.22032/dbt.34148>. – DOI 10.22032/dbt.34148. – Dissertation, Friedrich-Schiller-Universität Jena, 2017
- [17] WIPF, Andreas: *Statistical approach to quantum field theory: an introduction*. Bd. 864. Springer, 2012
- [18] CATTERALL, S. ; JHA, R. G. ; SCHAICH, D. ; WISEMAN, T.: Testing holography using lattice super-Yang-Mills theory on a 2-torus. In: *Phys. Rev. D* 97 (2018), Nr. 8, S. 086020. <http://dx.doi.org/10.1103/PhysRevD.97.086020>. – DOI 10.1103/PhysRevD.97.086020
- [19] PESKIN, Michael E.: *An introduction to quantum field theory*. CRC Press, 1995
- [20] In: GIES, Holger: *Introduction to the Functional RG and Applications to Gauge Theories*. Berlin, Heidelberg : Springer Berlin Heidelberg, 2012. – ISBN 978-3-642-27320-9, 287–348
- [21] LANDAU, David P. ; BINDER, Kurt: *A guide to Monte Carlo simulations in statistical physics*. Cambridge university press, 2014
- [22] FORCRAND, Philippe de ; WENGER, Urs: New baryon matter in the lattice Gross-Neveu model. In: *PoS LAT2006* (2006), S. 152
- [23] BINDER, Kurt: Finite size scaling analysis of Ising model block distribution functions. In: *Zeitschrift für Physik B Condensed Matter* 43 (1981), Nr. 2, S. 119–140
- [24] NIELSEN, Holger B. ; NINOMIYA, Masao: Absence of neutrinos on a lattice:(II). Intuitive topological proof. In: *Nuclear Physics B* 193 (1981), Nr. 1, S. 173–194
- [25] WILSON, Kenneth G.: *New phenomena in subnuclear physics*. 1977
- [26] BURDEN, C. ; BURKITT, A. N.: Lattice Fermions in Odd Dimensions. In: *EPL (Europhysics Letters)* 3 (1987), Nr. 5, 545. <http://stacks.iop.org/0295-5075/3/i=5/a=006>
- [27] NIELSEN, Holger B. ; NINOMIYA, Masao: Absence of neutrinos on a lattice:(I). Proof by homotopy theory. In: *Nuclear Physics B* 185 (1981), Nr. 1, S. 20–40
- [28] DRELL, Sidney D. ; WEINSTEIN, Marvin ; YANKIELOWICZ, Shimon: Strong-coupling field theory. I. Variational approach to  $\varphi^4$  theory. In: *Physical Review D* 14 (1976), Nr. 2, S. 487
- [29] DRELL, Sidney D. ; WEINSTEIN, Marvin ; YANKIELOWICZ, Shimon: Strong-coupling field theories. II. Fermions and gauge fields on a lattice. In: *Physical Review D* 14 (1976), Nr. 6, S. 1627
- [30] KARSTEN, Luuk H. ; SMIT, Jan: The vacuum polarization with SLAC lattice fermions. In: *Physics Letters B* 85 (1979), Nr. 1, S. 100–102

## References

- [31] BERGNER, Georg ; KAESTNER, Tobias ; UHLMANN, Sebastian ; WIPF, Andreas: Low-dimensional supersymmetric lattice models. In: *Annals of Physics* 323 (2008), Nr. 4, S. 946–988
- [32] AARTS, Gert: Introductory lectures on lattice QCD at nonzero baryon number. In: *Journal of Physics: Conference Series* Bd. 706 IOP Publishing, 2016, S. 022004
- [33] ALEXANDRU, Andrei ; BERGNER, Georg ; SCHAICH, David ; WENGER, Urs: Solution of the sign problem in the Potts model at fixed fermion number. In: *Phys. Rev. D* 97 (2018), 114503. <https://link.aps.org/doi/10.1103/PhysRevD.97.114503>
- [34] BRINK, Lars: PARTICLE PHYSICS AS REPRESENTATIONS OF THE POINCARÉ ALGEBRA. In: *Symposium Henri Poincaré, Brussels 2004*, 2005
- [35] CORNWELL, J.F.: *Group Theory in Physics*. Academic Press, 1984 (Group Theory in Physics Bd. 2). <https://books.google.de/books?id=bKQ7AQAATAAJ>. – ISBN 9780121898021
- [36] THIRRING, W. E.: A soluble relativistic field theory. In: *Annals of Physics* 3 (1958), S. 91–112. [http://dx.doi.org/10.1016/0003-4916\(58\)90015-0](http://dx.doi.org/10.1016/0003-4916(58)90015-0). – DOI 10.1016/0003-4916(58)90015-0
- [37] NOETHER, Emmy: Invarianten beliebiger Differentialausdrücke. In: *Nachrichten von der Gesellschaft der Wissenschaften zu Göttingen, mathematisch-physikalische Klasse* 1918 (1918), S. 37–44
- [38] NOETHER, E: Invariante variationsprobleme. In: *Nachr. d. König. Gesellsch. d. Wiss. zu Göttingen, Math-phys. Klasse (1918)* 235–257 (1918), S. 57
- [39] WARD, J. C.: An Identity in Quantum Electrodynamics. In: *Physical Review* 78 (1950), S. 182–182. <http://dx.doi.org/10.1103/PhysRev.78.182>. – DOI 10.1103/PhysRev.78.182
- [40] TAKAHASHI, Y.: On the generalized ward identity. In: *Il Nuovo Cimento* 6 (1957), S. 371–375. <http://dx.doi.org/10.1007/BF02832514>. – DOI 10.1007/BF02832514
- [41] HASENFRATZ, P. ; KARSCH, Frithjof: Chemical potential on the lattice. In: *Physics Letters, B* 125 (1983), Nr. 4, S. 308–310. [http://dx.doi.org/10.1016/0370-2693\(83\)91290-X](http://dx.doi.org/10.1016/0370-2693(83)91290-X). – DOI 10.1016/0370-2693(83)91290-X
- [42] BILIĆ, Neven ; GAVAI, Rajiv V.: On the thermodynamics of an ideal fermi gas on the lattice at finite density. In: *Zeitschrift für Physik C Particles and Fields* 23 (1984), Nr. 1, 77–83. <https://doi.org/10.1007/BF01558043>. – ISSN 1431-5858
- [43] 'T HOOFT, G.: A planar diagram theory for strong interactions. In: *Nuclear Physics B* 72 (1974), S. 461–473. [http://dx.doi.org/10.1016/0550-3213\(74\)90154-0](http://dx.doi.org/10.1016/0550-3213(74)90154-0). – DOI 10.1016/0550-3213(74)90154-0
- [44] DUNNE, Gerald V. ; THIES, Michael: Full time-dependent Hartree-Fock solution of large  $N$  Gross-Neveu models. In: *Phys. Rev. D* 89 (2014), 025008. <https://link.aps.org/doi/10.1103/PhysRevD.89.025008>

- [45] BRZOSKA, Andrej ; THIES, Michael: No first-order phase transition in the Gross-Neveu model? In: *Phys. Rev. D* 65 (2002), 125001. <https://link.aps.org/doi/10.1103/PhysRevD.65.125001>
- [46] THIES, Michael ; URLICHS, Konrad: Revised phase diagram of the Gross-Neveu model. In: *Phys. Rev. D* 67 (2003), 125015. <https://link.aps.org/doi/10.1103/PhysRevD.67.125015>
- [47] SCHERER, David D.: *Low-dimensional chiral physics: gross-neveu universality and magnetic catalysis*, Diss., 2012
- [48] DOLAN, Louise A. ; JACKIW, Roman: Symmetry behavior at finite temperature. In: *Phys. Rev. D* 9 (1974), 3320–3341. <https://link.aps.org/doi/10.1103/PhysRevD.9.3320>
- [49] WOOD, David: The Computation of Polylogarithms / University of Kent, Computing Laboratory. Version: 1992. <http://www.cs.kent.ac.uk/pubs/1992/110>. University of Kent, Canterbury, UK, 1992 (15-92\*). – Forschungsbericht. – 182–196 S.
- [50] FALK, Gottfried ; RUPPEL, Wolfgang: *Energie und Entropie: Die Physik des Naturwissenschaftlers. Eine Einführung in die Thermodynamik*. Springer-Verlag, 2013
- [51] WELLEGEHAUSEN, Björn H ; SCHMIDT, Daniel ; WIPF, Andreas: Critical flavor number of the Thirring model in three dimensions. In: *Physical Review D* 96 (2017), Nr. 9, S. 094504
- [52] CHANDRASEKHARAN, Shailesh: Fermion bag approach to lattice field theories. In: *Physical Review D* 82 (2010), Nr. 2, S. 025007
- [53] HÖFLING, F ; NOWAK, C ; WETTERICH, Christof: Phase transition and critical behavior of the  $d=3$  Gross-Neveu model. In: *Physical Review B* 66 (2002), Nr. 20, S. 205111
- [54] CHRISTOFI, Stavros ; HANDS, Simon ; STROUTHOS, Costas: Critical flavor number in the three dimensional Thirring model. In: *Physical Review D* 75 (2007), Nr. 10, S. 101701
- [55] TSAI, Shan-Ho ; SALINAS, Silvio R.: Fourth-order cumulants to characterize the phase transitions of a spin-1 Ising model. In: *Brazilian journal of physics* 28 (1998), Nr. 1, S. 58–65
- [56] GRACEY, J. A.: Four loop renormalization of  $\phi^3$  theory in six dimensions. In: *Physical Review D* 92 (2015), Nr. 2, S. 025012. <http://dx.doi.org/10.1103/PhysRevD.92.025012>. – DOI 10.1103/PhysRevD.92.025012
- [57] BROADBENT, S. R. ; HAMMERSLEY, J. M.: Percolation processes: I. Crystals and mazes. In: *Mathematical Proceedings of the Cambridge Philosophical Society* 53 (1957), Nr. 3, S. 629–641. <http://dx.doi.org/10.1017/S0305004100032680>. – DOI 10.1017/S0305004100032680
- [58] GATTRINGER, Christof: Coherent center domains in  $SU(3)$  gluodynamics and their percolation at  $T_c$ . In: *Physics Letters B* 690 (2010), Nr. 2, 179 - 182. <http://www.sciencedirect.com/science/article/pii/S0370269310006052>. – ISSN 0370–2693

## References

- [59] CONIGLIO, A ; KLEIN, W: Clusters and Ising critical droplets: a renormalisation group approach. In: *Journal of Physics A: Mathematical and General* 13 (1980), Nr. 8, 2775. <http://stacks.iop.org/0305-4470/13/i=8/a=025>
- [60] DEL DEBBIO, L. ; HANDS, S. J. ; MEHEGAN, J. C. ; UKQCD COLLABORATION: Three-dimensional Thirring model for small  $N_f$ . In: *Nuclear Physics B* 502 (1997), S. 269–308. [http://dx.doi.org/10.1016/S0550-3213\(97\)00435-5](http://dx.doi.org/10.1016/S0550-3213(97)00435-5). – DOI 10.1016/S0550-3213(97)00435-5
- [61] IKEDA, H. ET AL.: A detailed test of the CsI(Tl) calorimeter for BELLE with photon beams of energy between 20 MeV and 5.4 GeV. In: *Nuclear Instruments and Methods in Physics Research Section A: Accelerators, Spectrometers, Detectors and Associated Equipment* 441 (2000), Nr. 3, 401 - 426. [https://doi.org/10.1016/S0168-9002\(99\)00992-4](https://doi.org/10.1016/S0168-9002(99)00992-4). – ISSN 0168-9002
- [62] BUKIN, A. D.: Fitting function for asymmetric peaks. In: *ArXiv e-prints* (2007)
- [63] KHANNA, Faqir C. ; MALBOUISSON, Adolfo Pedro C. ; MALBOUISSON, Jorge Mário C. ; SANTANA, Ademir Eugênio de: Phase transition in the 3D massive Gross-Neveu model. In: *EPL (Europhysics Letters)* 92 (2010), Nr. 1, S. 11001
- [64] KHANNA, Faqir C. ; MALBOUISSON, Adolfo Pedro C. ; MALBOUISSON, Jorge Mário C. ; SANTANA, Ademir Eugênio de: Finite-size effects on the phase transition in the three-dimensional Gross-Neveu model. In: *EPL (Europhysics Letters)* 97 (2012), Nr. 1, S. 11002
- [65] SCHNETZ, O. ; THIES, M. ; URLICHS, K.: Phase diagram of the Gross Neveu model: exact results and condensed matter precursors. In: *Annals of Physics* 314 (2004), Dezember, S. 425–447. <http://dx.doi.org/10.1016/j.aop.2004.06.009>. – DOI 10.1016/j.aop.2004.06.009

# Selbstständigkeitserklärung

Ich, Julian J. Lenz, erkläre, dass ich die vorliegende Arbeit selbstständig und nur unter Verwendung der angegebenen Quellen und Hilfsmittel angefertigt habe. Seitens des Verfassers bestehen keine Einwände die vorliegende Masterarbeit für die öffentliche Benutzung im Universitätsarchiv zur Verfügung zu stellen.

in Jena, den

---

Julian Johannes Lenz